Department of Aerospace Engineering and Engineering Mechanics
University of Cincinnati

A STUDY OF EROSION IN HELICOPTER ENGINE

WITH INLET SEPARATOR

W. TABAKOFF AND A. HAMED

AUGUST 1986

AD-A173 288

DTIC FILE COPY

A STUDY OF COMPRESSOR EROSION IN HELICOPTER ENGINE WITH INLET SEPARATOR

BY

W. TABAKOFF AND A. HAMED

TABLE OF CONTENTS

A-1

LIST OF FIGURES

iii

ABSTRACT

The performance of aircraft engines operating in areas where the atmosphere is polluted by small solid particles can suffer due to blade surface erosion. The erosion damage can lead to significant reduction in engine efficiency as well as performance, due to the change in blade surfaces, tip leakages and blade pressure distribution. This report presents the results of an investigation of the solid particle dynamics and the resulting blade erosion through a helicopter engine with inlet particle separator. The particle trajectories are computed in the inlet separator which is characterized by considerable hub and tip contouring and radial variation in the swirling vane shape. The nonseparated particle trajectories are determined through the deswirling vanes and the five stage axial and one stage radial compressors. The impact data for a very large number of ingested particles is used to calculate the resulting blade surface erosion. The erosion pattern indicates the location of maximum blade erosion. In addition, the distribution of particle impact data which are pertinent to erosion such as the impact velocities, impact angles and in particular, the frequency of particle impacts are presented to suggest possible procedures to reduce the erosion in the critically affected blade areas.

NOMENCLATURE

C_D particle drag coefficient

d   particle diameter

$\bar{F}$ force of interaction between the gas and the particle

M   meridional distance

r   radial distance from the turbomachine axis

$\bar{V}$ velocity relative to the blade surface

z   axial coordinate

β particle impingement angle relative to the blade surface

γ frequency of particle impacts (total number of particle impacts per unit area of the blade surface per unit number of ingested particle)

ϵ blade surface erosion parameter, mg of eroded material per unit area of the blade surface per unit mass of ingested particles $(mg/m^2/gm)$

θ angular coordinate

ρ gas density

ρ_p particle material density

τ time

ω rotor speed (radians/s)

Subscripts

I   refers to particle impact conditions relative to the surface

p   particle

r   component in radial direction

R   refers to particle rebound conditions relative to the surface

z   component in axial direction

θ component in circumferential direction

INTRODUCTION

The problem of a gas-flow mixed with solid particles in axial and radial flow turbomachines has great importance in aeronautical, industrial, and naval applications. The performance of the aircraft engines is known to deteriorate rapidly when they operate in areas where the atmosphere is laden with solid particles. In general, these particles do not follow the flow streamlines in the engine and tend to impact the blade surfaces due to their higher inertia. These blade impacts can cause severe erosion damage that is manifested in the pitting and cutting of the leading and trailing edges, and a general increase in the blade surface roughness [1]. Excessive erosion damage can lead to the structural failure of the blades.

The erosion problems in military and commercial airplane gas turbine engines are generally recognized in industry. The operating life of helicopter engines performing in sandy areas is very short, from 50 to 250 hours [2]. Recently, many reported industrial gas turbine engine failures have been connected to their exposition to particulate flows [3]. Research efforts are still needed to provide a thorough knowledge of the various parameters which influence the extent of erosion damage.

The erosion of metals by solid particle laden flow have been investigated experimentally [4, 5, 6] to determine the parameters that affect the erosion rate and to arrive at empirical equations for the target material erosion in terms of these parameters. The results of these investigations demonstrate that for a given particle-target material combination, the erosion rate is affected by the impacting velocity, impingement angle, and by the metal and the gas temperatures. Prediction of turbomachine blade erosion hence requires that a large number of particle trajectory calculations are carried throughout the machine to determine the pattern and frequency of particle blade impacts as well as the magnitude and direction of the impacting velocities relative to the blade. This data can then be combined with the empirical equation to calculate the blade erosion pattern and intensity.

Erosion cascade tunnels have also been used to determine experimentally the change in compressor cascade performance due to erosion [7]. The changes in the airfoil configuration and its surface roughness were found to influence both the blade loading and the cascade loss coefficient. However, blade erosion in multistage turbomachines differ significantly from the

1

cascade erosion due to the difference in the particle impact locations as well as in their impacting velocities and impingement angles relative to these surfaces. Since the particles impact the blades as well as the casings, the geometrical configuration of the latter would also influence the blade erosion. It was shown that the hub contour geometry [8] and the radial variation in the blade shape [9] not only affect the particle trajectory but also their radial and circumferential distribution after the blade row. Furthermore, since the particles are generally redistributed in the radial direction under the influence of the centrifugal forces as they travel through the machine and repeatedly impact the different blade rows [10, 11, 12], the erosion of the blades in the multistage machines is dependent on their stage locations.

This work presents the results of a detailed study of blade and vane surface erosion through the inlet separator, in the deswirling vanes, and the five stage axial compressor, and the radial compressor of the G.E. T700 helicopter gas turbine engine described in reference [13]. The inlet is characterized by swirling vanes placed in a highly contoured hub zone to centrifuge the particles for separation. The unscavanged flow proceeds through deswirling vanes placed in an annulus zone with decreasing inner and outer radii before the five stage axial flow compressor.

Two separate computer codes, one for predicting the particle dynamics, and another for predicting the erosion are used to obtain the presented results. The three dimensional particle trajectory calculation, in the various components of the machine [12, 14, 15, 16], provide the particle blade impact locations and the magnitude and direction of the particle impacting velocity relative to each blade [3]. A computer code that is especially developed to predict the blade surface erosion uses the computed blade impact data and the experimental results for blade material erosion. The presented results show the magnitude and pattern of blade erosion in the various blade rows. The results indicate that the deswirling and swirling vane erosion is strongly influenced by the inlet separator geometry. The multistage axial compressor blade erosion is found to be strongly influenced by the blade row location. The results also indicate that the erosion intensity in the compressor increases in the latter stages and that higher local values of erosion are generally encountered in the rotor blades than in the stator blades. The results of the radial compressor indicate that

2

the impeller blade pressure surface encounters on erosion intensity higher than that of the splitter surfaces. It was also found that the erosion intensity of the radial impeller is as high as the axial compressor later stages.

ANALYSIS

The equations governing the particle motion, in the turbomachinery flow field are written in cylindrical polar coordinates relative to a frame of reference fixed with respect to the rotating blade.

$$\frac{d^2 r_p}{d\tau^2} = F_r + (\frac{d\theta_p}{d\tau} + \omega)^2 \tag{1}$$

$$r_p \frac{d^2 \theta_p}{d\tau^2} = F_\theta - \frac{2 dr_p}{d\tau} (\frac{d\theta_p}{d\tau} + \omega) \tag{2}$$

$$\frac{d^2 z_p}{d\tau^2} = F_z \tag{3}$$

where r_p, θ_p, z_p define the particle location in cylindrical polar coordinates, and ω the blade angular velocity. The centrifugal acceleration and Coriolis acceleration are represented by the last terms on the right hand side of equations (1) and (2). The first term on the right hand side of equations (1) through (3) represents the force of interaction between the two phases, per unit mass of particles. This force is dependent on the relative velocity between the particles and the gas flow, as well as the particle size and shape. Under the particulate flow conditions in turbomachines, the effect of the forces due to gravity and to interparticle interactions are negligible compared to those due to the aerodynamic and centrifugal forces. In addition, the force of interaction between the two phases is dominated by the drag due to the difference in velocity between the solid particles and the flow field. The force of interaction per unit mass of solid particles is given by

$$F = \frac{3}{4} \frac{\rho}{\rho_p} \frac{C_D}{d} [(V_r - \frac{dr_p}{d\tau})^2 + (V_\theta - \frac{d\theta_p}{d\tau})^2$$

$$+ (V_z - \frac{dz_p}{d\tau})^2]^{1/2} (\bar{V} - \bar{V}_p) \tag{4}$$

where V_r, V_θ, V_z, represent the relative gas velocities in the radial, circumferential and axial directions, respectively and ρ, ρ_p are the gas and

4

solid particle material densities, d the particle diameter, and C_D the particle drag coefficient. This coefficient is dependent on the Reynolds number, which is based on the relative velocity between the particle and the gas. Empirical relations, as shown in reference [14], are used to fit the drag curve over a wide range of Reynolds numbers.

Trajectory Calculations

The particle trajectory calculations consist of the numerical integration of the equations (1)-(4) in the flow field, up to the point of blade, hub or tip impact. The magnitude and direction of particle rebounding velocity after these impacts are dependent on the impacting conditions and the particular particle and surface material combination under consideration.

The particle rebounding conditions are determined from empirical correlations of the restitution parameters. These correlations [17] are based on the experimental data obtained using LDV for particle laden flows over metal samples at various incidence angles and flow velocities in a special tunnel [5, 6]. The ratios were found to be mainly dependent upon the impingement angle [17] for a given particle-material combination.

In the present study the magnitude and direction of the particle rebounding velocity after impact were obtained using the following empirical equation which was obtained from [17] for Kingston fly ash particles impacting on a 410 stainless steel target.:

$$V_{P_R}/V_{P_I} = 1 - 0.90847 \, \beta_I + 0.3072 \, \beta_I^2 + 0.05695 \, \beta_I^3$$

$$(5)$$

and

$$\beta_R/\beta_I = 1 - 0.38746 \, \beta_I + 0.51442 \, \beta_I^2 + 0.45094 \, \beta_I^3$$

$$(6)$$

where V_{P_I} and β_I represent the particle impact velocity and impingement angle, while V_{P_R} and β_R are the rebound velocity and rebound angle measured from the impacted surface.

In the case of rotor blade impacts, the velocities and angles of impact and rebound are considered relative to the rotating blade. Furthermore, in

5

order to use the empirical correlations obtained from two dimensional measurements, in the three dimensional particle trajectories, a knowledge of the geometry of the solid surface at the impact location is required. Geometrical data describing the blade, hub and tip configuration need to be available during the trajectory calculations for use in the determination of the impact location and the impingement angle relative to the surface.

Blade Passage Geometric Representation

The accurate representation of the blade passage geometry is crucial in the particle trajectory calculations and blade erosion prediction as it influences the predicted blade impact locations and particle impact velocity and impingement angle relative to the blades. In addition, the particle trajectory after each impact is also affected by these impact conditions through the rebound restitution correlations of equations (5) and (6). Even if the particle distribution is uniform as particles enter the blade row, they are generally redistributed in a nonuniform pattern as they leave due to blade surface impacts [16]. The blade airfoil shape and inner and outer casing geometry must therefore be accurately represented in the trajectory analysis as it strongly influences the predicted particle dynamics. In addition, the radial variation in the blade shape is also important as it affects the particle rebound characteristics in the three dimensional trajectories [3], and might influence the particle redistribution in the radial direction. The inner and outer casing coordinates and the blade surface coordinates at several sections between the hub and tip are used in the trajectory calculations to determine the blade surface coordinates at other locations using interpolation. At least two blade sections are required but more sections can be used to describe the hub to tip variation in the blade shape.

Flow Field Representation

The flow field affects the particle trajectories, through the aerodynamic forces of interaction consisting mainly of the drag force. Pitchwise as well as radial and axial flow field variations must be represented in the particle trajectory calculation. Careful consideration must be given to the flow field description in the particle trajectory calculations [8], in order to represent the important flow field

characteristics without excessive computer storage requirements. The radial variation in the flow field is affected by the radial variation in blade loading and by inner and outer casing radii contours.

Referring to Fig. 1, one can observe that the inner and outer casings are highly contoured in the inlet separator and through the deswirling vanes, than through the five stage axial flow compressor. The flow field representation in the particle trajectory calculation was hence chosen accordingly to reflect the important three dimensional flow characteristics. The flow field on a mean hub to tip stream surface and a blade to blade velocity gradient [18] are used to represent the flow field in the particle trajectory code for the inlet separator with the swirling vanes [16] and in the deswirling vanes. On the other hand, in the axial compressor particle trajectory calculations, the flow field in the compressor blade passage is synthesized from a number of blade-to-blade stream surface solutions Each flow field solution on a blade-to-blade stream surface [18] provides accurate description of the pitchwise and streamwise variation in the flow properties. The stream surface shapes and stream filament thickness as determined from a mid channel hub to tip stream surface solution [19] model the influence of the inner and outer casing contours and the hub to tip variation in the blade shapes.

Calculation of the three dimensional flow field through the radial compressor impeller was conducted in two steps [20]. The first step uses the code of Ref. [18] to get the flow in the hub shroud meridional plane and the stream tube filament thickness which are the input parameter for the second step. The second step uses the panel method [21] to obtain the blade to blade solutions on a number of stream surfaces stacked from hub to shroud.

Particle Trajectory Computation Procedure:

One can conclude from the previous discussion that the spanwise, pitchwise and chordwise variations in flow properties are therefore represented in the particle trajectory calculations. In addition the effect of the radial variation in the blade shape and hub and tip contouring is taken into consideration in the particle trajectory calculations. The output of the particle trajectory calculation code consists of three files. The first file provides the input for particle trajectory plots. The second

particle trajectory output file contains all particle exit conditions for a given blade row and is used as input to provide the initial conditions for the particle trajectories in the following blade row. This data is first adapted to the new frame of reference, which is fixed in each blade row. The particle axial and radial location is not affected by the relative motion between successive blade rows. The circumferential variation in the particle distibution at the exit of a given blade row, is in reality evened out at the inlet to the following blade row due to the relative motion between successive blade rows. This effect is simulated in the computations by re-distributing the particles randomly in the circumferential direction, in the new frame of reference which is fixed relative to the subsequent blade row. The third file contains all computed particle impact data, including impact locations, and the impact velocity and impingement angle relative to the solid surfaces, for use in the code for blade surface erosion computations.

Blade Mass Erosion Prediction

The computation of the blade surface erosion combines the empirical correlations for the mass erosion parameter for a given particle target material combination [4, 5] with the results of the particle trajectory calculations for a large number of particle trajectories in the form of the impact velocities and impingement angles.

The experimental measurements in the erosion tunnel indicate that the target erosion was found to be dependent upon the particle impact velocity, impingement angle and on the flow and target temperatures. Experimental measurements were obtained in the erosion tunnel for quartz particles (165 micron diameter) impacting 510 stainless steel at different impacting velocities and impingement angles.

The experimental data was used to obtain the following empirical equation for the erosion mass parameter, ϵ, which is defined as the ratio of the eroded mass of the target material to the mass of impinging particles.

$$\epsilon = K_1 [1 + CK(K_{12} \sin(\frac{90}{\beta_o} \beta_1))]^2 V_1^2 \cos^2\beta_1 (1 - R_t^2)$$

$$+ K_3 (V_1 \sin\beta_1)^4$$

where V_1 and β_1 are the impact velocity and impingement angle, respectively.

8

$$R_t = 1 - 0.0016 \ V_1 \ \sin\beta_1$$

β_o = angle of maximum erosion

$CK = 1$ for $\beta_1 \leq 2\beta_o$

$CK = 0$ for $\beta_1 > 2\beta_o$

K_1, K_{12} and K_3 are material constants which were found to be as follows:

$$K_1 = 0.5225 \times 10^{-5}$$

$$K_{12} = 0.266799$$

$$K_3 = 0.549 \times 10^{-12}$$

The erosion computer code was especially developed to calculate the blade surface erosion distribution. The program input consists of the blade surface geometrical data and the particle blade impact data as determined by the particle trajectory calculations. A blade surface fitted grid is generated and the impact data is then combined with the empirical equations to predict the mass erosion intensity and pattern. The mesh size was carefully selected, according to the finite number of particles trajectories, to give the most accurate representation of the blade surface erosion.

The output from this program includes the blade erosion distribution as well as the distribution of the impact velocity, impingement angles and the frequency of particle impacts on the blade surface. The detailed distribution of all these significant erosion parameters over each blade surface in a multistage compressor is essential for taking specific measures to alleviate blade erosion problems.

RESULTS AND DISCUSSION

The results of the particle trajectory computations and blade surface erosion analysis are presented for 165 micron diameter quartz particles through the inlet separator, the axial and the radial flow compressors of the G.E. T700 helicopter engine which is shown in Fig. 1. Three sets of results are presented in each component, the first shows the particle trajectory projections on the blade to blade surface and on a hub to tip surface. The second set of data is also pertinent to the particle trajectory computations and shows the actual locations of particle blade surface impacts. The third set presents the results of blade surface erosion analysis in the form of the distribution over the blade surface, of the frequency of particle impacts, the magnitudes of the impacting velocity and impact angle relative to the blade, and finally the predicted blade erosion.

Inlet Separator

Figure 1 shows the geometry of the inlet separator which combines a highly contoured inner casing with the swirling vanes to deflect the particles in the radial direction. The particle initial conditions were taken statistically to represent uniform particle loading with uniform axial velocity upstream of the engine inlet. The particle trajectory calculations were performed in the inlet separator as described in reference [16]. The results of the particle trajectory computations are presented in figures 2 and 3 which show the projection of sample particle trajectories in the blade to blade cylindrical surface and the meridional plane through the machine axis, respectively. One can observe that the trajectories of these large particles deviate considerably from the flow streamlines because of their high inertia. These particles can be seen to continue in their axial motion uninfluenced by the flow field until they impact the blade or casing. One can see that some of the particles near the tip traverse the twisted blades without any impacts. Many of these particles are still separated however because of their outward radial location relative to the splitter between the engine and scavanged flow. The particles that impact the swirling vanes pressure surface, rebound with a smaller radially outward velocity component and a larger circumferential velocity component that causes their centrifugion. These particles impact the tip casing and acquire a radially

10

inward velocity after rebounding which causes them to enter the engine. On the other hand, many of the particles that impact the inner casing are reflected in the radially outward direction towards the tip annulus. Many of these particles also impact the outer casing and acquire a radial inwarad velocity after rebounding and later enter the engine. The very few particles exempt from this behavior are those impacting the inner casing further downstream, much closer to the hump, and might miss entering the engine due to their later impact locations with the outer casing, which causes them to separate.

Figures 4 and 5 show the particle impact locations on the swirling vanes suction and pressure surfaces respectively. It is obvious from these figures that the particles impact the vane pressure surface much more frequently than the suction surface. Figure 5 also shows that the particle impacts with the vane increases towards the hub and the trailing edge.

The particle impact frequency impinging velocity and angle distribution over the vane surface was determined from a large number of particle trajectories and the results are shown in Figs. 6 through 8 respectively for the pressure surface. Figure 6 confirms that generally the particle impact frequency increases towards the hub except at the trailing edge. A high intensity impact region extends over most of the vane chord towards the hub. Two other regions of high impact frequency are also predicted at the corner of the trailing edge and outer casing, and the opposite corner of the leading edge and inner casing. Figure 7 shows the distribution of the particle impacting velocity on the pressure surface of the swirling vanes. The highest impacting velocities (60 m/s or more) can be seen in a triangular part of the blade near the leading edge and the tip which extends up to 75% of both the span and chord. This corresponds to the particle inlet velocities, which remain practically unchanged until the first particle impact. The low impact velocities in the other parts of the blade can be attributed to the lower velocity of many of the particles, impacting this area after encountering previous impacts with the blade surface, the hub or tip casing which causes a loss in their momentum. The higher impacting velocity regions near the trailing edge reflect first time impacts for the particles that traverse most of the blade chord with no previous interactions to their blade impacts near the trailing edge. Figure 8 shows the impact angle distribution over the swirling vanes pressure surface. The

11

highest impact angles are seen at the leading edge area which then decreases towards the mid chord, and then increases again towards the trailing edge as the blade angle increases.

An erosion code was especially developed to predict the blade surface erosion based on the blade surface impact data for a large number of particles and the empirical equations from the experimental measurements for the particle target material. Figure 9 shows the distribution of the calculated erosion parameter on the pressure surface as determined from a large number of particle trajectories. This figure shows that the maximum blade erosion is predicted at the corner of the blade between the trailing edge and the hub. The particle impact angle of 25-30 degrees in this region is close to β_o the impact angle corresponding to the maximum erosion for this particle target material combination. Both impact velocity and frequency of particles impact are also high in this region.

Deswirling Vanes

The unseparated particles enter the engine with the unscavenged air which follows the inner part of the flow path through the separator. Figures 10 and 11 present sample particle trajectories through the deswirling vanes viewed, in the z-θ plane and in the z-r plane respectively. Many of the unseparated particles enter with very small radial velocities and consequently impact the contoured outer casing. Some of these and the other particles impact either the pressure side or the suction side of the vanes.

Figures 12, 13 show the locations of particle impacts with the deswirling vane surfaces. One can see that, over the vane suction surface, the particle impacts are confined to one third the vane chord towards the leading edge, and in another narrower band that extends from the leading edge blade corner at the tip to about one quarter the blade span at the trailing edge. On the other hand the particle impacts with the pressure surface are concentrated towards the outer half of the blade span, and extend more over the vanes leading edge and trailing edge and less in between. These particle impact patterns are a result of the combined effect of the particle distribution as they enter the vanes and the geometry of the twisted vanes and the highly contoured annulus.

12

Figures 14 through 17 present the distribution of the erosion parameters θ, V, β and ϵ over the suction side of the deswirling vanes. One can see from figure 14 that the highest values of particle impact frequencies are encountered near the tip and leading edge corner and decrease gradually towards the hub and the trailing edge. In addition, Fig. 15 shows that the impacting velocities are highest in the same areas of higher impact frequencies. Figure 16 shows that the particle impact angles are generally low with the highest values of impacting angles close to $\beta_o=25°$, at the leading edge close to the tip. This corresponds to the impact angle of maximum erosion. All three effects combined together result in the highest erosion rate on the blade suction surface at the leading edge tip corner as shown in Fig. 17.

Figures 18 through 21 present the erosion parameters distribution on the deswirling vanes pressure surface. Comparing Figs. 18 and 14, one can see that more particles impact the pressure surface than the suction surface. The particle impact frequency distribution is also different, with maximum values on the pressure surface near the vane mid chord at the tip. Figure 19 shows that the particle impact velocities do not change drastically over the deswirling vanes pressure side. Comparing Figures 19 and 15, one can see that the particle impacting velocities are generally lower over the pressure surface than the suction surface. Figure 20 shows that the particle impact angles are generally higher than β_o, the impact angle of maximum erosion. The lowest values of the particle impact angles are at the vane tip near the leading corner where it is close to the value of, $\beta_o=25°$, the angle of maximum erosion. Figure 21 shows that the erosion pattern on the pressure side of the deswirling vanes is somewhat similar to that of the impacting frequency, with the maximum at the tip of the blade near the mid-chord. Comparing Figs. 21 and 17 one can see that the maximum value of the deswirling vane pressure surface erosion is almost the same as for the suction surface, in spite of the much higher impacting frequencies over the pressure surface. This can be attributed to the higher impacting velocities on the suction surface, Fig. 15.

13

Axial Compressor

The blade erosion characteristics of the G.E. T700 helicopter engine five stage axial flow compressor were studied on the basis of the trajectory data presented in reference [3]. The particle trajectory calculation, for 165 microns diameter particles, were performed throughout the five stages axial flow compressor. The results of the first and last stages particle trajectory are shown in Figs. 22 through 29, respectively. One can notice from Figs. 23, 25 and 27 that only the pressure side of the rotor and stator blades are subjected to particle impacts. Details of the trajectory results and the location of particle impacts on the blade surfaces can be found in reference [3].

The data required by the code which was specially developed for analyzing the erosion characteristics on the machine blade surfaces consisting of the impact characteristics of a large number of particles was obtained from the trajectory computations. Only the blade pressure surfaces data was considered because the blade suction surface erosion is insignificant. Figures 30 through 34 present the important blade erosion parameters, namely, particle impacting velocity V, particle impingement angle β, the frequency of particle impacts θ, and particle erosion parameter ϵ, for the five rotors, of the axial compressor. One can observe from these figures that both particle impact frequency and impact velocity patterns over the rotor pressure surface are somewhat similar. The impingement angle pattern is different, and changes from a maximum value at the hub to a minimum near the tip towards the trailing edge. The blade erosion pattern is similar to both particle impact frequency and impact velocity patterns with the maximum erosion at the blade leading edge tip corner, then diminishing towards the trailing edge hub corner. A region of the rotor blade pressure surface at the hub trailing edge corner extending diagonally over one third of the blade chord near the hub to about two thirds of the blade span at the trailing edge is not subjected to any particle impacts and hence suffer no erosion.

Figures 35 through 39 show the variation of the erosion parameters v, β, θ, and ϵ on the pressure surfaces of the five stators of the axial flow compressor. One can see from these figures that the stator blade pressure surface erosion pattern is very similar to the particle impact frequency pattern. The maximum stator blade erosion is always at the tip but is not

14

necessarily near the leading edge. A small portion of the stator blade at the leading edge near the hub is not subjected to particle impacts. This is due to the effect of the preceding rotor impacts which centrifuge the particles in the radially outward direction. However, the particles are distributed more uniformly in the radial direction as they leave the stator blades. This explains the difference in the location of the non impacted blade surfaces in stationary and rotating blade rows. In general the erosion intensity increases in the latter stages due to the reduced flow path. The maximum value of stator blade erosion are generally lower than the maximum rotor blade erosion.

Centrifugal Compressor

The particle trajectories as well as the study of the erosion parameters were conducted through the centrifugal compressor. In order to determine the particle inlet conditions at the centrifugal compressor. The trajectory calculations for the 165 micron particles were continued through the annular gap, between the axial and the centrifugal compressors. The particle trajectory computations were carried out in this axisymmetric flow field as determined using the computer code of reference [18]. The centrifugal compressor impeller configuration, as shown in Fig. 4, has two different size splitters between the blades.

Figure 41a and 41b show a sample of the particle trajectories projected in the M-θ and r-z planes respectively through the impeller of the compressor. One can also see that the particles initially have a small radial inward velocity component which they had as they left the fifth stator of the axial compressor. Shortly, the particles outward radial migration starts and is more pronounced after they impact either the blade or the hub surface. It is clear from Fig. 41a that the particles impact the pressure surfaces of the impeller blade and the second splitter. Figure 41b shows many particle impacts with the hub and very few particle impacts ;with the shroud.

The particle impact locations with the blade and splitter surfaces are shown in Fig. 42. One can see from this figure that the first splitter suction surface is subjected to some particle impacts, while most of the particle impacts are with the second splitter pressure surface and the full blade pressure surface.

15

The particle impact locations for the impeller's hub and casing, are presented in Fig. 43. Inspection of this figure shows that the impeller hub encounters more impacts than the casing. The particle distribution at the impeller exit is given in Fig. 44, which shows that the particles are more concentrated near the pressure side of the impeller blade and the second splitter.

The conditions of impact (velocity, angle and location) provided by the calculations of the particle trajectories through the radial impeller were used as input. An erosion study of the radial compressor impeller was conducted using the same procedures outlined previously for the axial flow compressor. The results are presented for the erosion parameters, namely the impact velocity, impact angle, impact frequency and the mass erosion parameter over the affected blade and splitter surfaces. Figure 45 shows the distribution of the particle impact velocities on the impeller blade pressure surface. One can see that the highest impact velocities are at inlet, and close to the impeller casing at outlet. The distribution of the impact angles on the same blade surface, is given in Fig. 46. Inspection of this figure shows that the whole blade pressure side area is subjected to impact angles that correspond to maximum erosion. The impeller area that is subjected to the highest impacting frequencies constitutes the second half of the impeller, close to the outlet region, as shown in Fig. 47. The resulting blade surface erosion over the blade pressure surface is given in Fig. 48, which shows high values of erosion at the impeller inlet.

The distributions of the erosion parameters over the pressure surface of the second splitter vane are displayed in Figs. 49 through 52. Figure 49 shows the distribution of the particle impact velocities over the pressure side of the second splitter. The velocities are generally high comparable to those on the pressure surface of the impeller blade. The highest velocities are close to the impeller casing. The distribution of the impact angles, Fig. 50, show that most of the surface is subjected to impact angles close to that corresponding to the maximum erosion. The areas that are subjected to the maximum frequency of impacts are the same areas that show the maximum rate of mass erosion as shown in Figs. 51 and 52 respectively.

Figures 53 through 56 show the distribution of the same erosion parameters over the suction side of the first impeller, where the particle impacts are only limited to a small region of the splitter area close to the

16

leading edge, (Fig. 47). Figure 53 shows that the impact velocities are relatively low compared to those on the blade pressure surface (Fig. 45). The impact angle distribution over the same splitter surface is presented in Fig. 54, which shows that smaller impact angles than that corresponding to maximum erosion, β_o. Figure 55 shows the area of the splitter vane subject to the highest impact frequencies. Figure 56 shows that the mass erosion distribution on the same splitter surface is similar to the impact frequency pattern because of the moderate variation in both impact velocity and the impact angle distribution.

CONCLUSION

The dynamics of the suspended solid particles which are entrained by the air through the helicopter engine inlet separator and its axial and centrifugal compressors were investigated. The distribution of the unseparated particles and the locations of the particle-blade impacts were determined from the particle trajectory computations and presented throughout the five stage axial flow compressor and the single stage centrifugal compressor. The trajectories of the 165 micron sand particles are generally dominated by their impacts with the blade pressure surfaces, after which they tend to migrate in the radial direction under the influence of the centrifugal forces. This process is initiated at the first rotor and continues throughout the five stages leading to increased particle concentration toward the outer annulus and the absence of the particles near the inner annulus. This in turn affects the particle blade impact locations and the resulting blade erosion pattern in the various stages. The presented results indicate that most of particle blade impacts are with the pressure surface in both the axial and radial flow compressors. The results also show a nonuniform particle distribution in both the centrifugal and radial directions between each pair of sequential blade rows. In the axial flow compressor, the maximum stator blade erosion is always at the tip, but not at the leading edge, and the maximum rotor blade erosion is near the leading edge at the tip. In the axial compressor, the maximum blade erosion is generally observed in the rotors, not the stator. In the centrifugal compressor, the maximum erosion occurs on the pressure surface of the impeller blade closer to the impeller inlet. The results also indicate that the maximum erosion in the centrifugal compressor is comparable to that of the axial compressor earlier stages, but generally lower than the axial compressor lower stages. This can be attributed to the higher particle impact velocities relative to the axial compressor blade surfaces in the latter stages.

REFERENCES

1. Tabakoff, W., "A Study of the Surface Deterioration due to Erosion," Journal of Engineering for Power, October 1983, pp. 834-839.

2. Tabakoff, W., "Review - Turbomachinery Performance Deterioration Exposed to Solid Particulates Environment," Journal of Fluids Engineering, Vol. 106/125, June 1984.

3. Tabakoff, W. and Hamed, A., "Installed Engine Performance in Dust-Laden Atmosphere," AIAA Paper II, AIAA/AHS/ASEE Aircraft Design Systems and Operations Meeting, San Diego, California, Oct. 31-Nov. 2, 1984.

4. Grant, G. and Tabakoff, W., "Erosion Prediction in Turbomachinery Resulting from Environomental Solid Particles," Journal of Aircraft, Vol. 12, No. 5, 1975, pp. 471-478.

5. Tabakoff, W., Hamed, A. and Ramachandran, J., "Study of Metals Erosion in High Temperature Coal Gas Streams," Journal of Engineering for Power, Vol. 102, January 1980, pp. 148-152.

6. Tabakoff, W. and Hamed, A., "Investigation of Gas Particle Flow in Erosion Wind Tunnel," 7th Annual Conference on Materials for Coal Conversion and Utilization, National Bureau of Standards, Gaithersburg, MD, November 16-18, 1982.

7. Tabakoff, W., Hamed, A. and Balan, C., "Performance Deterioration of an Axial Flow Compressor stage with Presence of Solid Particles," Proceedings of the 5th intern. Symposium on Airbreathing Engines, 1980.

8. Hamed, A., "Solid Particle dynamic Behavior through Twisted Blade Rows," Proceedings of the Symposium on Particle Laden Flows in Turbomachinery, 1982, ASME, New York, pp. 33-41.

9. Beacher, B., Tabakoff, W. and Hamed, A., "Improved Particle Trajectory Calculations Through Turbomachinery Affected by Coal Ash Particles," Journal of Engineering for Power, Vol. 104, January 1982, pp. 64-68.

10. Tabakoff, W. and Hamed, A., "Installed Engine Performance in Dust Laden Atmosphere," AIAA Paper 84-2488, November 1984.

11. Hussein, M.F. and Tabakoff, W., "Computation and Plotting of Solid Particle Flow in Rotating Cascades," Computers and Fluids, Vol. 2, 1974, pp. 1-15.

12. Hussein, M.F. and Tabakoff, W., "Three Dimensional Dynamic Characteristics of Solid Particles Suspended by Polluted Air Flow in a Turbine Stage," AIAA Paper No. 73-140, January 1973.

13. Yaffe, M., "T700 Aims at Low Combat Maintenance," Aviation Week and Space Technology, Vol. 100, No. 4, January 1974, pp. 45-53.

14. Hussein, M.F. and Tabakoff, W., "Dynamic Behavior of Solid Particles Suspended by Polluted Flow in a Turbine Stage," Journal of Aircraft, Vol. 10, No. 7, July 1973, pp. 434-440.

15. Hussein, M.F. and Tabakoff, W., "Computation and Plotting of Solid Particles Flow in Rotating Cascade," Computers and Fluids, Vol. 2, 1974, pp. 1-15.

16. Hamed, A., "Particle Dynamics of Inlet Flow Fields with Swirling Vanes," Journal of Aircraft, Vol. 19, No. 9, Sept. 1982, pp. 707-712.

17. Tabakoff, W. and Malak, M.F., "Laser Measurements of Fly Ash Rebound Parameters for Use in Trajectory Calculations," ASME Paper No. 85-GT-161, 30th International Gas Turbine Conference and Exhibit, Houston, Texas, March 17-21, 1985.

18. Katsanis, T. and McNally, W.D., "Revised Fortran Program for Calculating Velocities and Streamlines on the Hub-Tip Mid Channel Stream Surface of an Axial, Radial, or Mixed Flow Turbomachine or Annular Duct, Vols. 1 and 2," NASA TND-8430 and NASA-TND 8431, 1977.

19. Katsanis, T., "Fortran Program for Calculating Transonic Velocities on a Blade-to-Blade Stream Surface of a Turbomachine," NASA TND-2809, May 1965.

20. Elfeki, S. and Tabakoff, W., "Particulate Flow Solutions Through Centrifugal Impeller with Two Splitters," ASME Paper No. 86-GT-130.

21. McFarland, E.R., "A Rapid Blade-to-Blade Solution for Use in Turbomachinery Design," ASME Journal of Engineering for Gas Turbines and Power, Vol. 106, 1984, pp. 376-383.

FIG. 1. SCHEMATIC OF ENGINE SEPARATOR WITH COMPRESSOR.
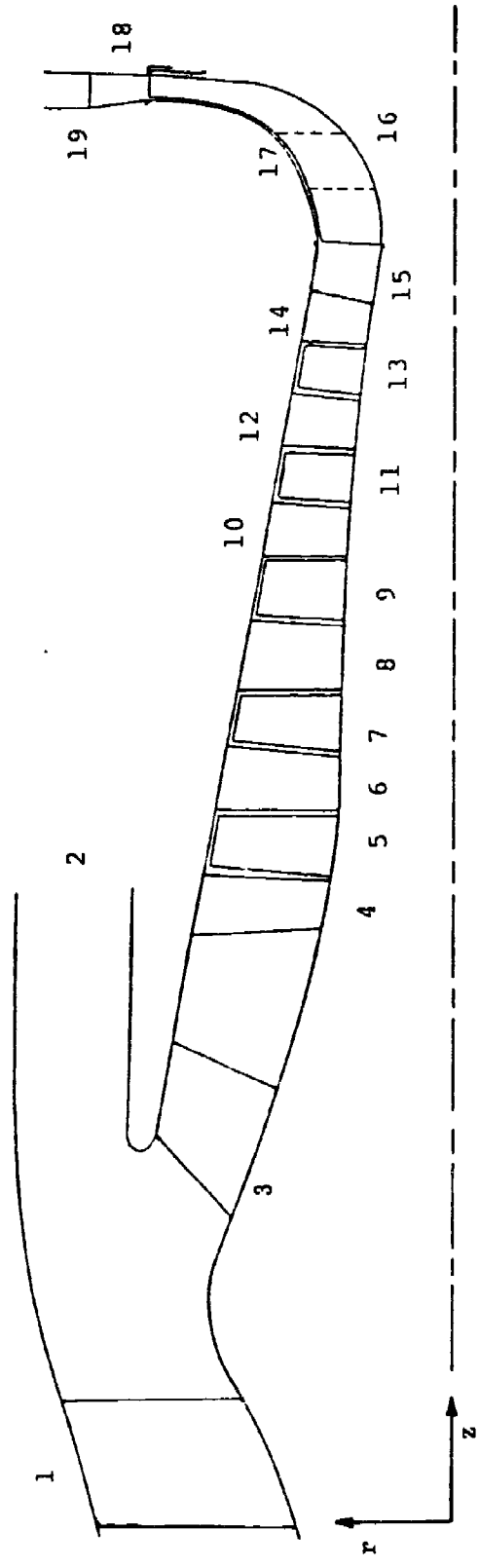
1. INLET SWIRL VANE
2. SCAVENGE AIR COLLECTOR
3. DESWIRL VANE
4. COMPRESSOR INLET GUIDE VANE

5. ROTOR 1
6. STATOR 1
7. ROTOR 2
8. STATOR 2
9. ROTOR 3

10. STATOR 3
11. ROTOR 4
12. STATOR 4
13. ROTOR 5
14. STATOR 5

15. GAP
16. IMPELLER
17. CASING
18. VANELESS DIFFUSER
19. VANED DIFFUSER

21

HUB SECTION

TIP SECTION
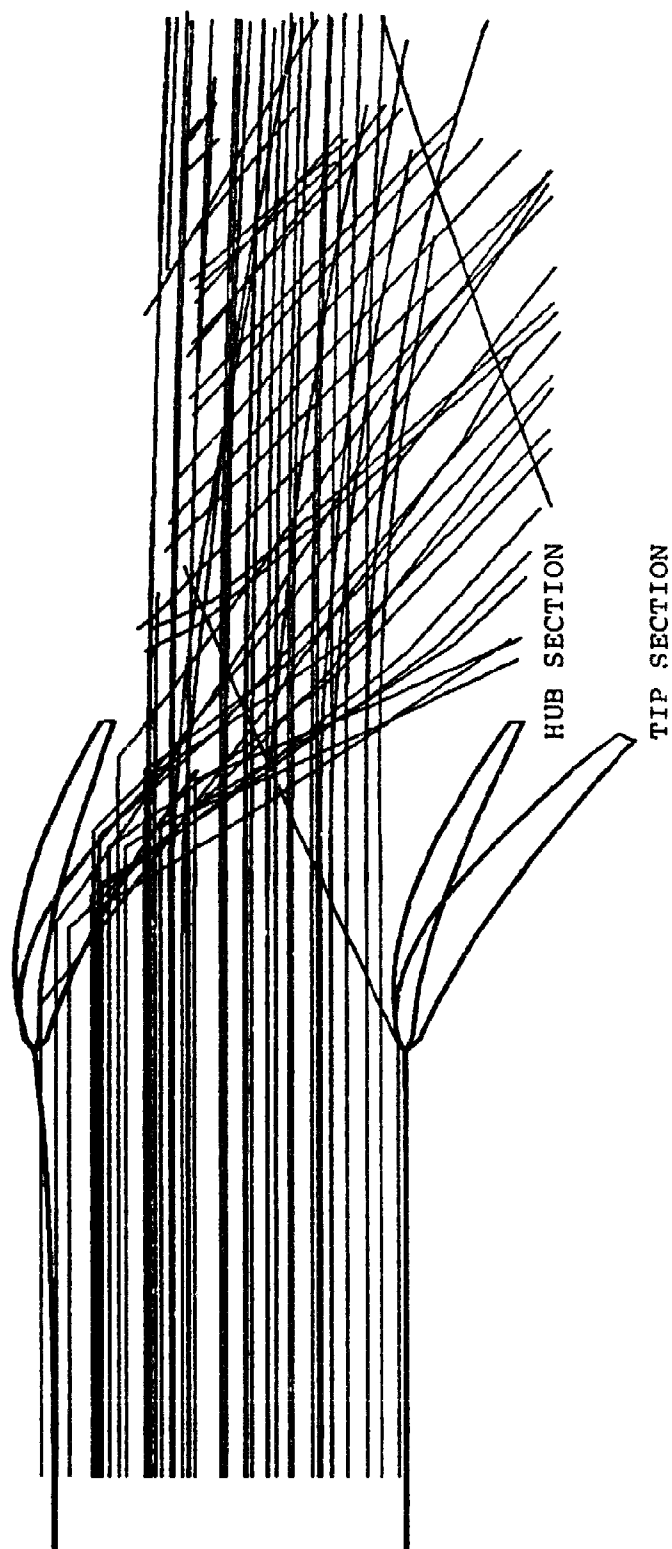
FIG. 2. PARTICLE TRAJECTORY VIEW, IN THE $z-\theta$ PLANE, THROUGH THE INLET SEPARATOR.
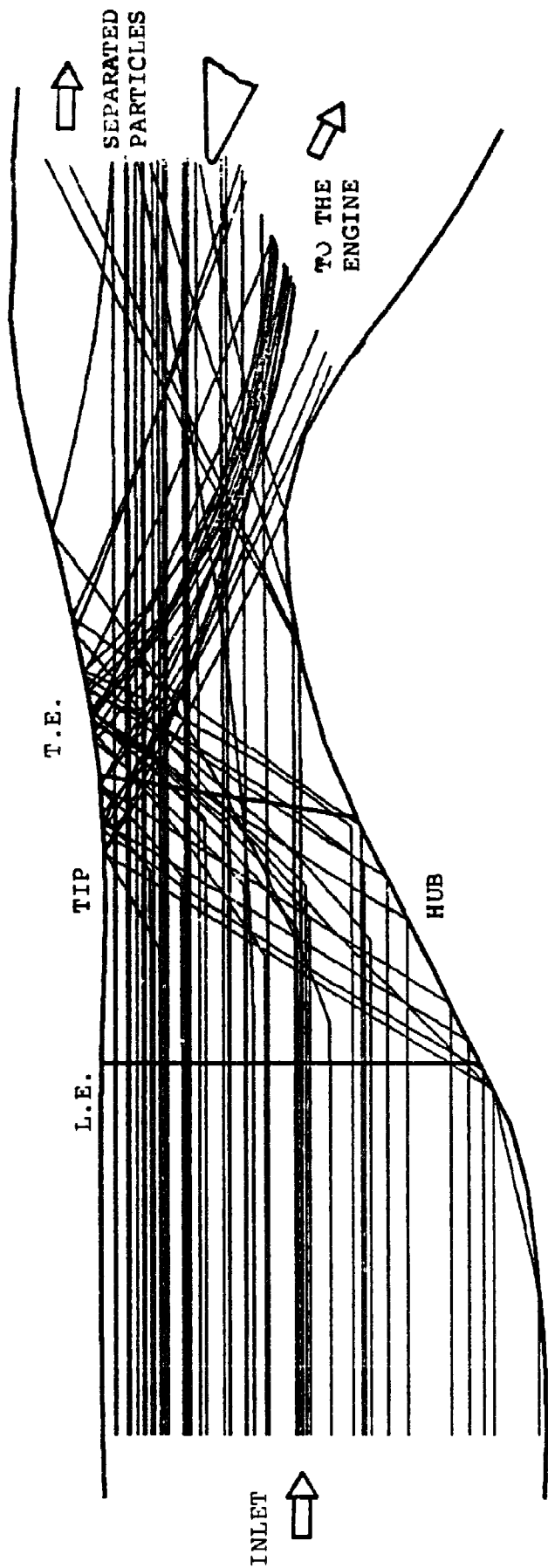
FIG. 3. PARTICLE TRAJECTORY VIEW, IN THE z-r PLANE, THROUGH THE INLET SEPARATOR.

23
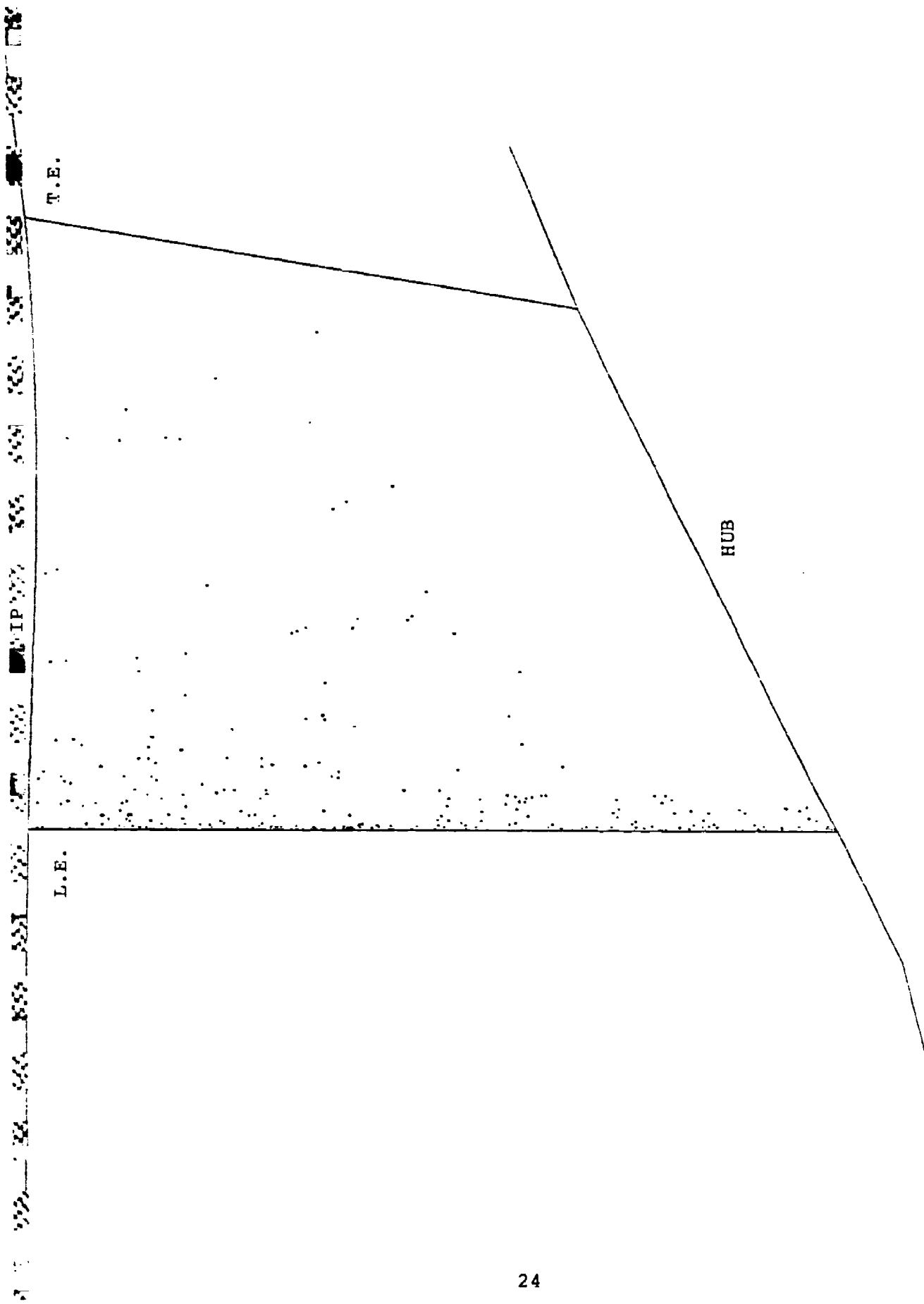
FIG. 4. PARTICLE IMPACT LOCATIONS ON THE SUCTION SURFACE OF THE SWIRLING VANES.

24
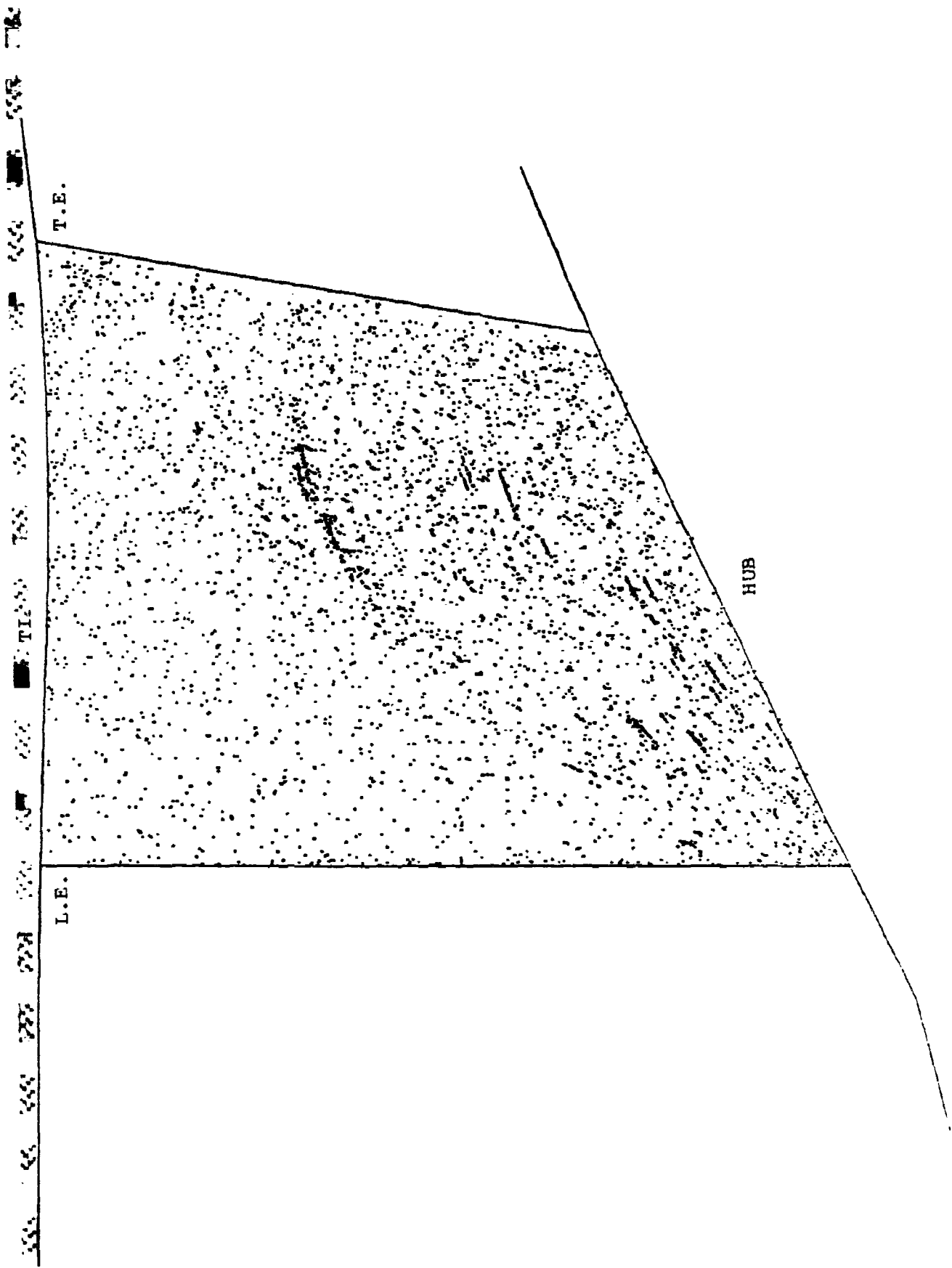
FIG. 5. PARTICLE IMPACT LOCATIONS ON THE PRESSURE SURFACE OF THE SWIRLING VANES.

25
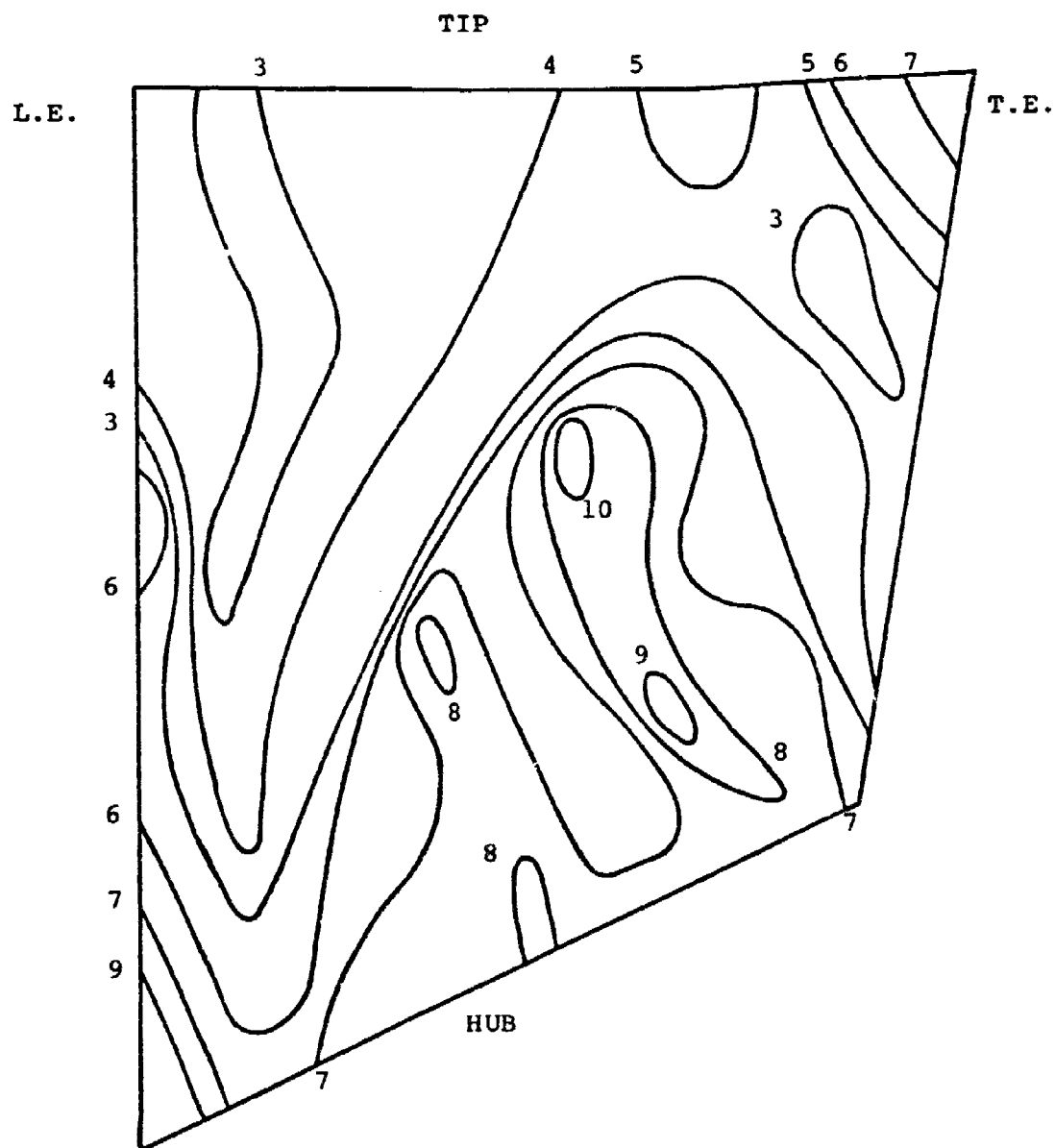
FIG. 6.   DISTRIBUTION OF THE PARTICLE FREQUENCY OF IMPACT, γ,
ON THE SWIRLING VANE PRESSURE SURFACE.
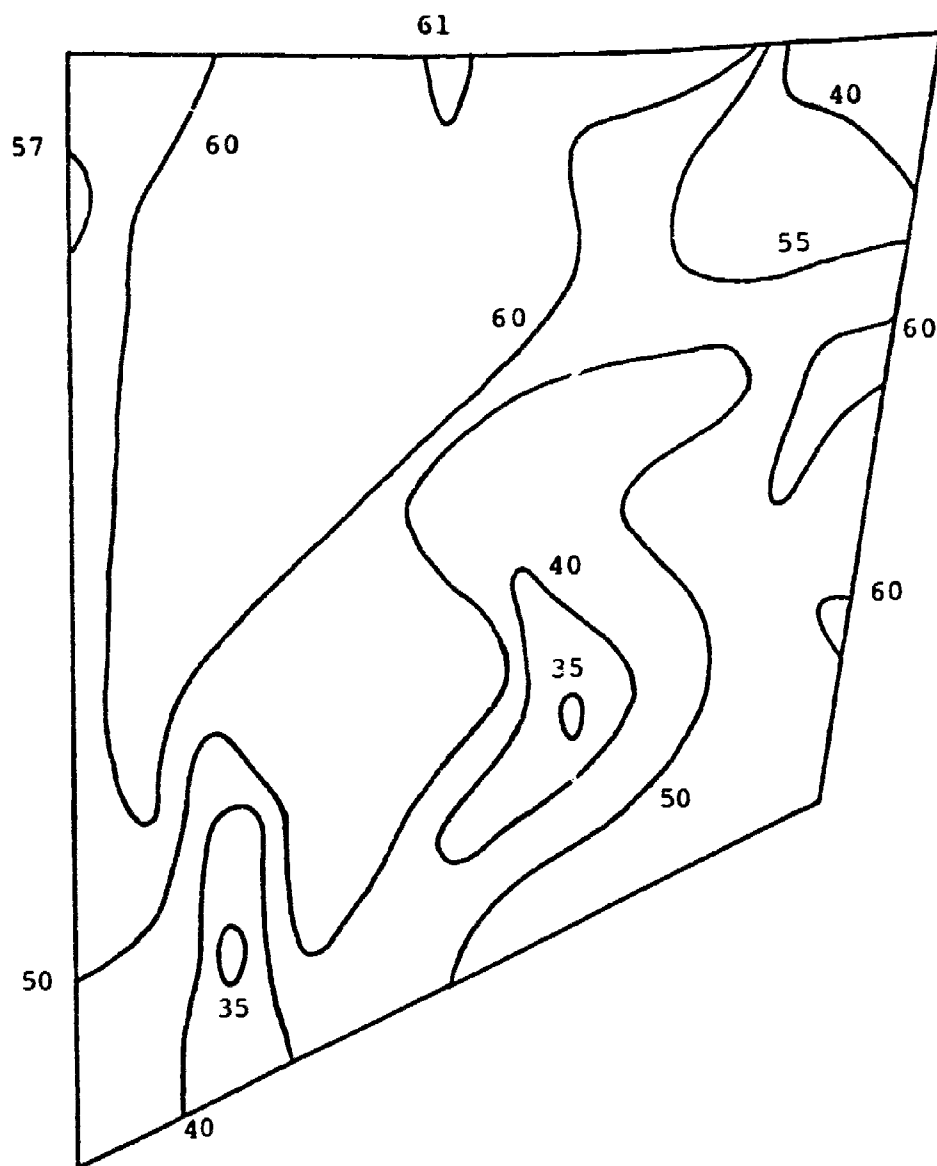
FIG. 7.   DISTRIBUTION OF THE PARTICLE IMPACTING VELOCITY (m/s)
ON THE PRESSURE SURFACE OF THE SWIRLING VANE.
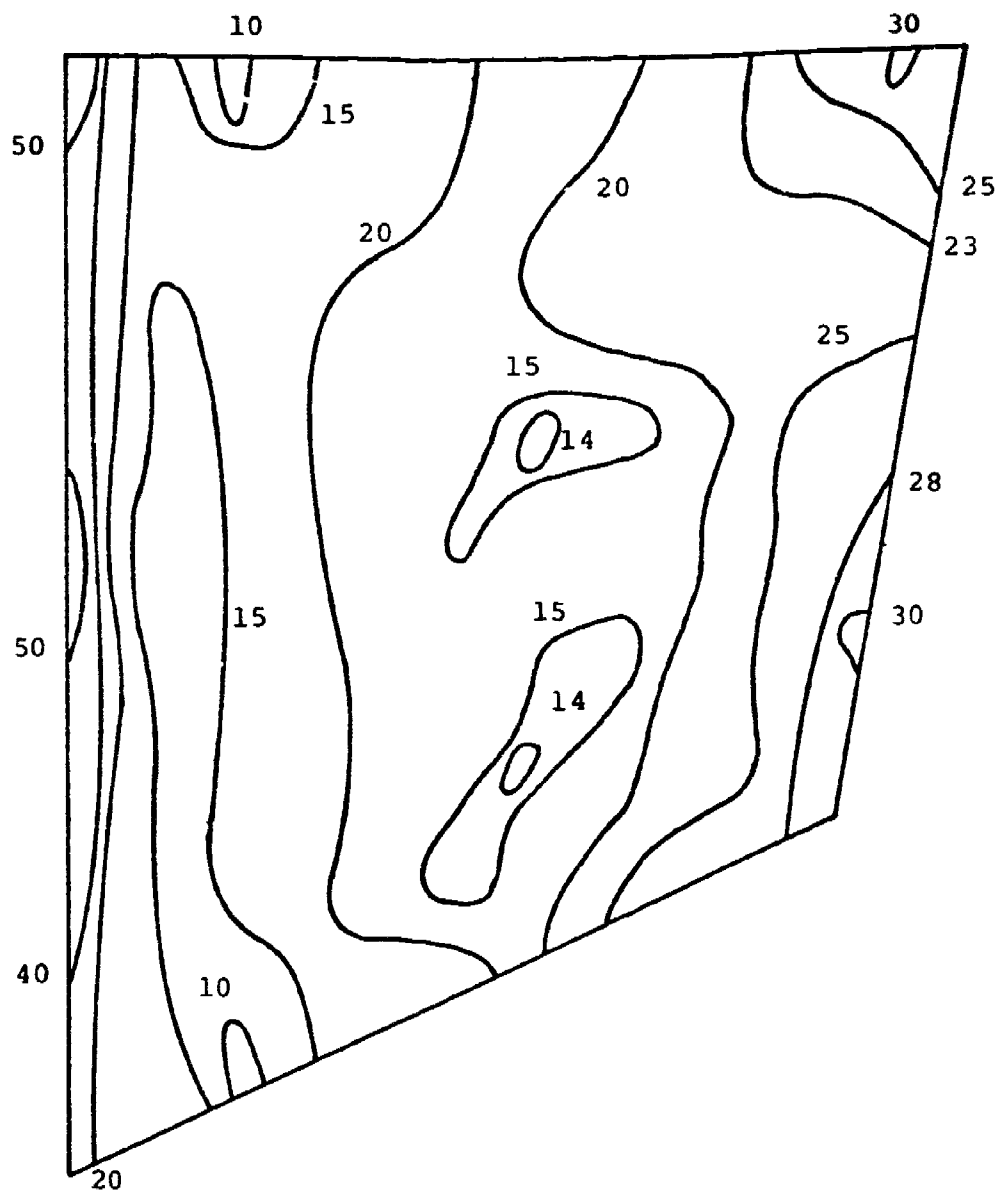
FIG. 8.   DISTRIBUTION OF THE PARTICLE IMPACTING ANGLE (DEGREE)
ON THE PRESSURE SURFACE OF THE SWIRLING VANE.

28
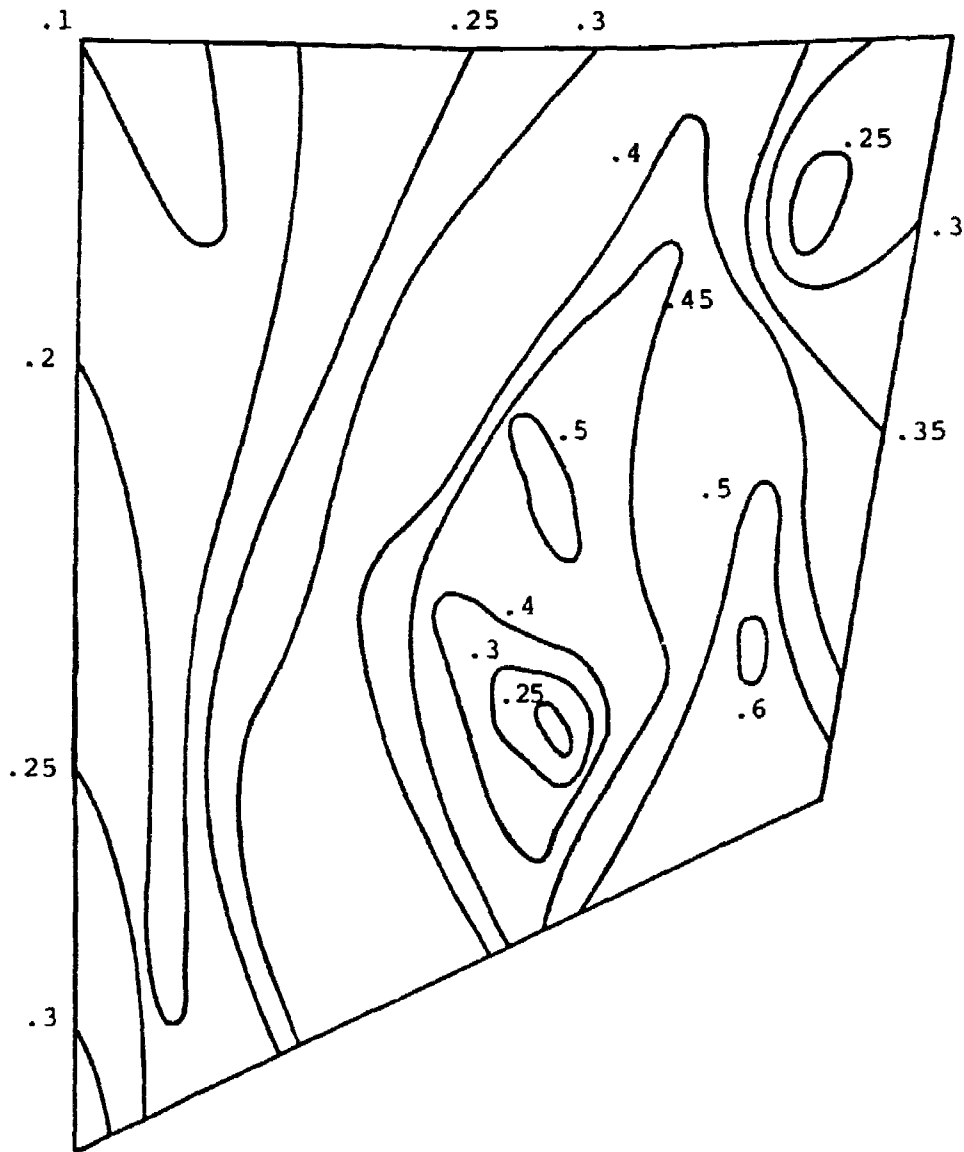
FIG. 9. DISTRIBUTION OF THE EROSION RATE, ε, ON THE
SWIRLING VANE PRESSURE SURFACE.

HUB BLADE SECTION

TIP BLADE SECTION

INLET

OUTLET
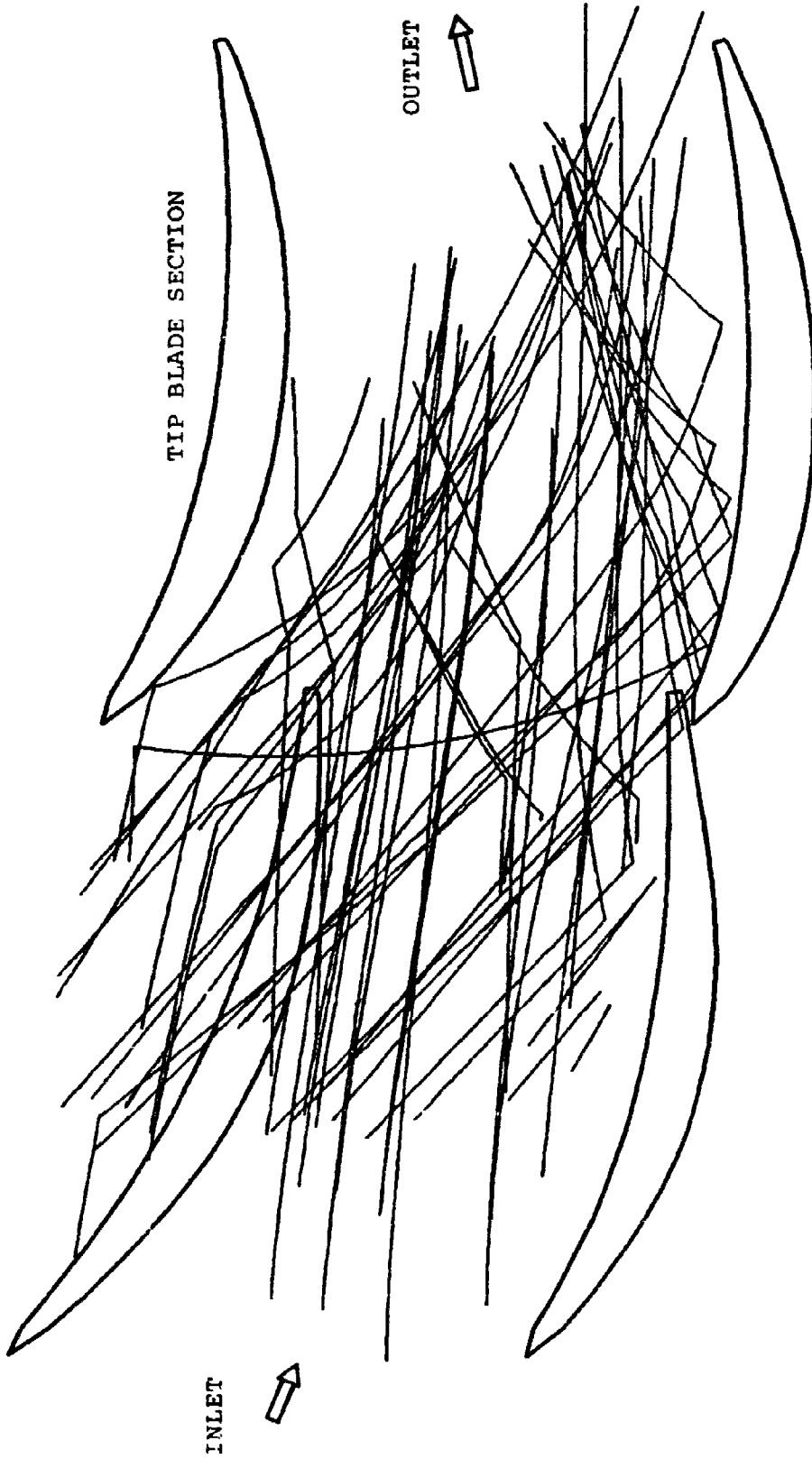
FIG. 10. PARTICLE TRAJECTORY VIEW, IN THE $z-\theta$ PLANE, THROUGH THE DESWIRLING VANES.
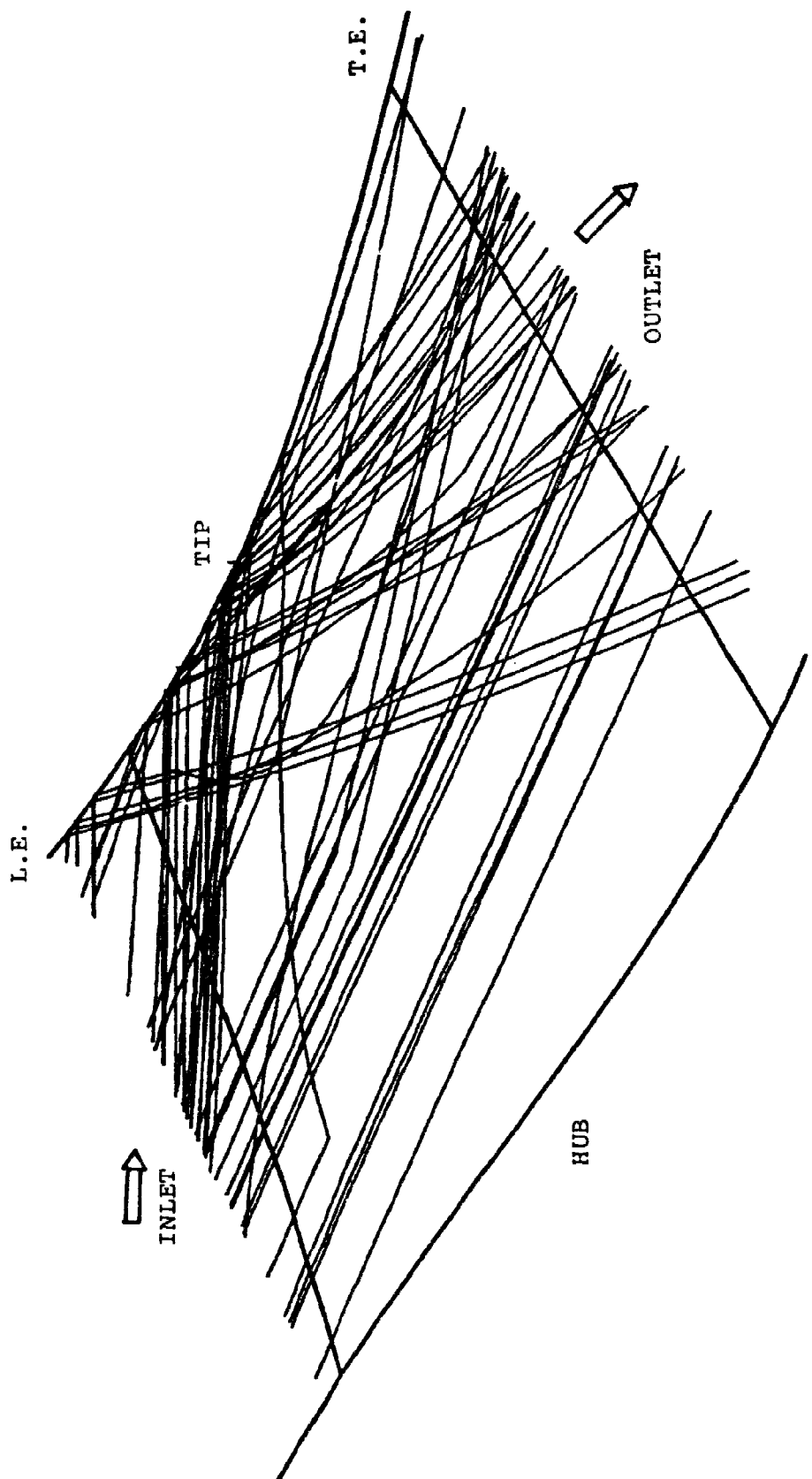
FIG. 11. PARTICLE TRAJECTORY VIEW, IN THE Z-R PLANE, THROUGH THE DESWIRLING VANES.

31
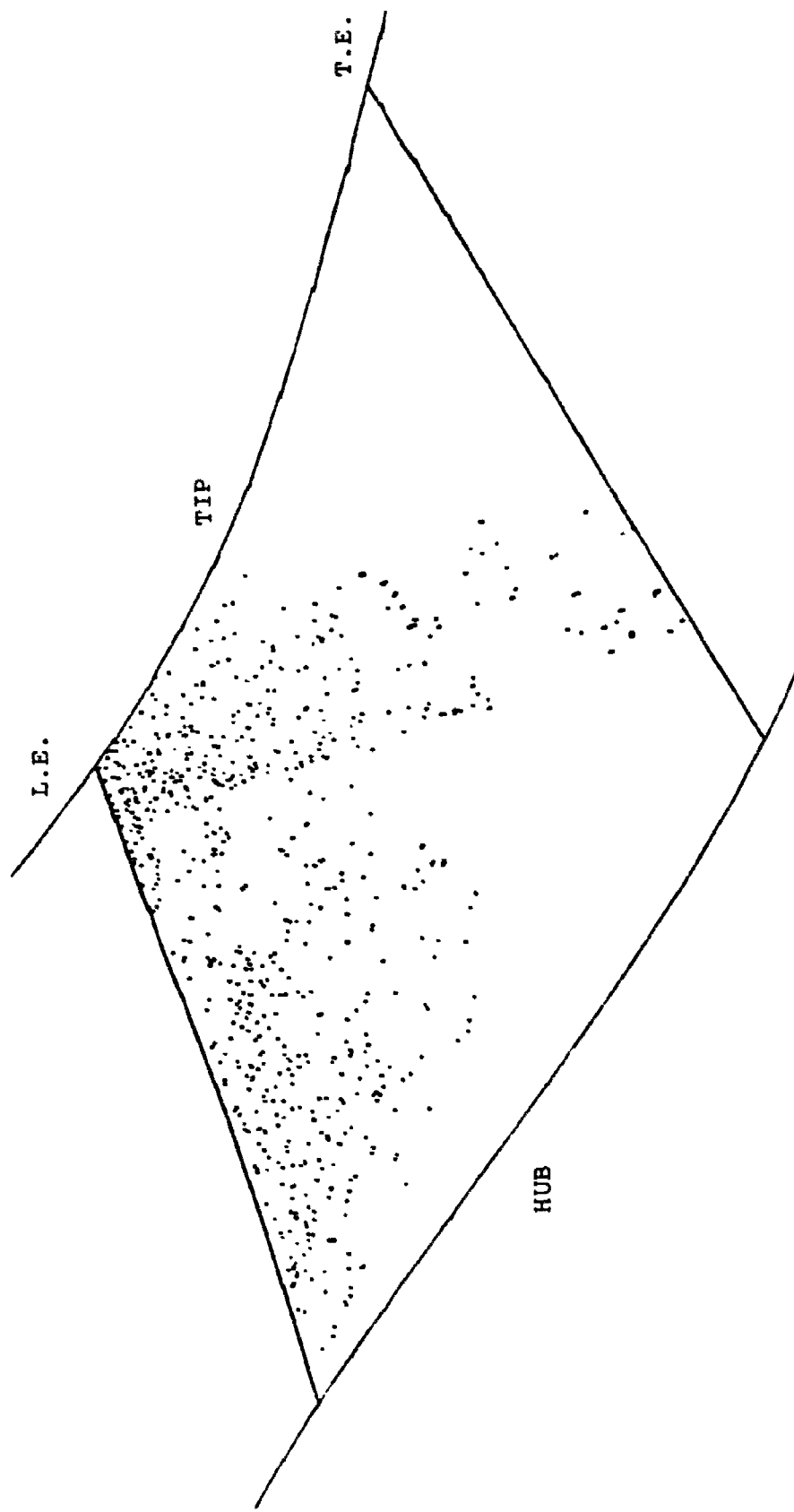
FIG. 12. PARTICLE IMPACT LOCATIONS ON THE SUCTION SIDE OF THE DESWIRLING VANES.
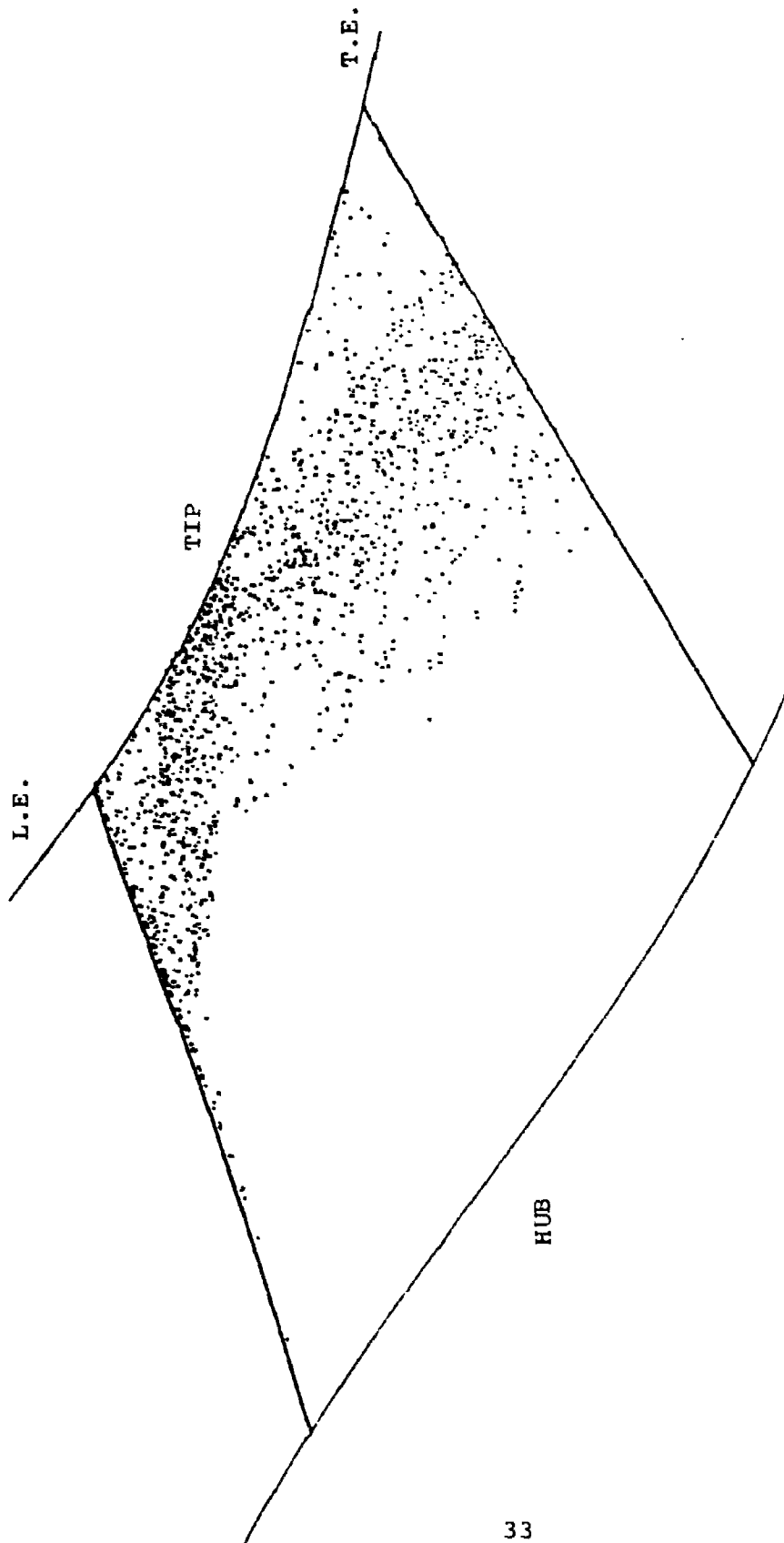
FIG. 13. PARTICLE IMPACT LOCATIONS ON THE PRESSURE SIDE OF THE DESWIRLING VANES.

33
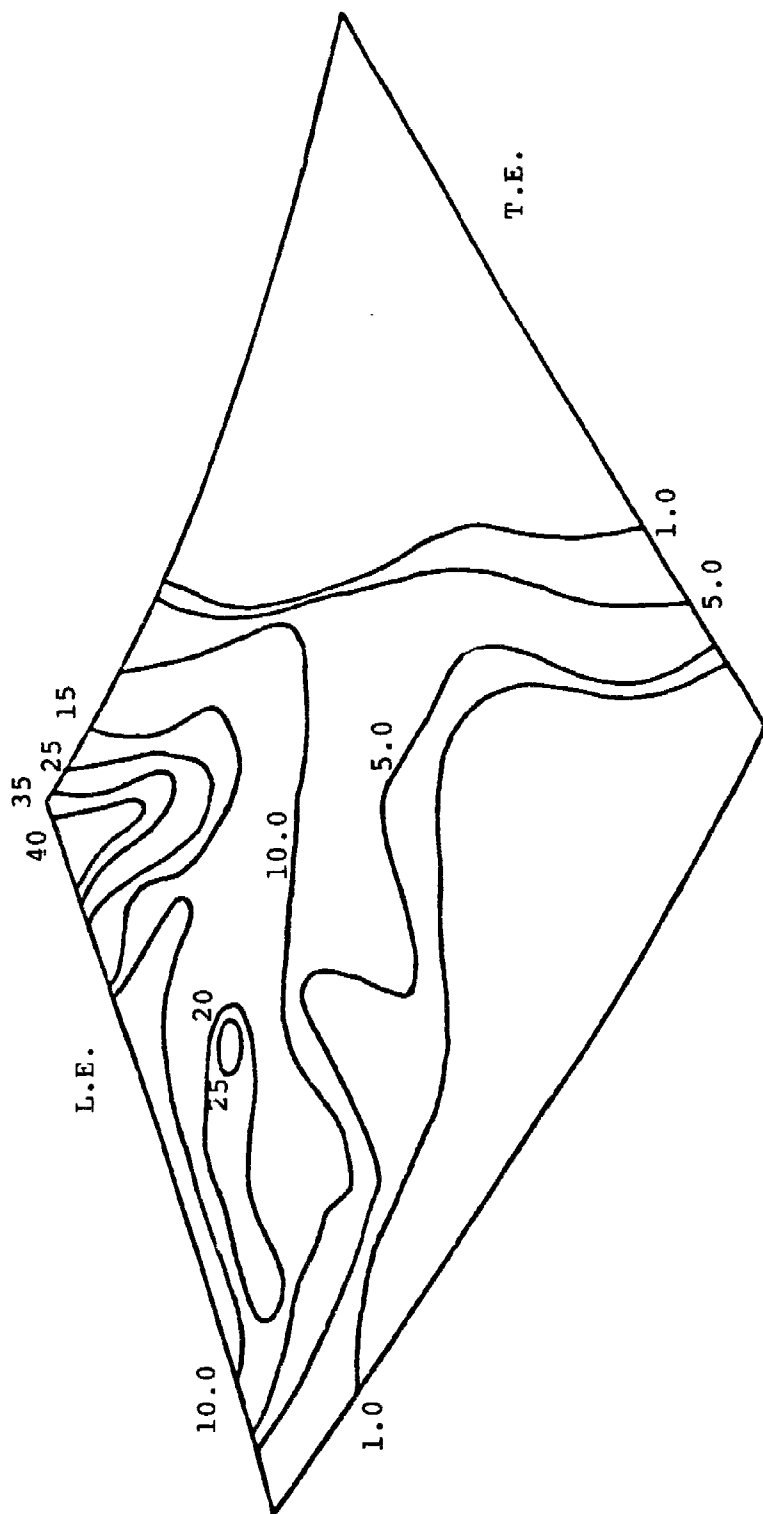
FIG. 14. DISTRIBUTION OF THE PARTICLE IMPACTING FREQUENCY ON THE DESWIRLING VANES SUCTION SURFACE.
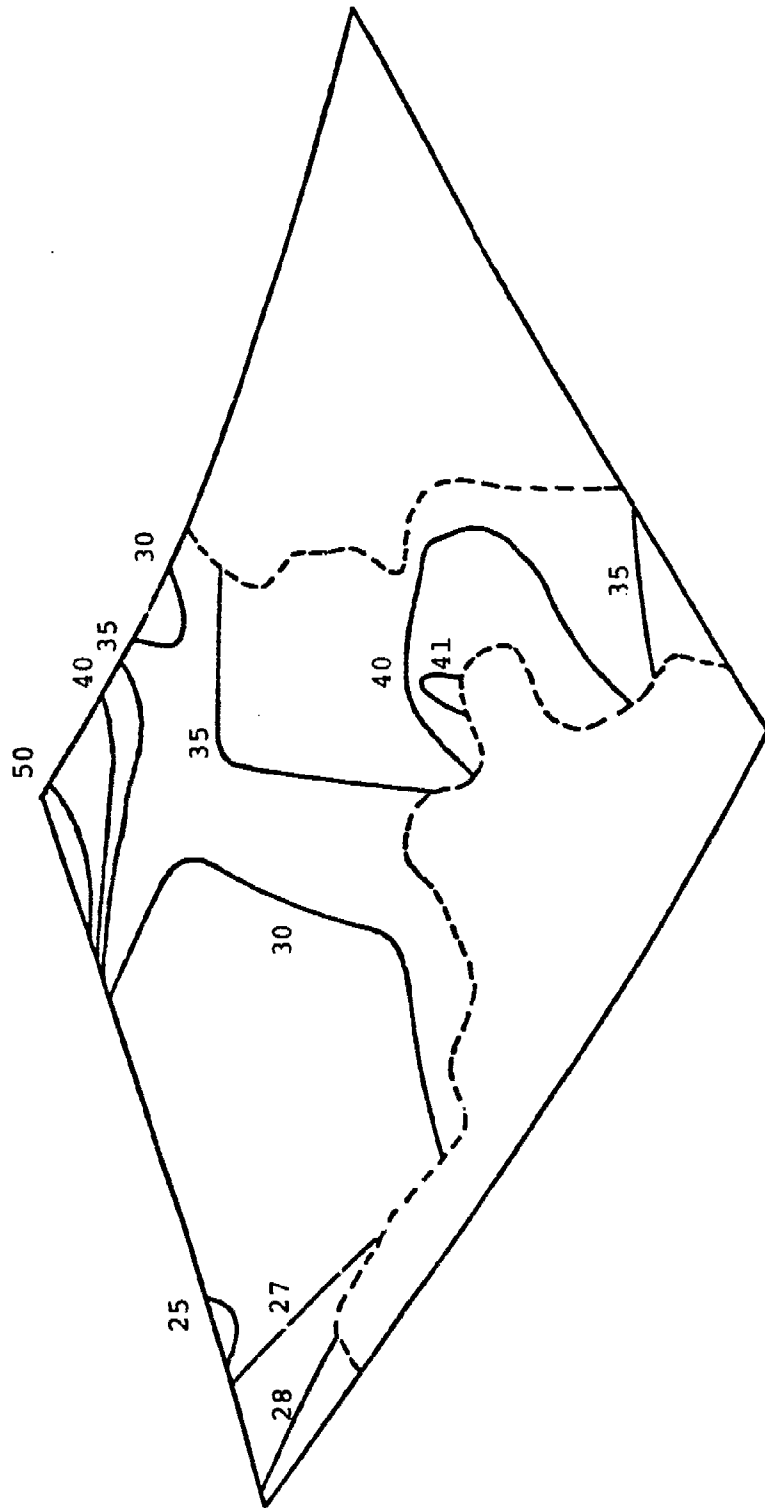
FIG. 15. DISTRIBUTION OF THE PARTICLE IMPACTING VELOCITY (M/S) ON THE DESWIRLING VANES SUCTION SURFACE.
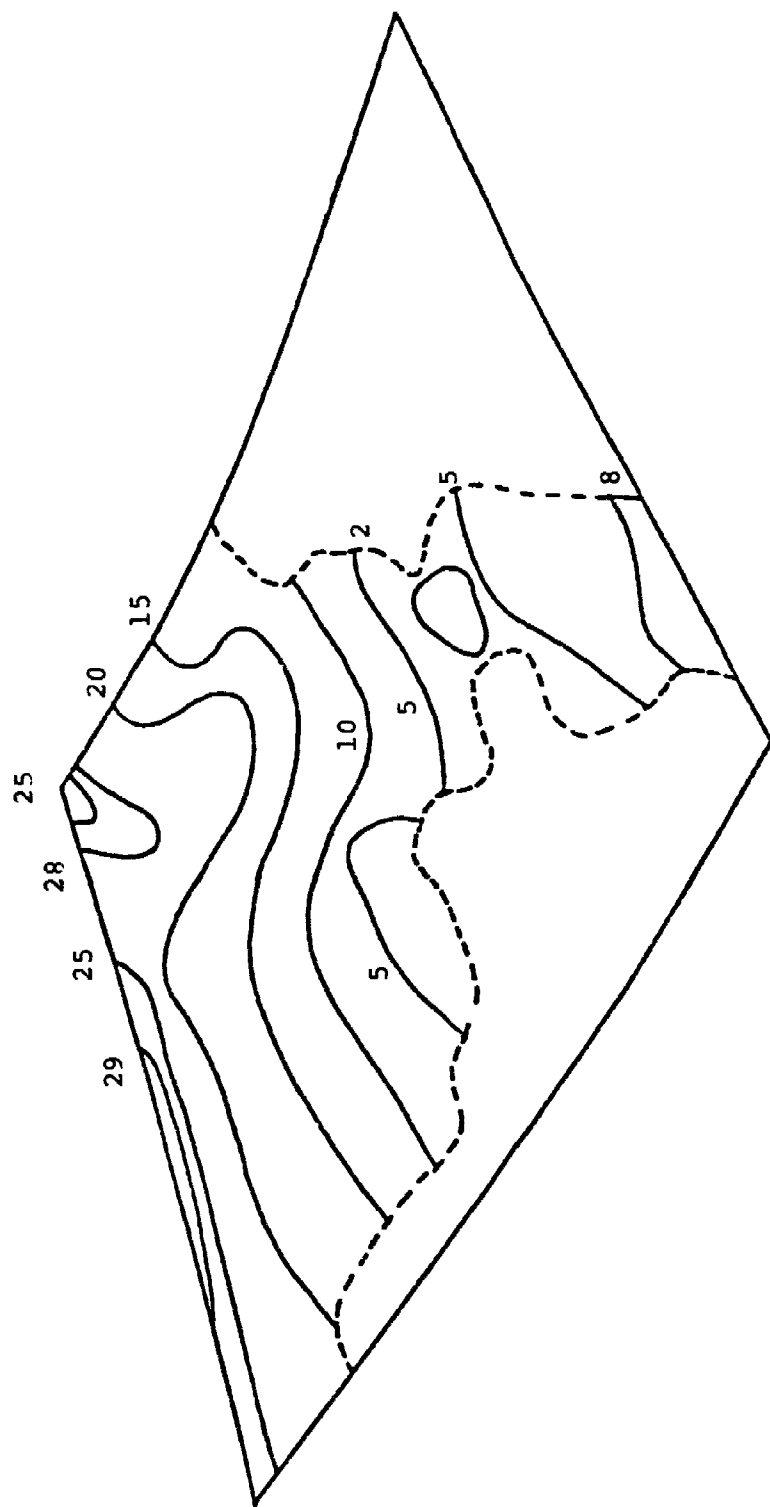
FIG. 16.   DISTRIBUTION OF THE PARTICLE IMPACTING ANGLE (DEGREES) ON THE
DESWIRLING VANES SUCTION SURFACE.
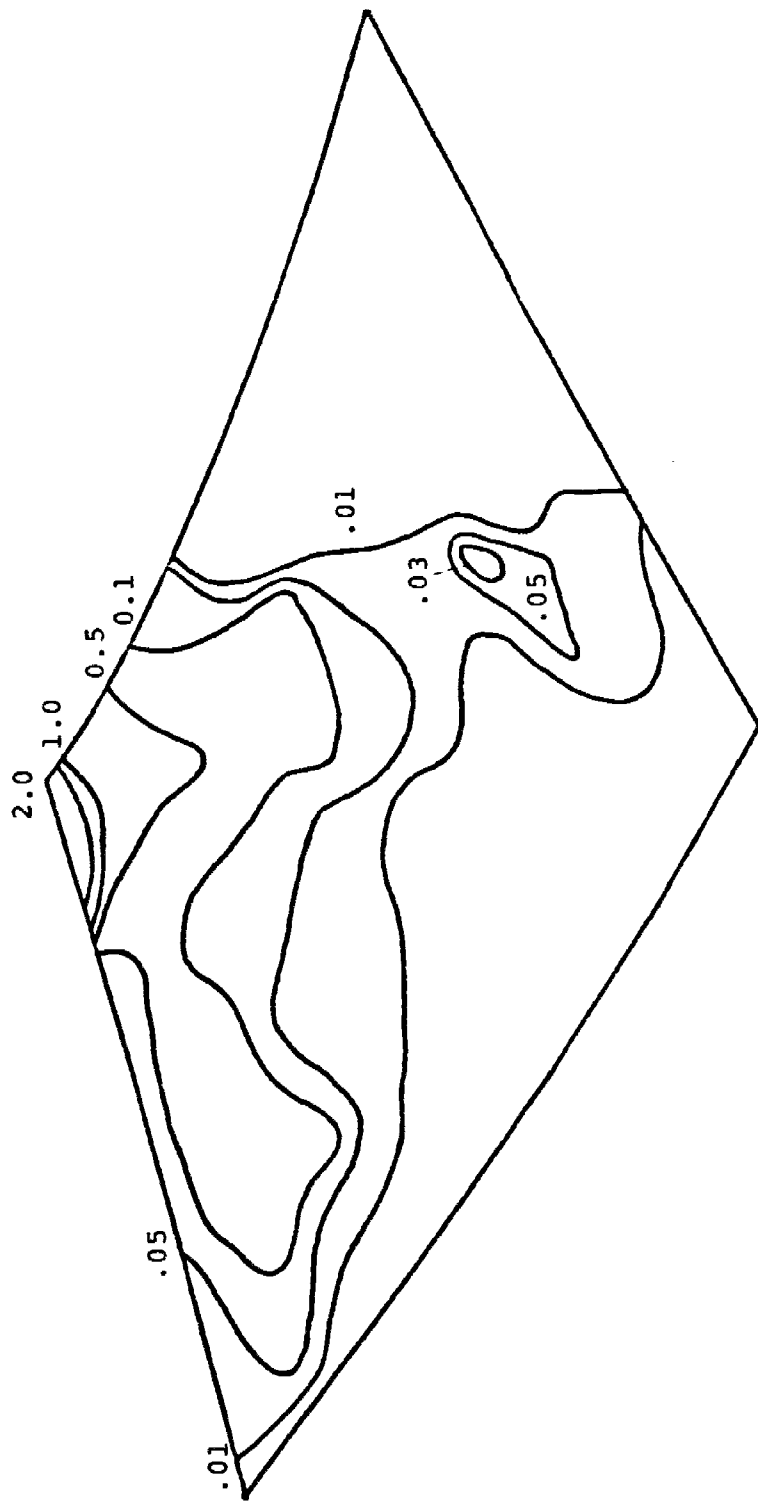
FIG. 17. DISTRIBUTION OF THE EROSION PARAMETER ON THE DESWIRLING VANE SUCTION SURFACE.

37
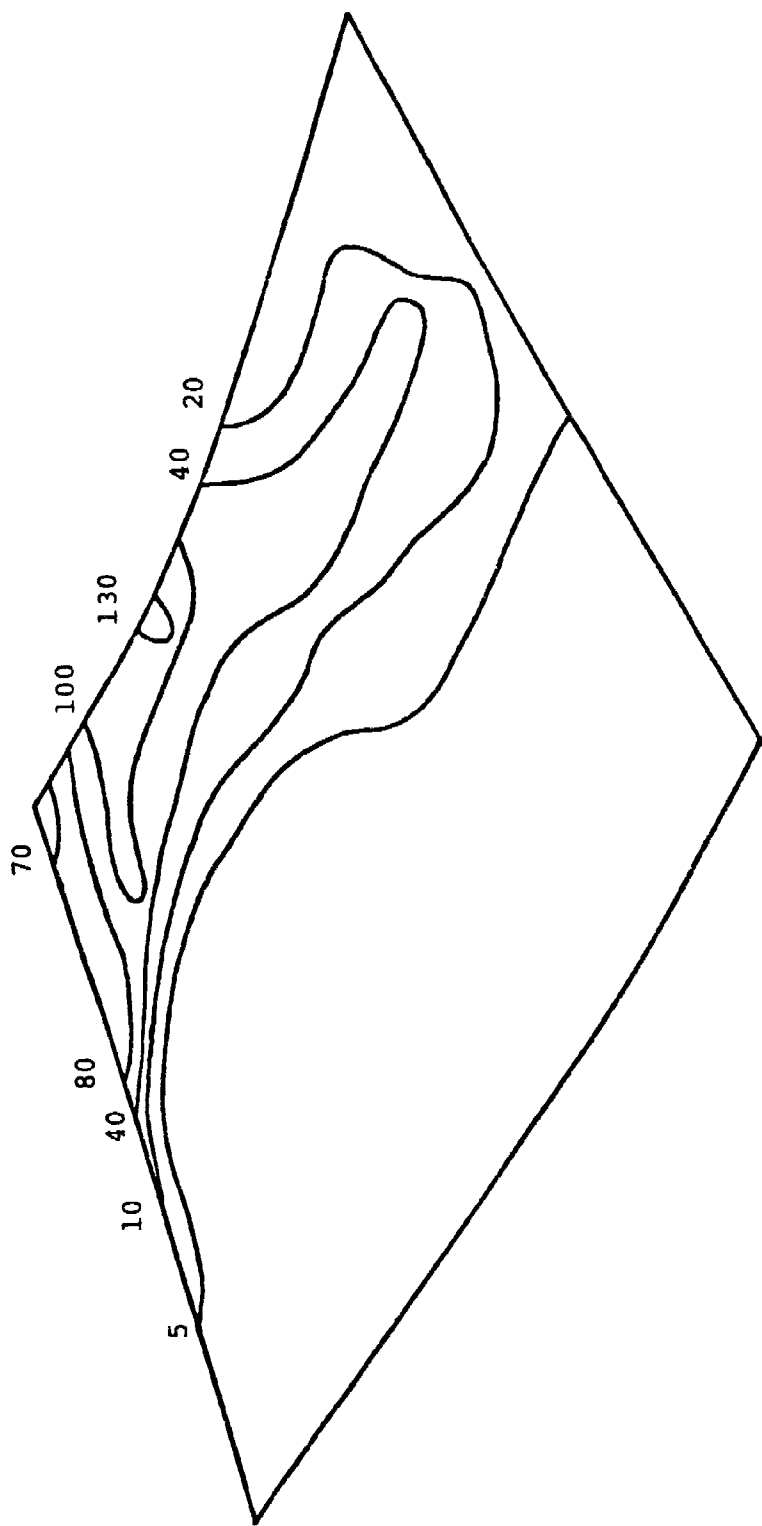
FIG. 18. DISTRIBUTION OF THE PARTICLE IMPACTING FREQUENCY ON THE DESWIRLING
VANE PRESSURE SURFACE.

38
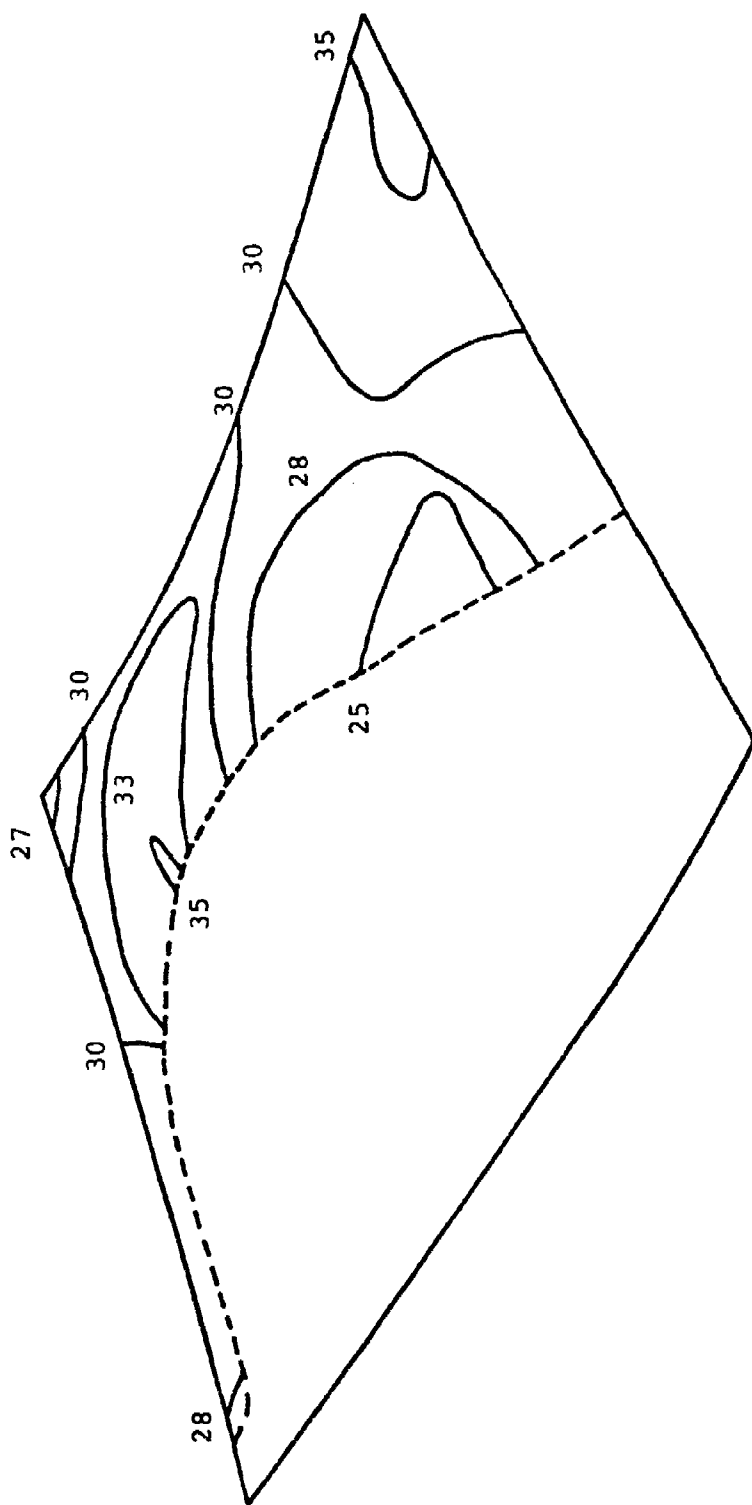
FIG. 19. DISTRIBUTION OF THE PARTICLE IMPACTING VELOCITY (M/S) ON THE DESWIRLING VANE PRESSURE SURFACE.

39
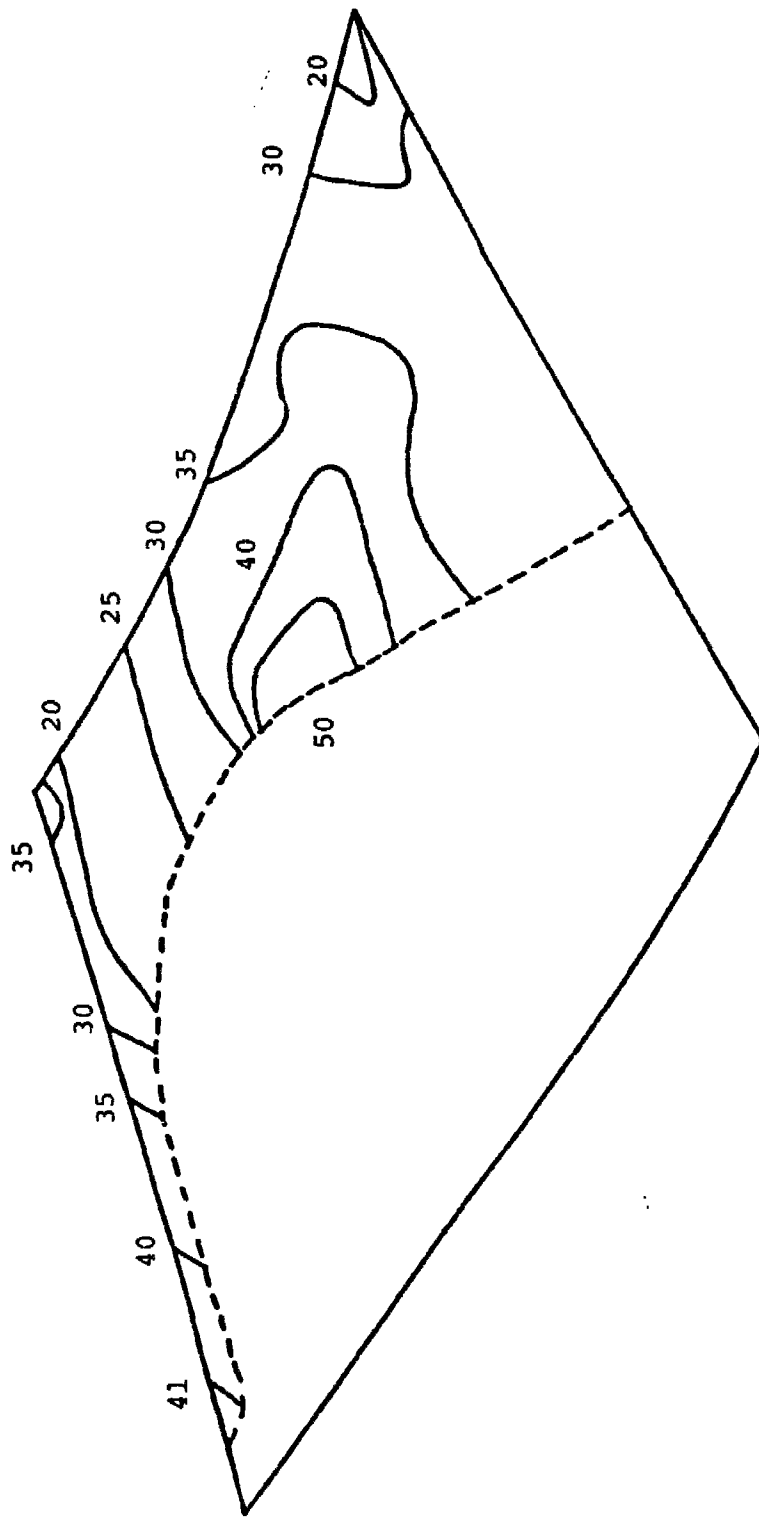
FIG. 20. DISTRIBUTION OF THE PARTICLE IMPACTING ANGLE (DEGREES) ON THE DESWIRLING VANES PRESSURE SURFACE.
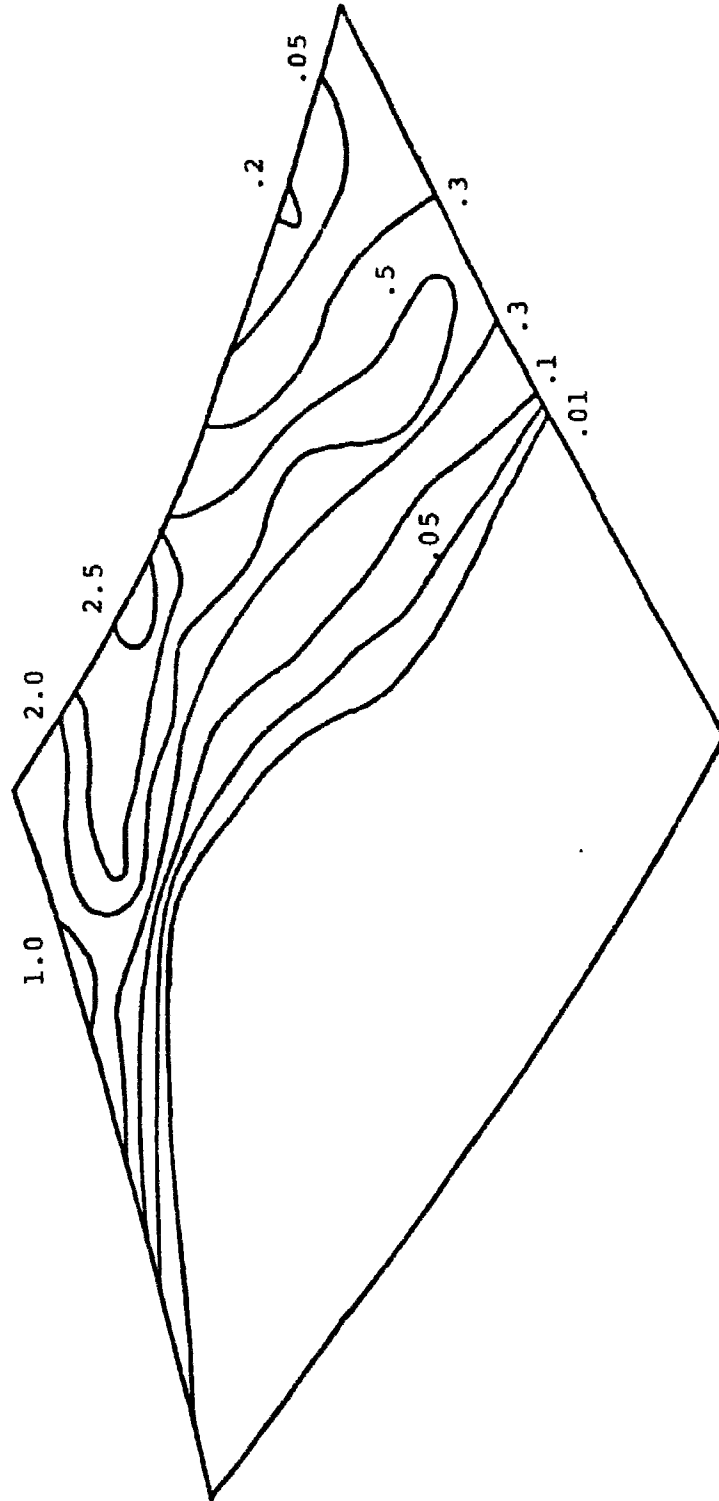
FIG. 21.. DISTRIBUTION OF THE EROSION PARAMETER ON THE DESWIRLING VANE PRESSURE SURFACE.

41

Tip

In ⟹

Out ⟹

Hub
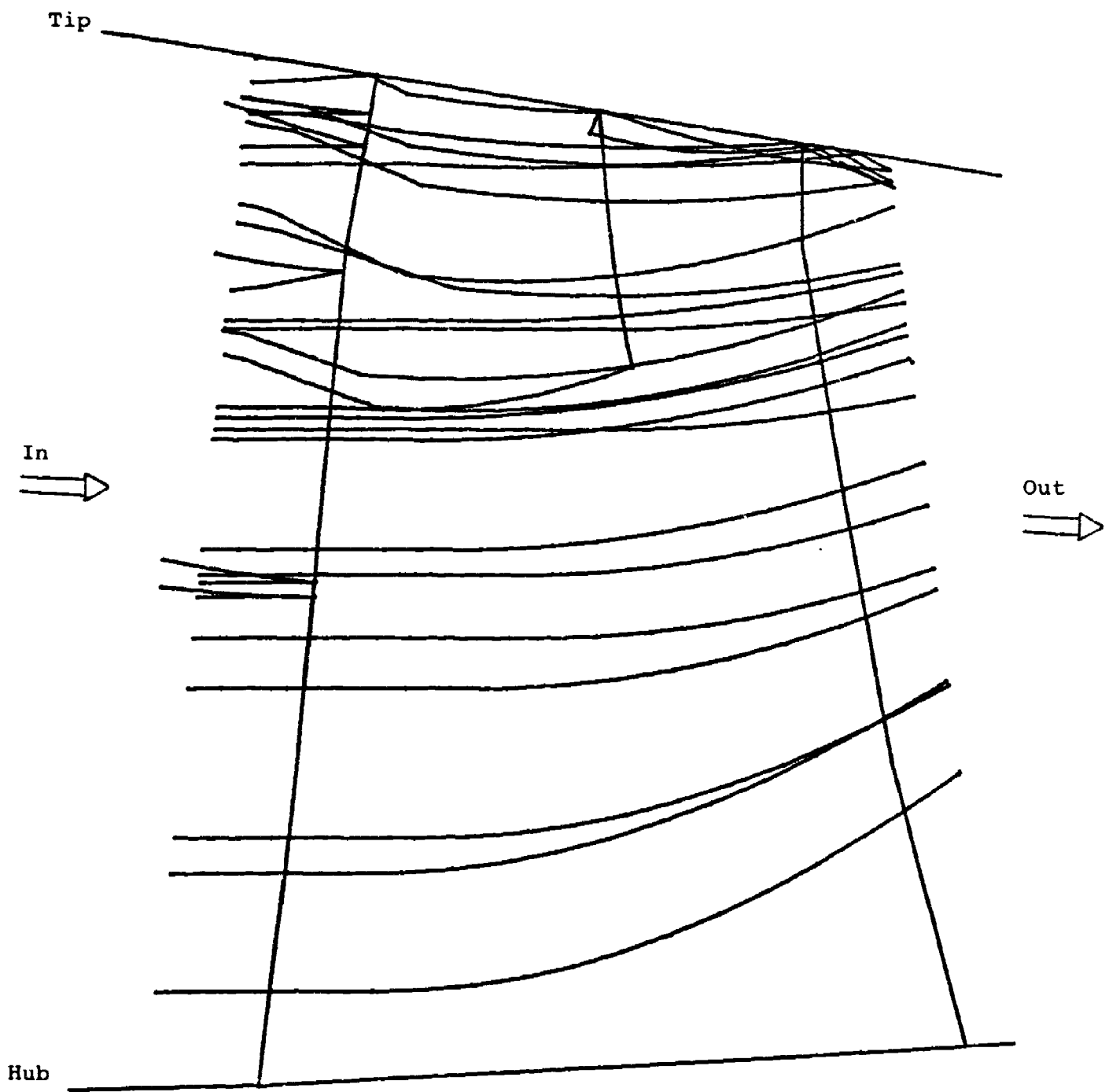
FIG. 22. HUB-TO-TIP PARTICLE TRAJECTORIES THROUGH THE FIRST ROTOR.
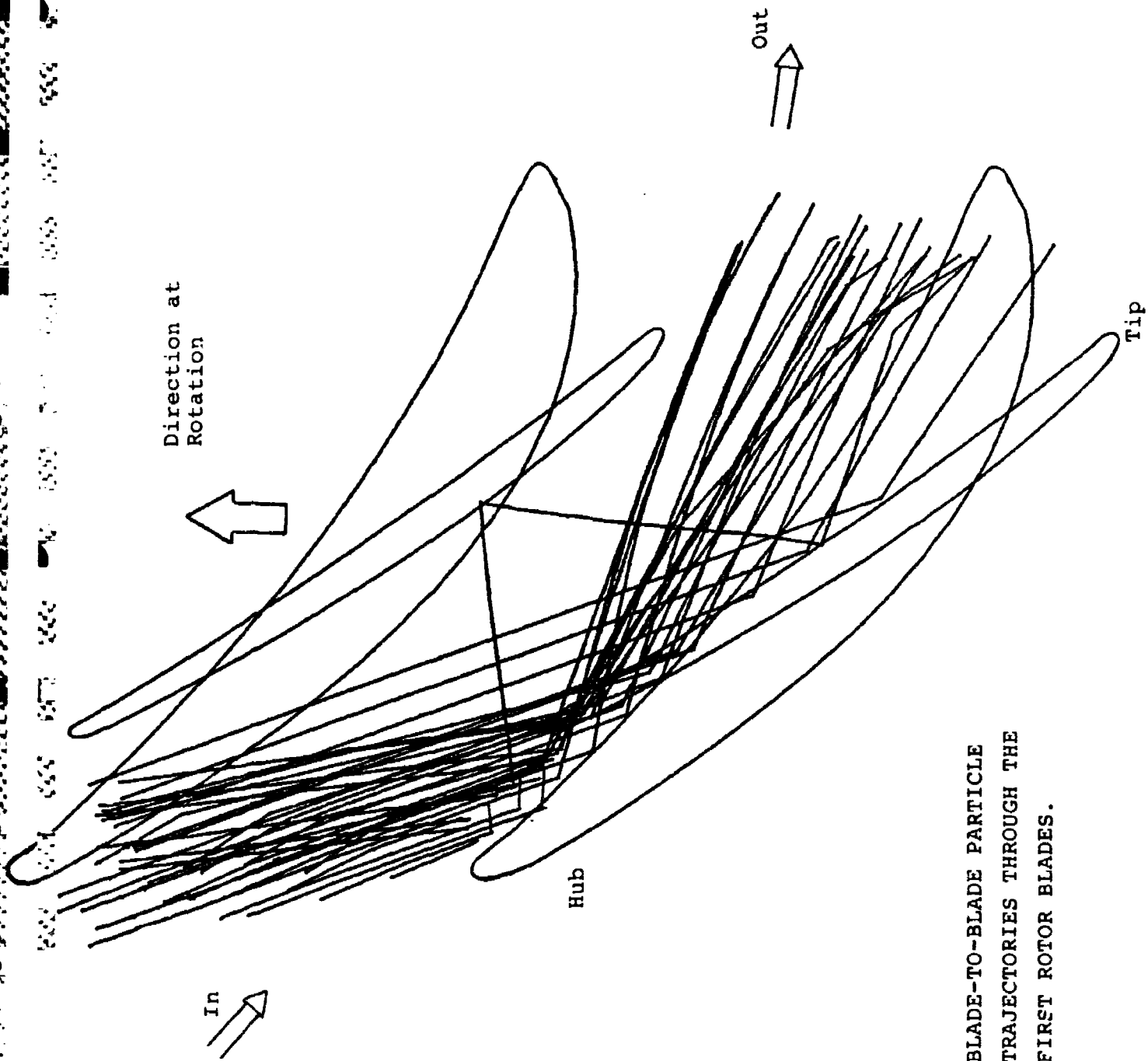
FIG. 23. BLADE-TO-BLADE PARTICLE TRAJECTORIES THROUGH THE FIRST ROTOR BLADES.
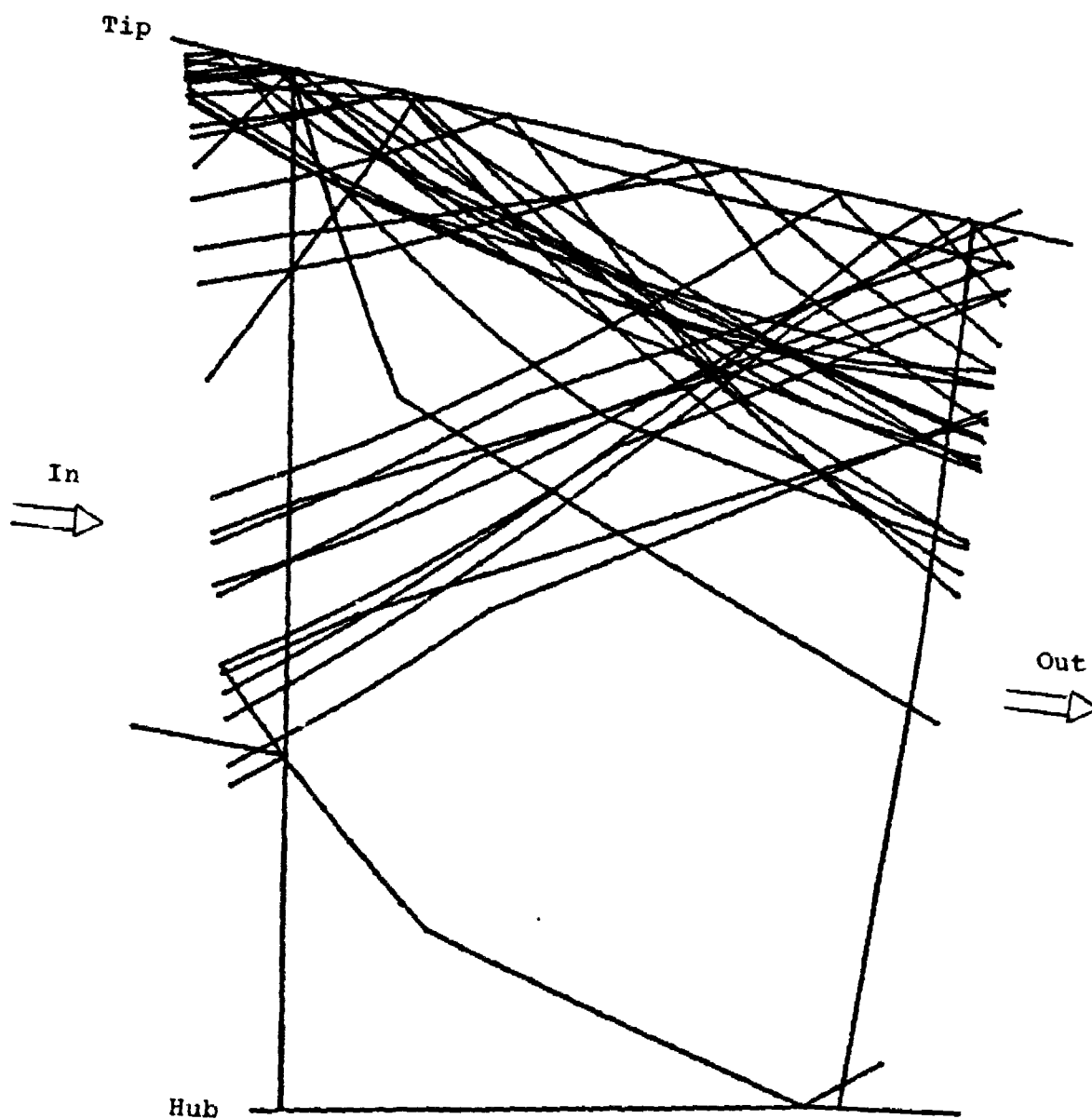
FIG. 24.   HUB-TO-TIP PARTICLE TRAJECTORIES THROUGH
THE FIRST STATOR.
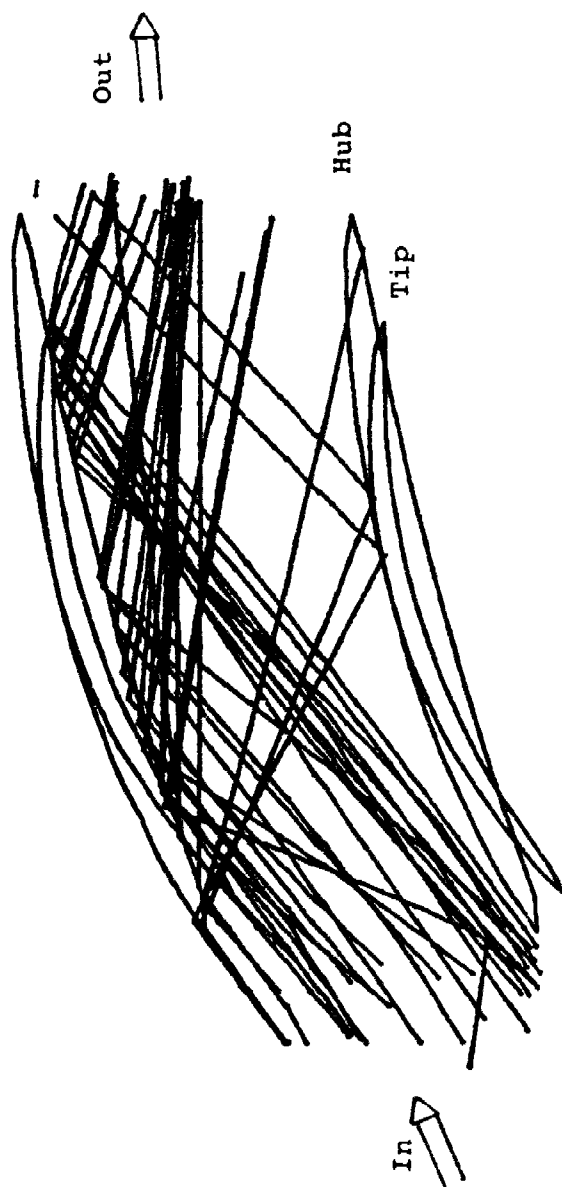
FIG. 25. BLADE-TO-BLADE PARTICLE TRAJECTORIES THROUGH
THE FIRST STATOR BLADES.
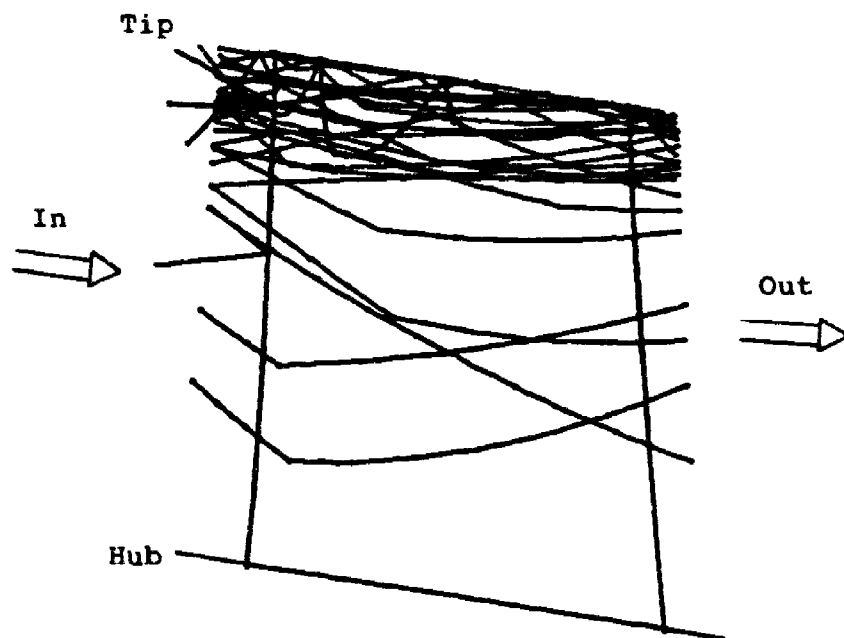
FIG. 26. HUB-TO-TIP PARTICLE TRAJECTORIES
THROUGH THE FIFTH ROTOR.
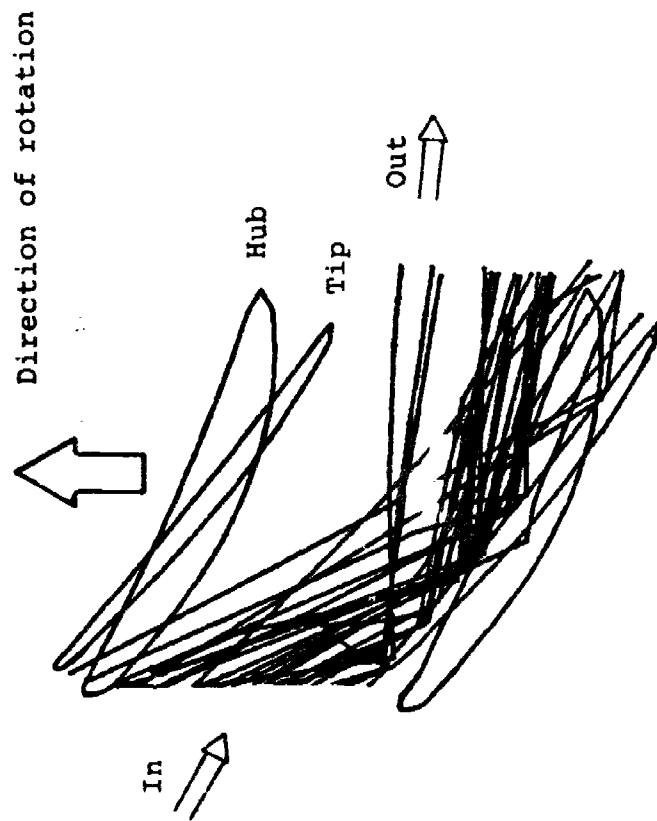
FIG. 27. BLADE-TO-BLADE PARTICLE TRAJECTORIES
THROUGH THE FIFTH ROTOR BLADES.

47
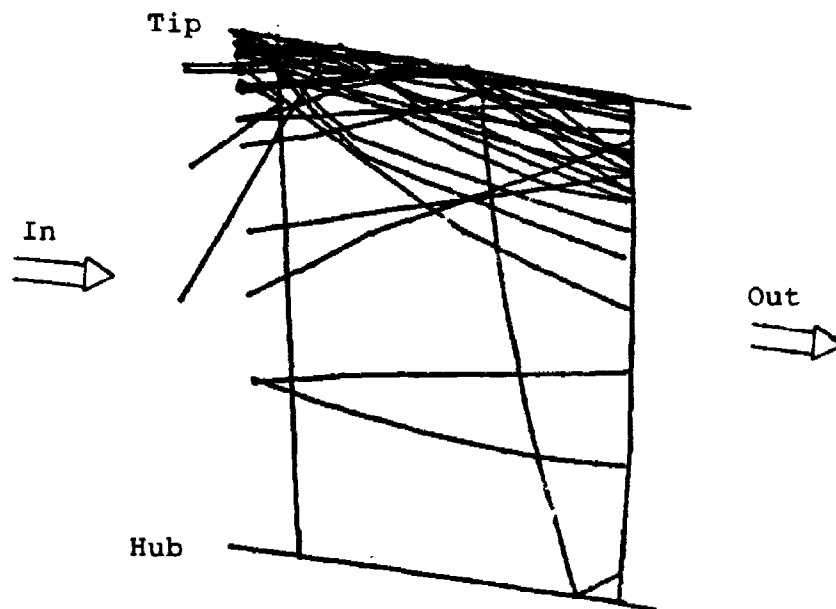
FIG. 28. HUB-TO-TIP PARTICLE TRAJECTORIES
THROUGH THE FIFTH STATOR.

48
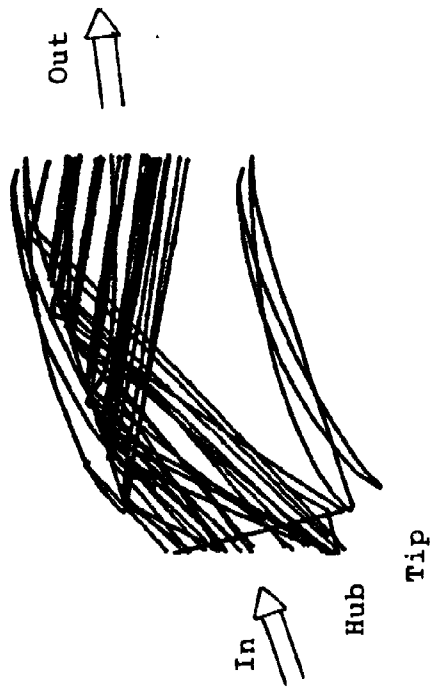
FIG. 29. BLADE-TO-BLADE PARTICLE TRAJECTORIES
THROUGH THE FIFTH STATOR BLADES.

49

$V = m/sec.$

β

(a)

Average Particle Impact Velocity

(b)

Average Particle Impingement Angle

FIG. 30. FIRST ROTOR

50

50

ε

Blade Erosion Parameter

(d)

400

300

200

150

100

50

10

1

Particle Impact Frequency

(c)

1

10

25

50

100

γ

FIG. 30. (CONT'D) FIRST ROTOR

β

20°

25°

30°

35°

40°

Average Particle Impingement Angle

(b)

v = m/sec.

100

200

250

260

100

100

Average Particle Impact Velocity

(a)
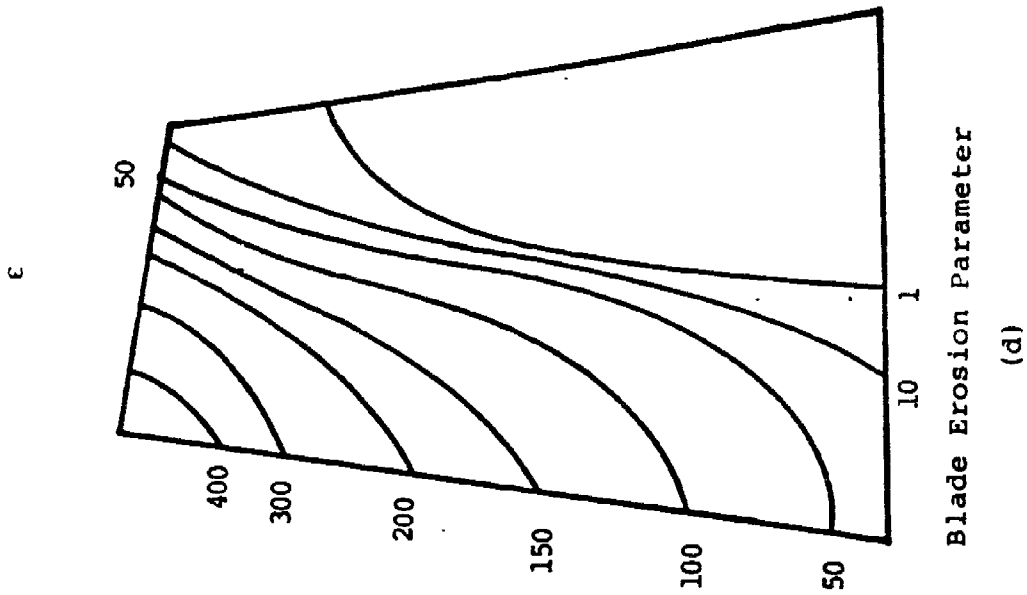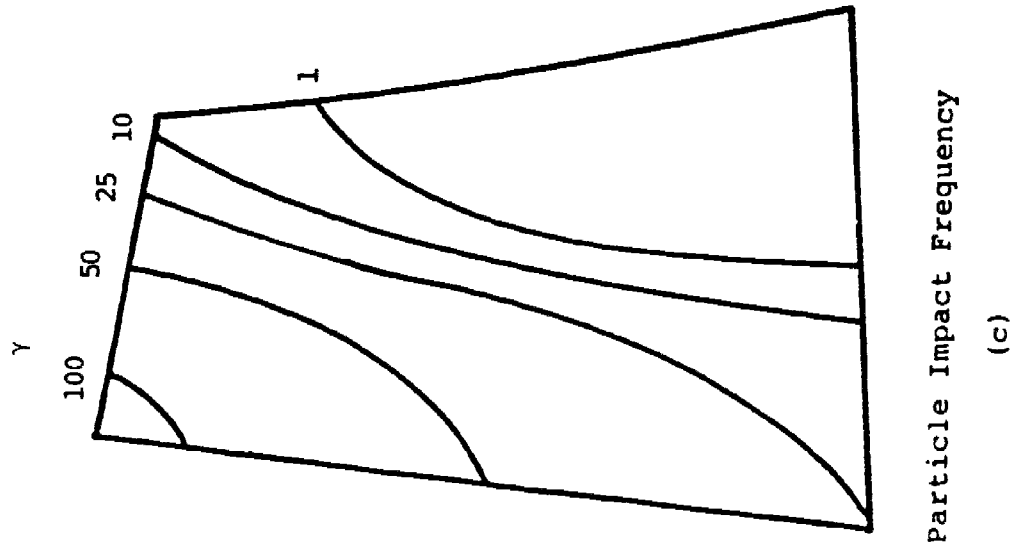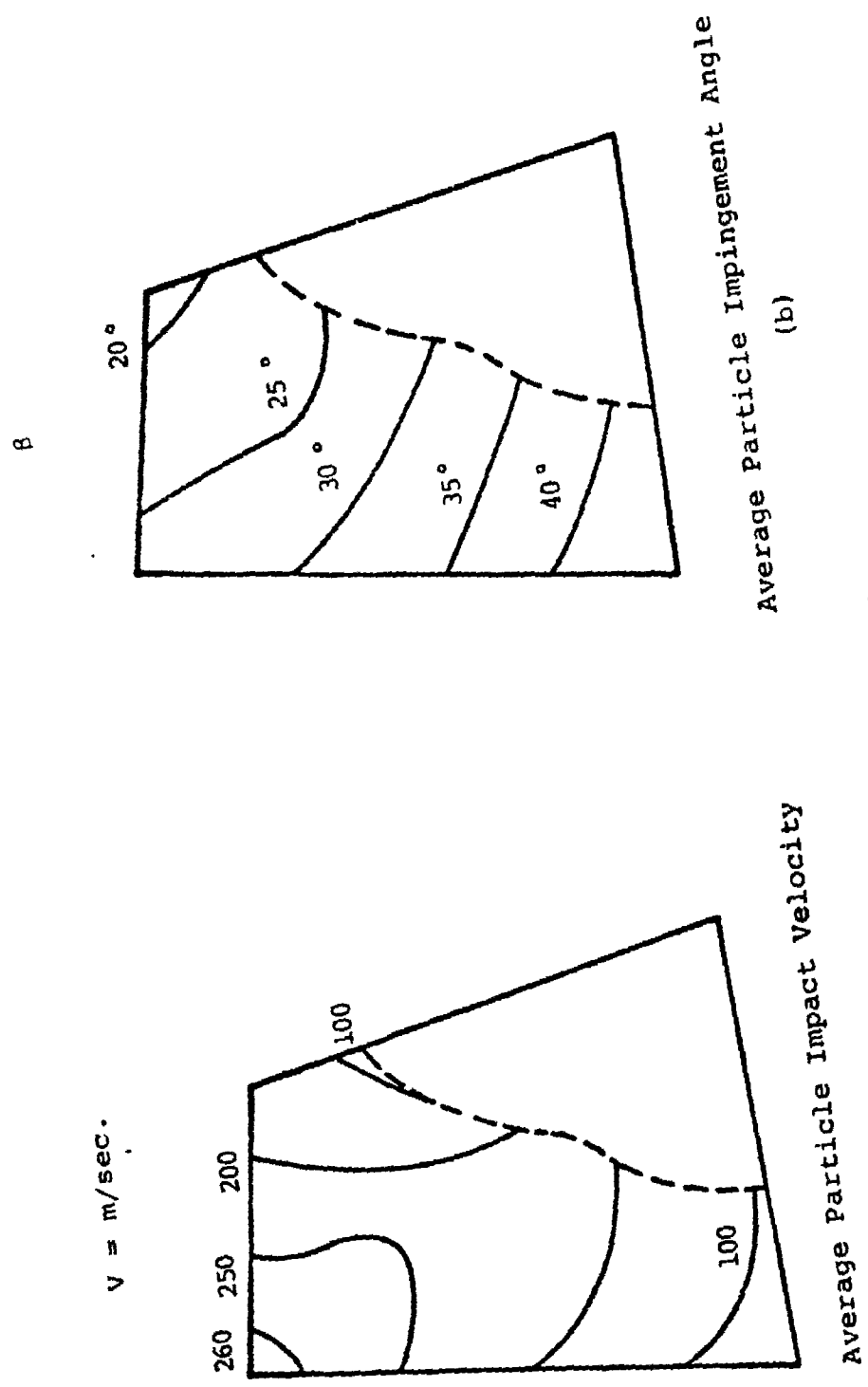
FIG. 31. SECOND ROTOR

Blade Erosion Parameter

(d)

Particle Impact Frequency

(c)
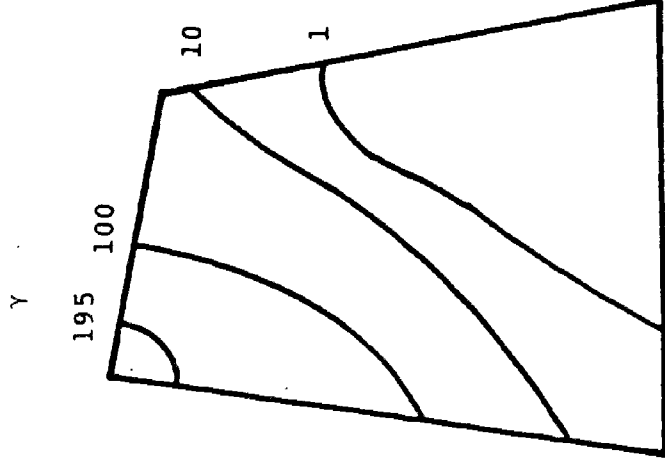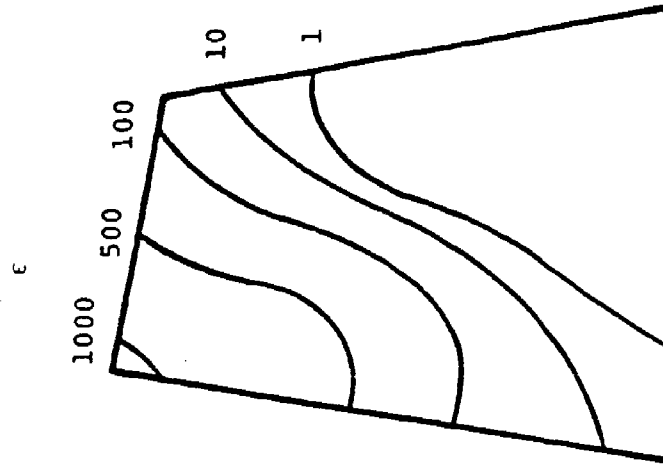
FIG. 31. (CONT'D) SECOND ROTOR

53

V = m/sec.

Average Particle Impact Velocity

(a)

β
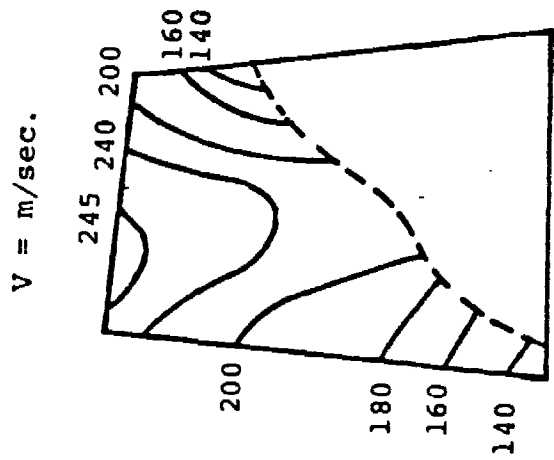
Average Particle Impingement Angle

(b)

FIG. 32. THIRD ROTOR

54

ε

900 500 100

10

Blade Erosion Parameter

(d)

γ

200 100

10

Particle Impact Frequency

(c)
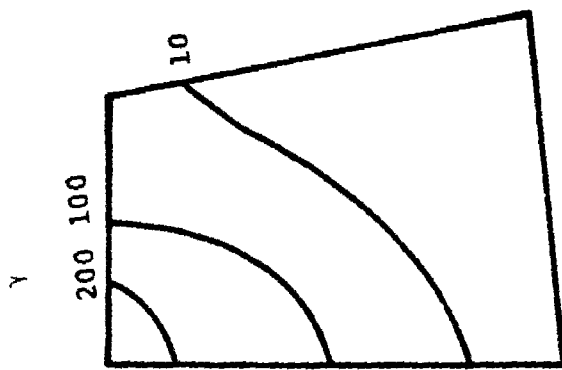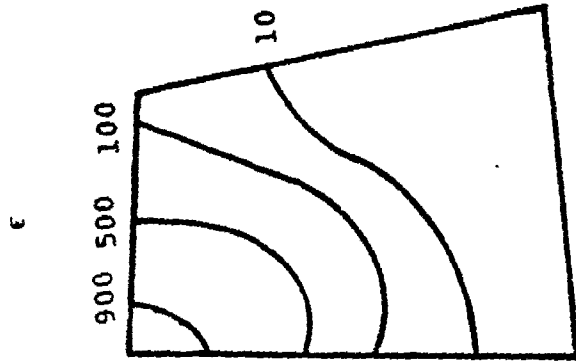
FIG. 32. (CONT'D) THIRD ROTOR

FIG. 33. FOURTH ROTOR

Average Particle Impact Velocity
(a)

Average Particle Impingement Angle
(b)

Particle Impact Frequency
(c)

Blade Erosion Parameter
(d)

56

V = m/sec.

Average Particle Impact Velocity

(a)

Average Particle Impingement Angle

(b)

Particle Impact Frequency

(c)
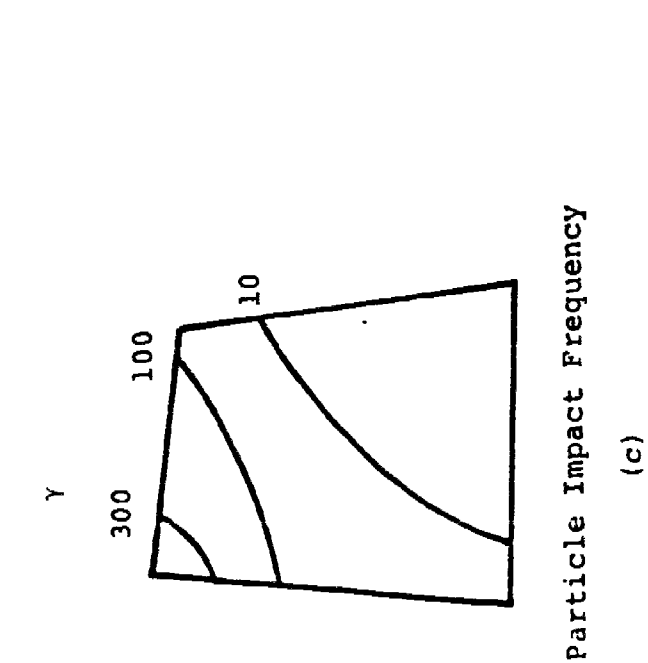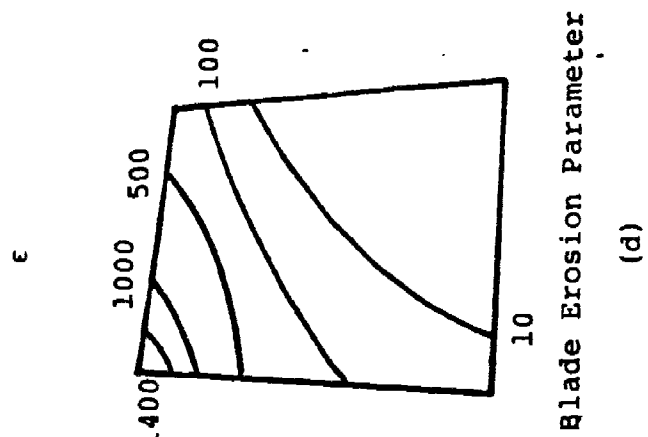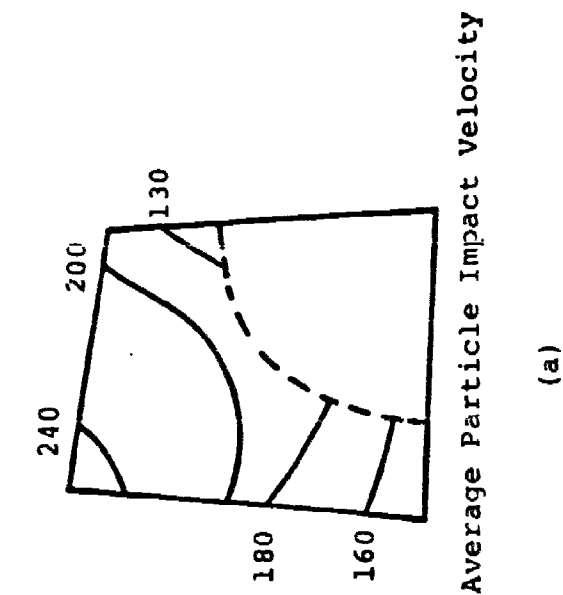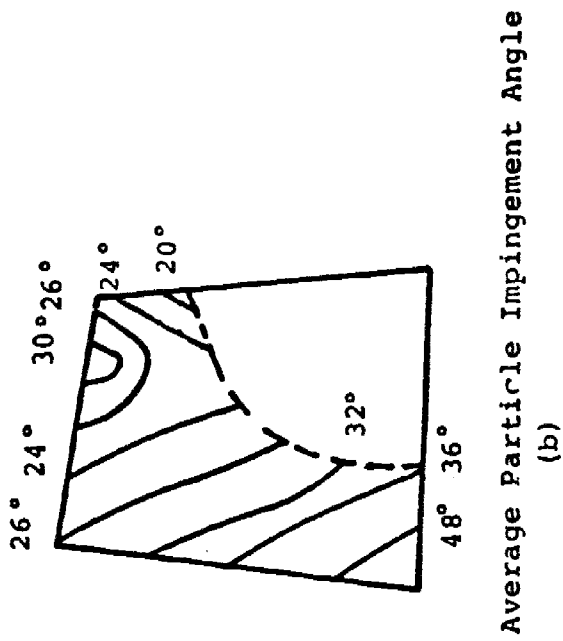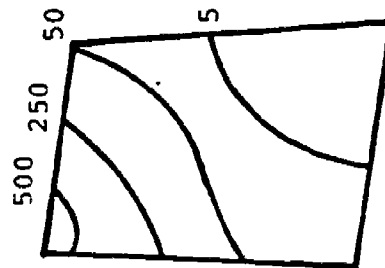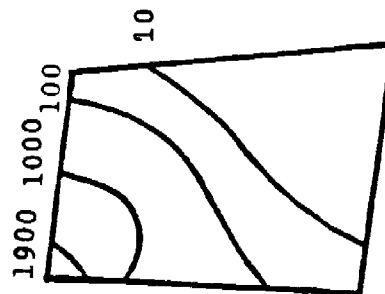
Blade Erosion Parameter

(d)

FIG. 34. FIFTH ROTOR
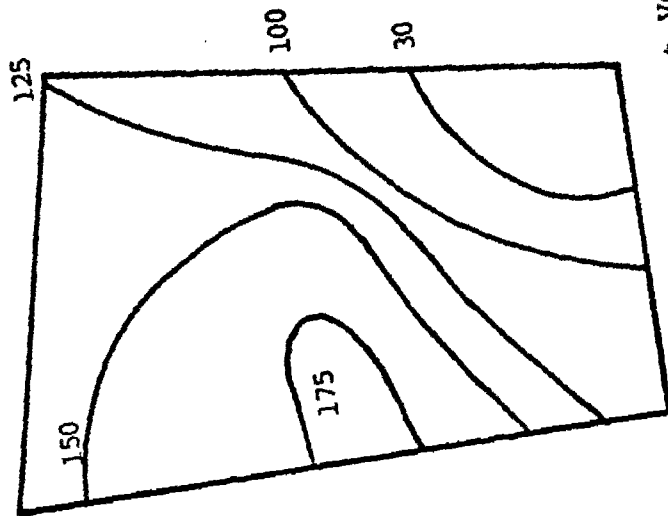
57

β

30°

30°

20°

30°

40°

50°

Average Particle Impingement Angle

(b)

v = m/sec.

125

100

30

150

175

Average Particle Impact Velocity

(a)
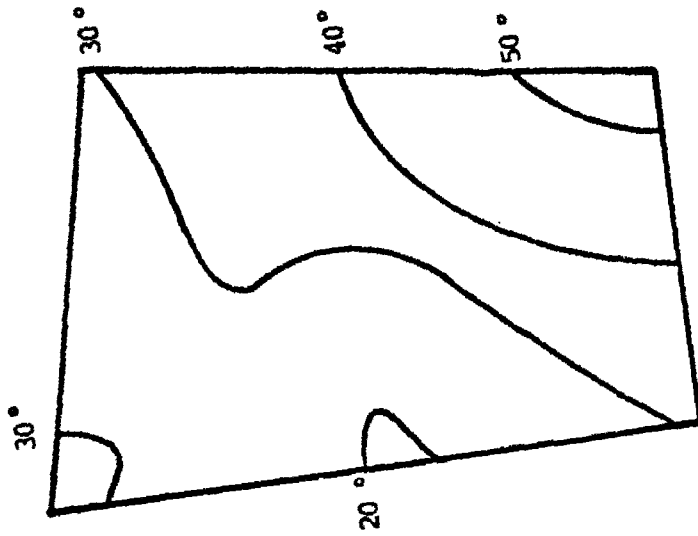
FIG. 35. FIRST STATOR

58

Blade Erosion Parameter

(d)

Particle Impact Frequency

(c)
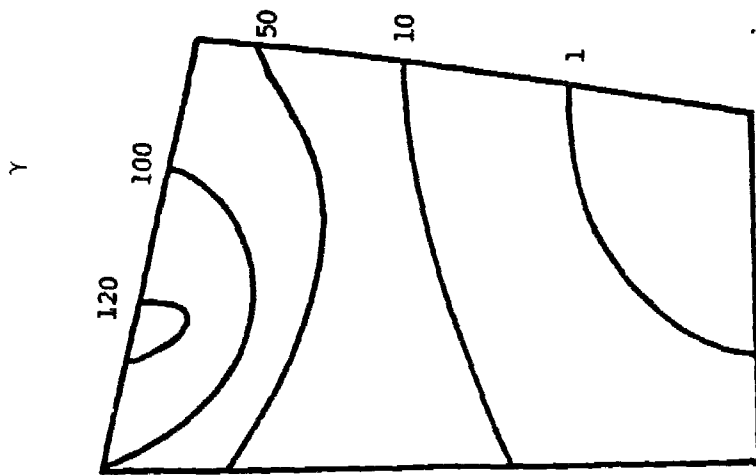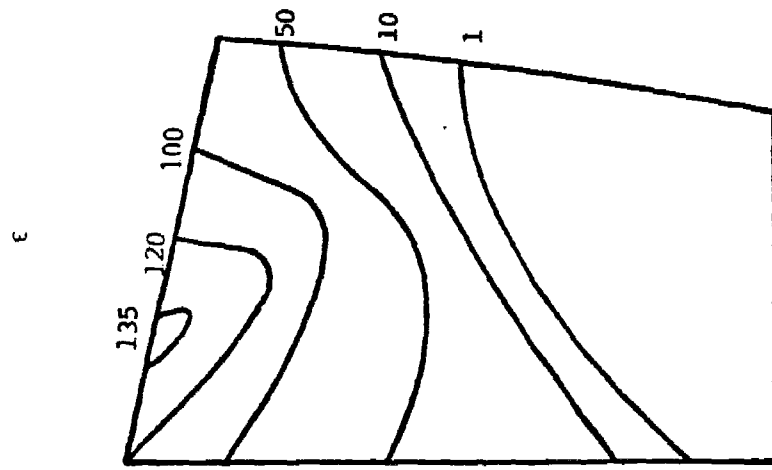
FIG. 35. (CONT'D) FIRST STATOR

V = m/sec.

125 ⟍ 150

200

50

(a)

Average Particle Impact Velocity

.β

32°

35°
40°

42°

(b)
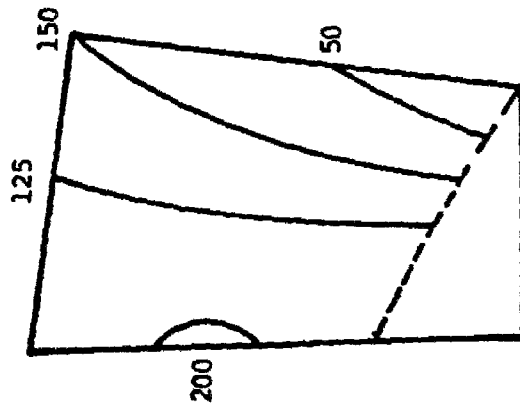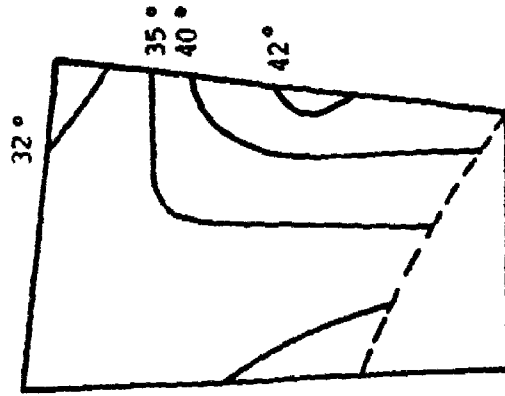
Average Particle Impingement Angle

FIG. 36 . SECOND STATOR

60

ε

Blade Erosion Parameter

(d)

γ

Particle Impact Frequency

(c)
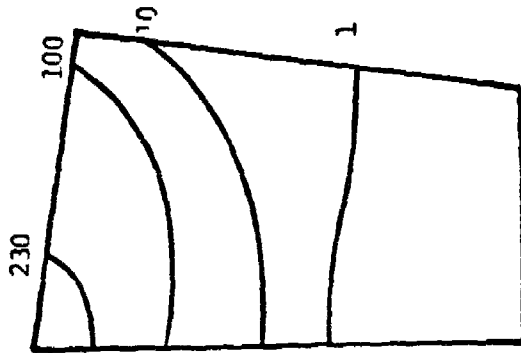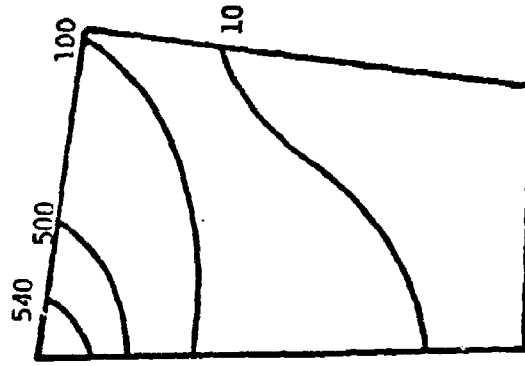
FIG. 36. (CON'T) SECOND STATOR
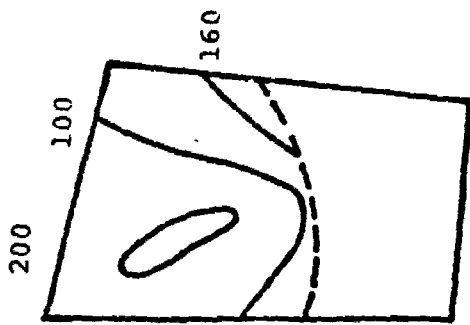
Average Particle Impact Velocity
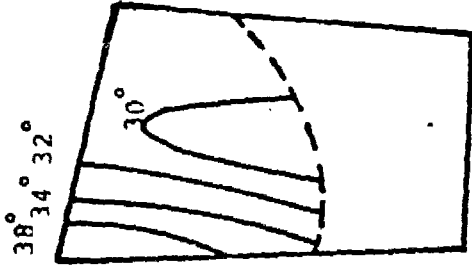
(a)

Average Particle Impingement Angle

(b)

Particle Impact Frequency

(c)
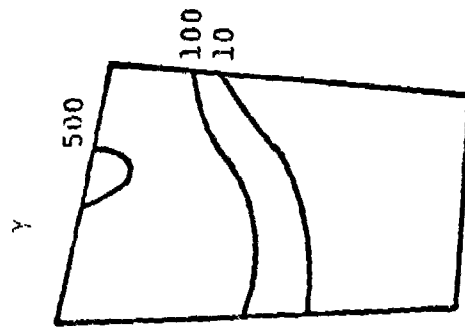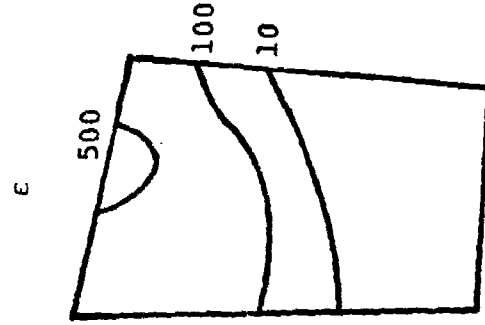
Blade Erosion Parameter

(d)

FIG. 37. THIRD STATOR
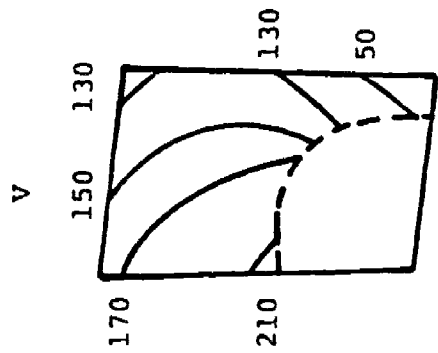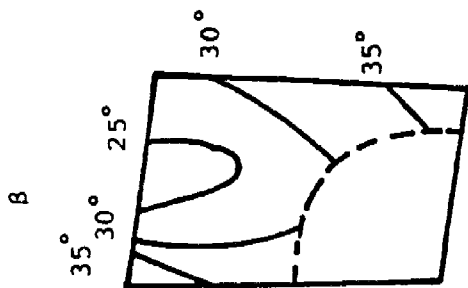
62

β

35° 30° 35° 30° 25° 30°

Average Particle Impingement Angle

(b)

ϵ

800 500 100 10

Blade Erosion Parameter

(d)

V

150 130 130 170 210 50

Average Particle Impact Velocity

(a)

$\dot{\gamma}$

500 100 10

Particle Impact Frequency

(c)
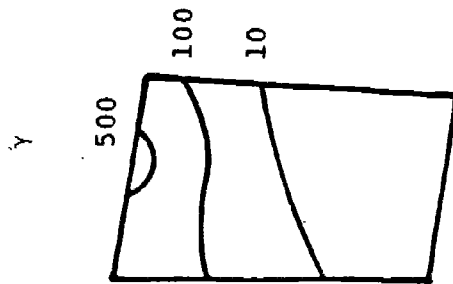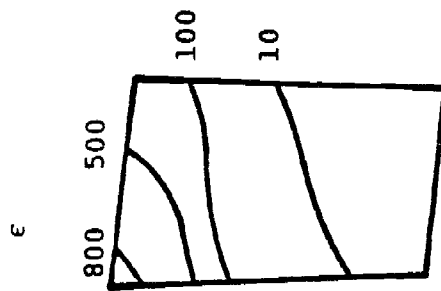
FIG. 38. FOURTH STATOR

V = m/sec.
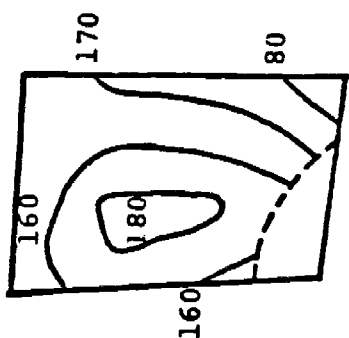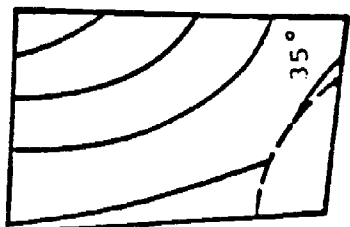
170

180

160

160

80

Average Particle Impact Velocity

(a)

γ

β

35° 30° 25° 20°

35°

Average Particle Impingement Angle

(b)

ε

100

50

10

400

Particle Impact Frequency

(c)

100

10

600
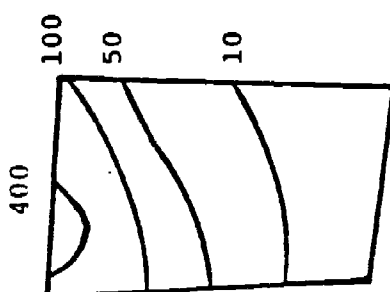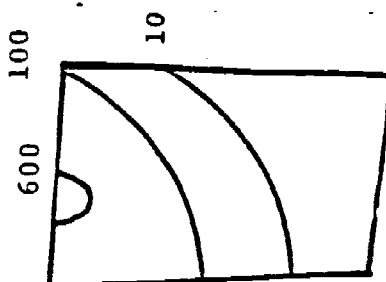
Blade Erosion Parameter

(d)

FIG. 39. FIFTH STATOR

64
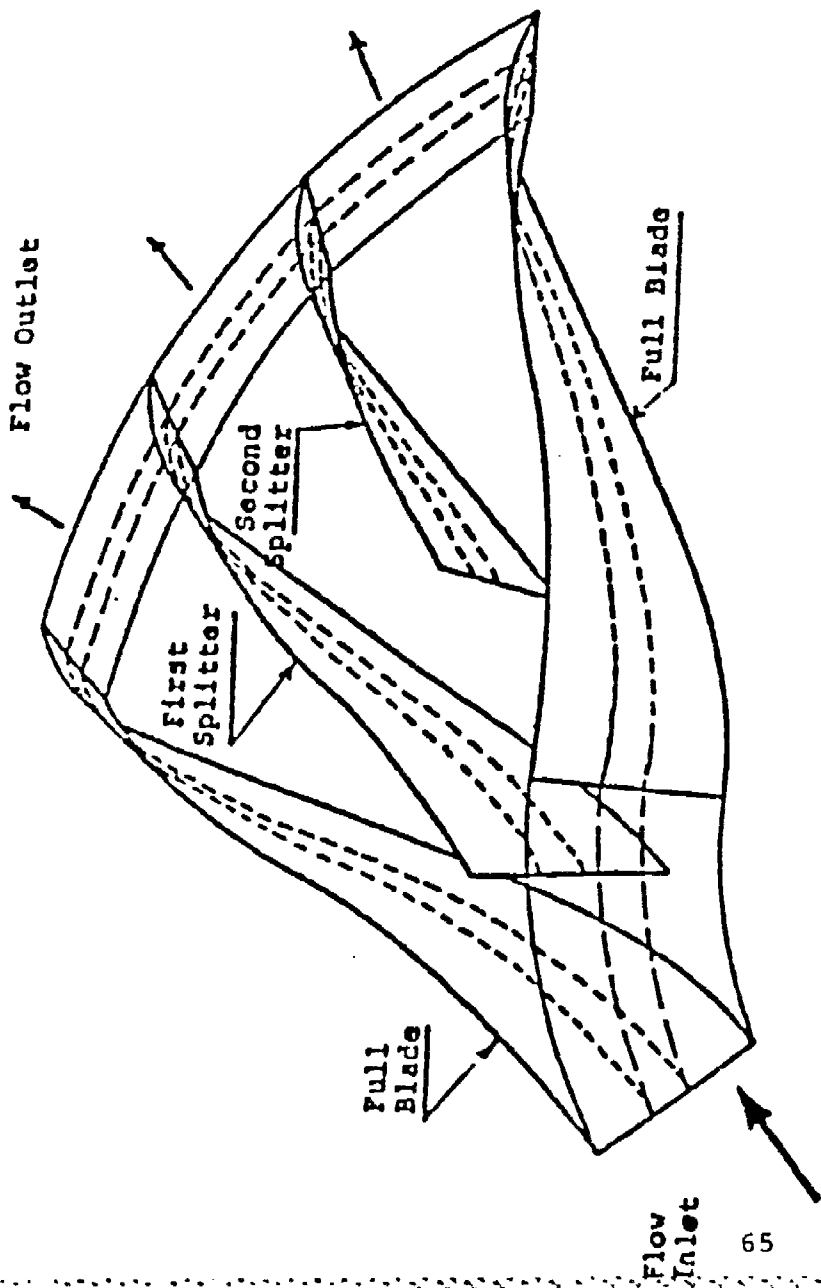
FIG. 40a. SCHEME OF IMPELLER SECTOR WITH TWO
DIFFERENT SIZE SPLITTERS.
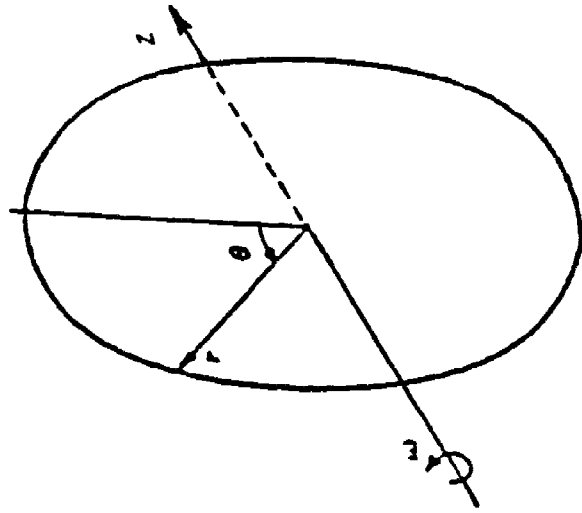
FIG. 40b. THE COORDINATE SYSTEM
(r, θ, z) USED IN
CALCULATION.

65

direction of
rotation

blade suction
surface

first splitter

second splitter

blade pressure
surface

a)

b)
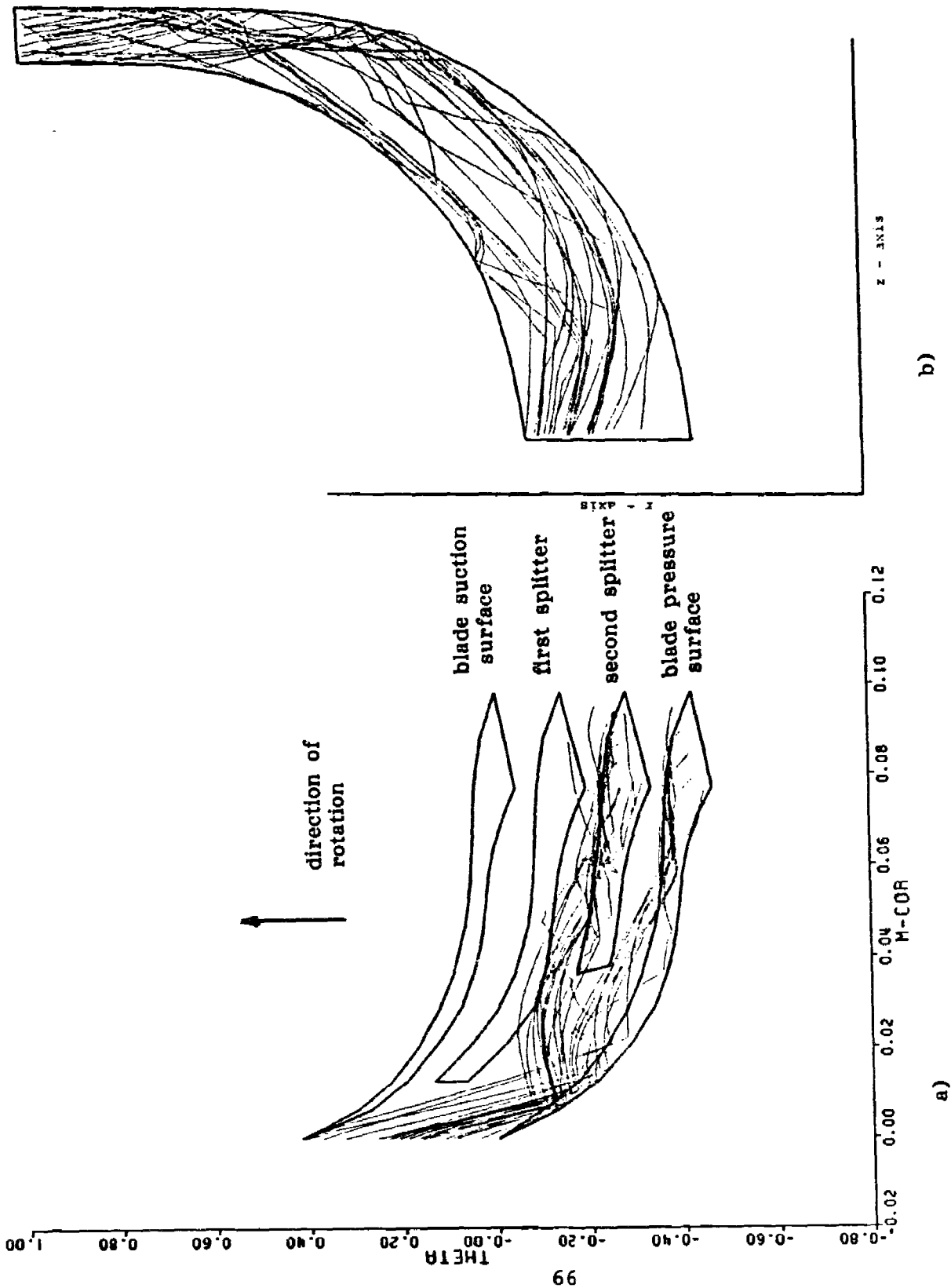
FIG. 41. PARTICLE TRAJECTORY VIEWS IN THE a) M-θ and b) r - Z PLANES, THROUGH THE
RADIAL COMPRESSOR IMPELLER.

T.E.

hub

shroud

L.E.

a) first splitter
   suction surface

b) second splitter
   pressure surface

c) Impeller blade
   pressure surface
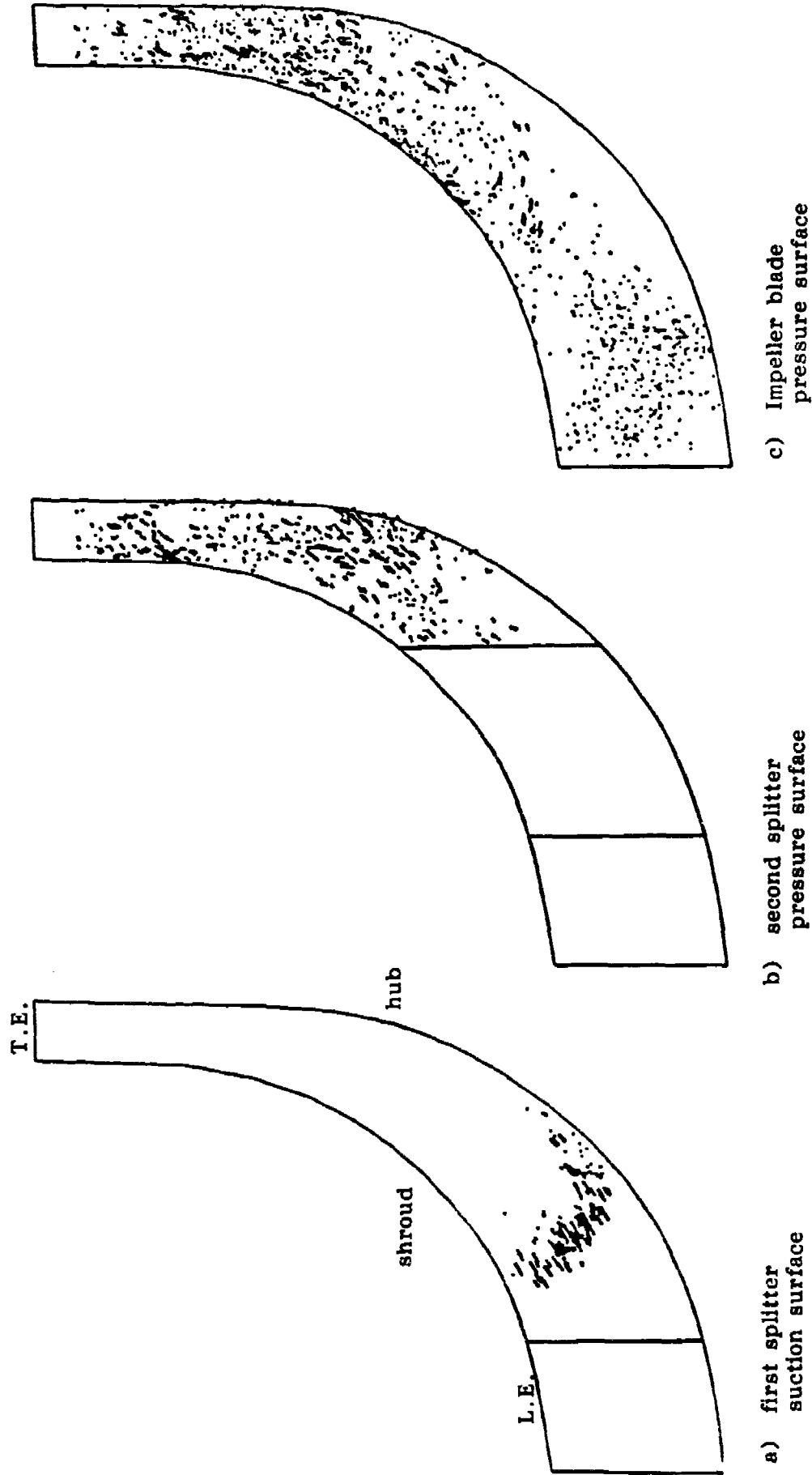
FIG. 42. DISTRIBUTION OF THE PARTICLE IMPACT LOCATIONS ON THE SPLITTERS AND THE
BLADE SURFACES THAT MOST SUBJECTED TO PARTICLE IMPACTS.
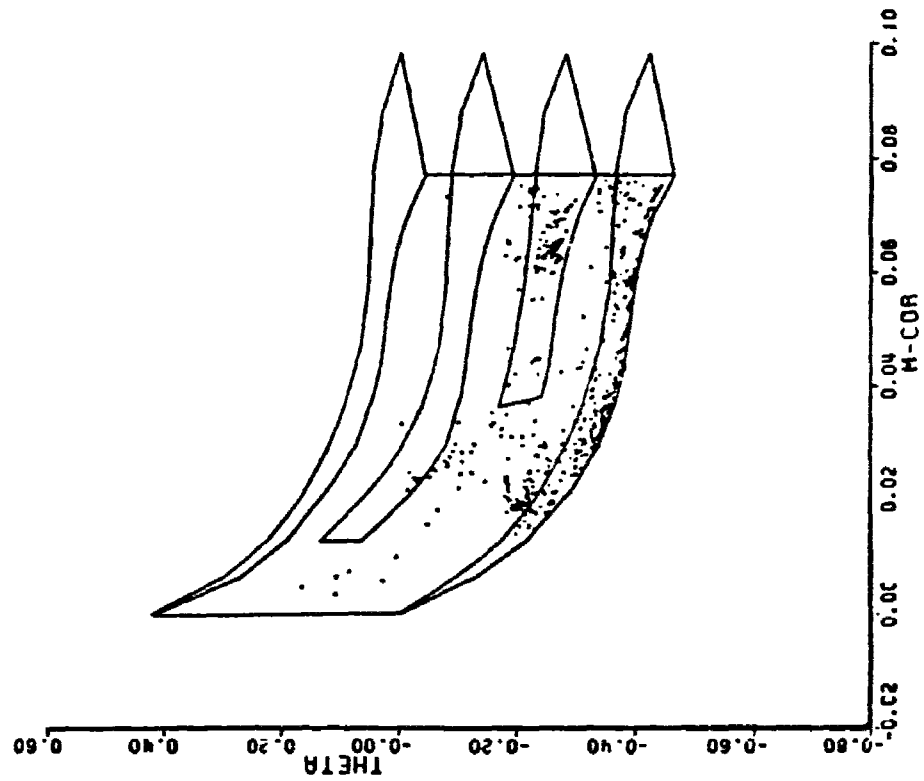
impeller hub
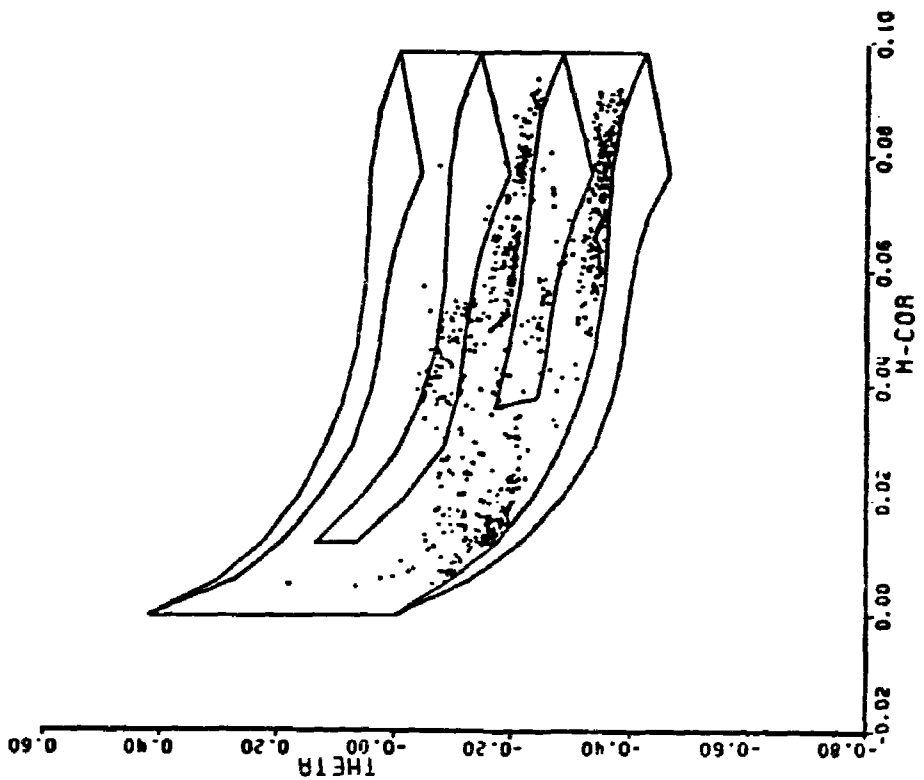
impeller casing

FIG. 43. DISTRIBUTION OF PARTICLE IMPACT LOCATIONS ON THE HUB AND THE CASING SURFACES OF THE RADIAL IMPELLER.
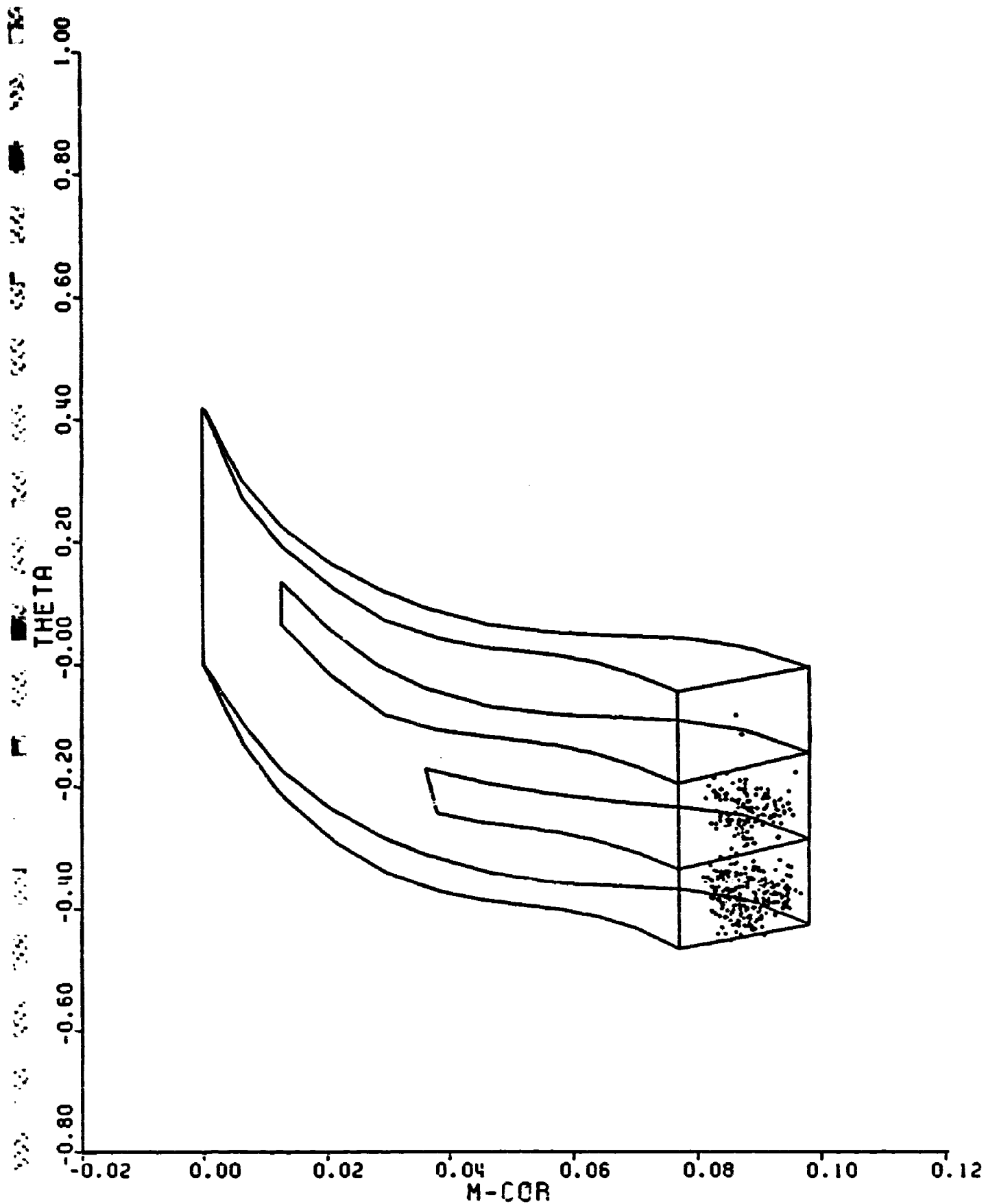
FIG. 44. PARTICLE LOCATIONS AT THE RADIAL IMPELLER EXIT.
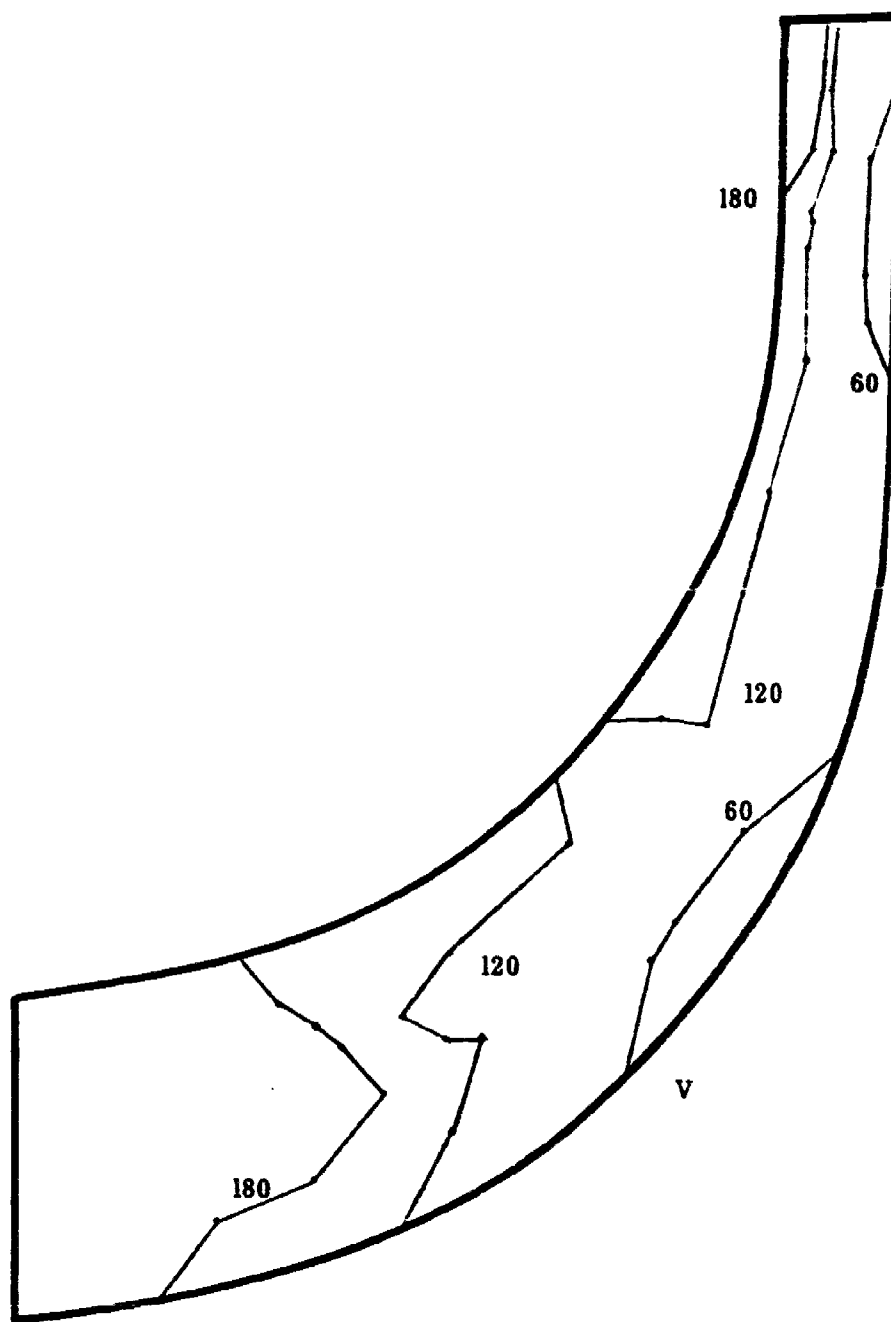
FIG. 45. DISTRIBUTION OF THE PARTICLE IMPACTING VELOCITY ON
THE PRESSURE SURFACE OF THE RADIAL IMPELLER BLADE (m/s)
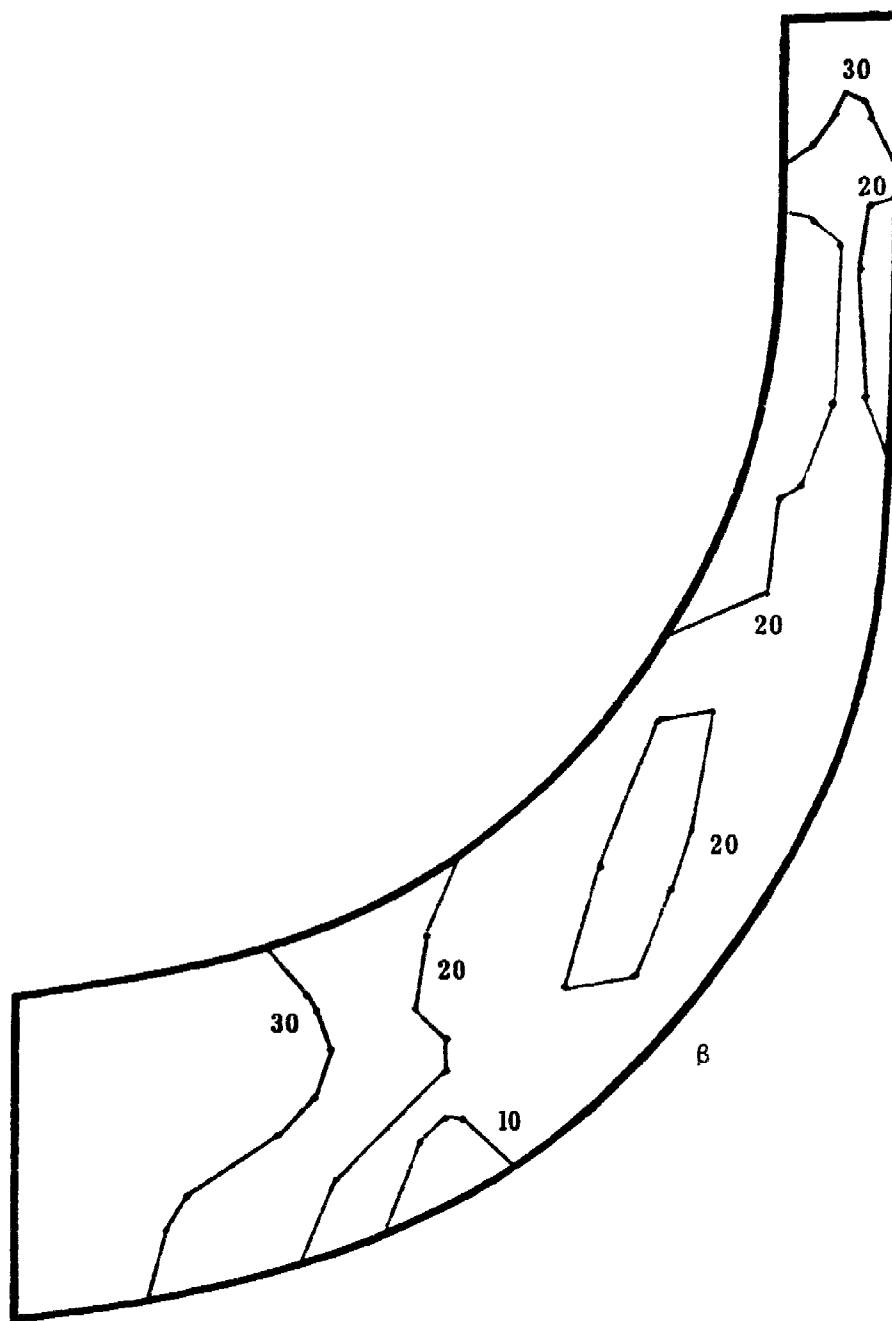
FIG. 46. DISTRIBUTION OF THE PARTICLE IMPACTING ANGLES ON
THE PRESSURE SIDE OF THE RADIAL IMPELLER (DEGREES)
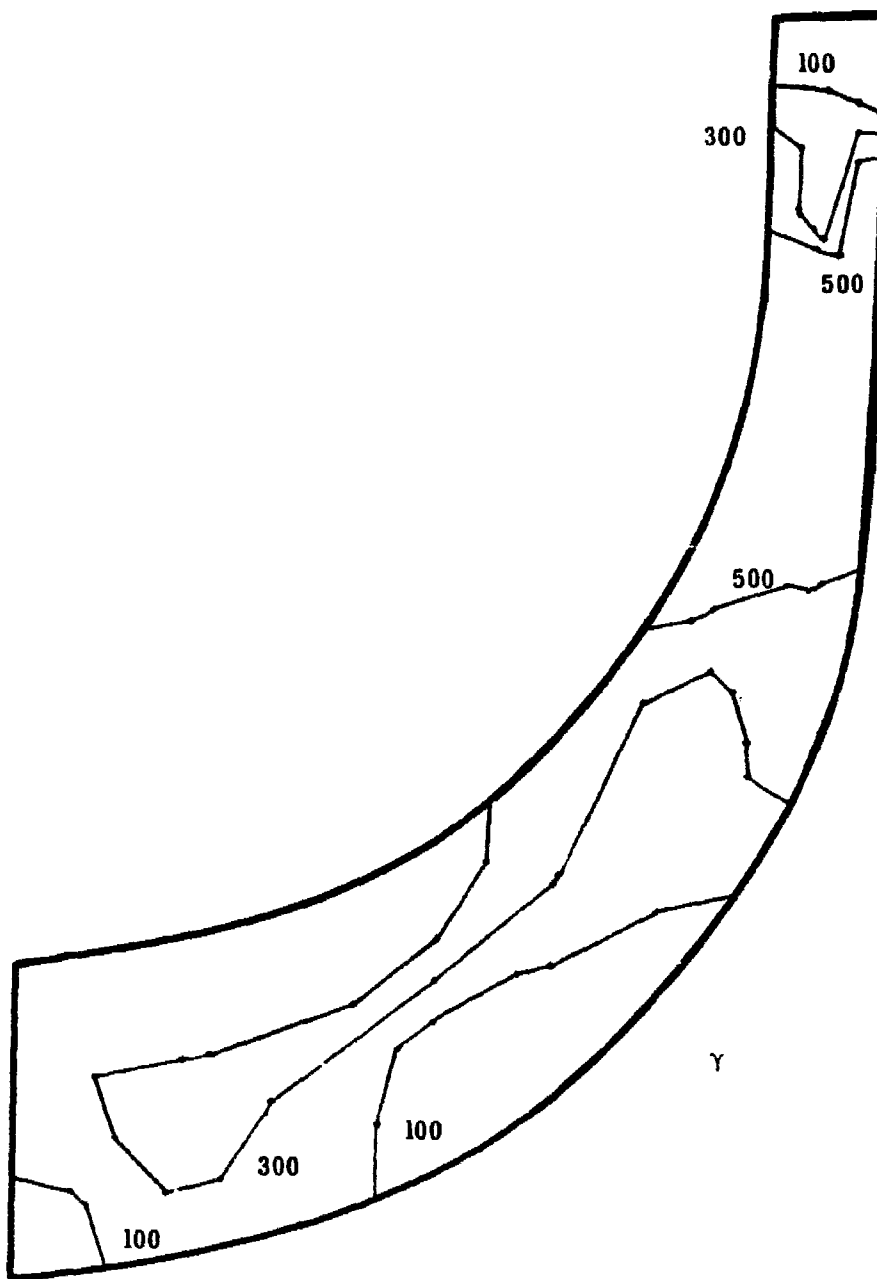
FIG. 47. DISTRIBUTION OF THE FREQUENCY OF IMPACTS ON THE
PRESSURE SIDE OF THE RADIAL IMPELLER.
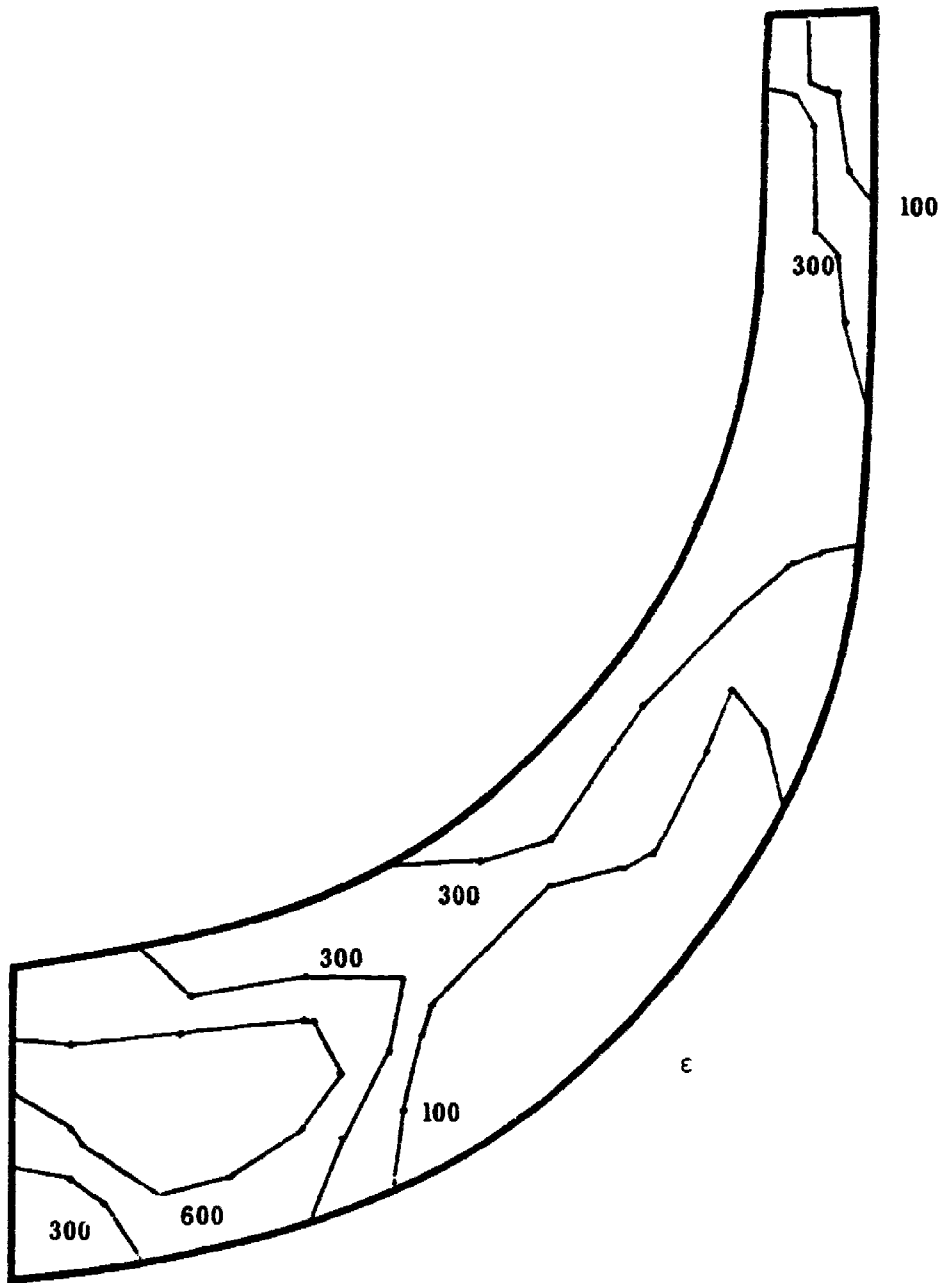
FIG. 48. DISTRIBUTION OF THE MASS EROSION PARAMETER ON THE
PRESSURE SIDE OF THE RADIAL IMPELLER.
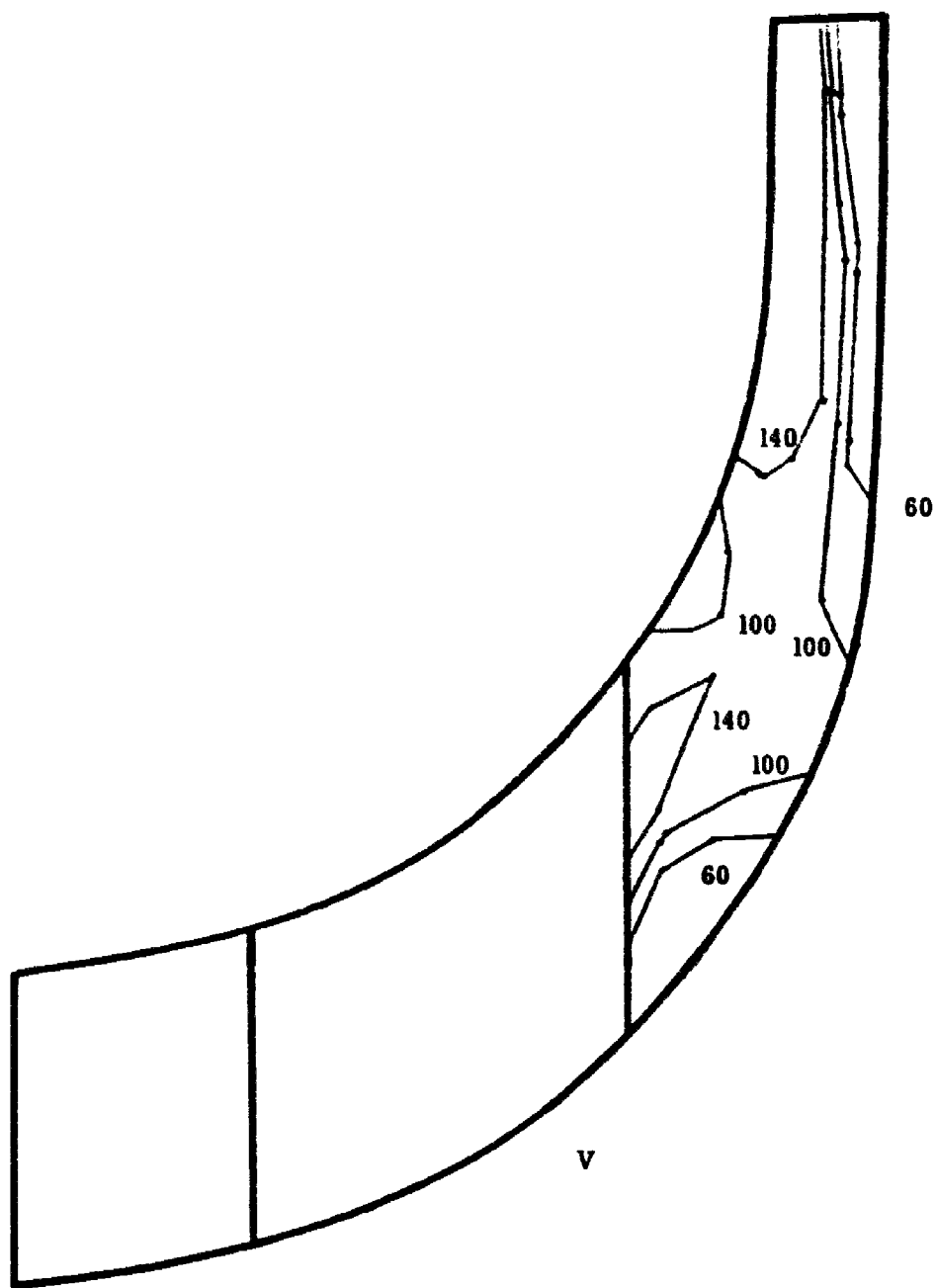
FIG. 49. DISTRIBUTION OF THE PARTICLE IMPACT VELOCITIES ON THE
PRESSURE SIDE OF THE SECOND SPLITTER VANE (METER/SEC)
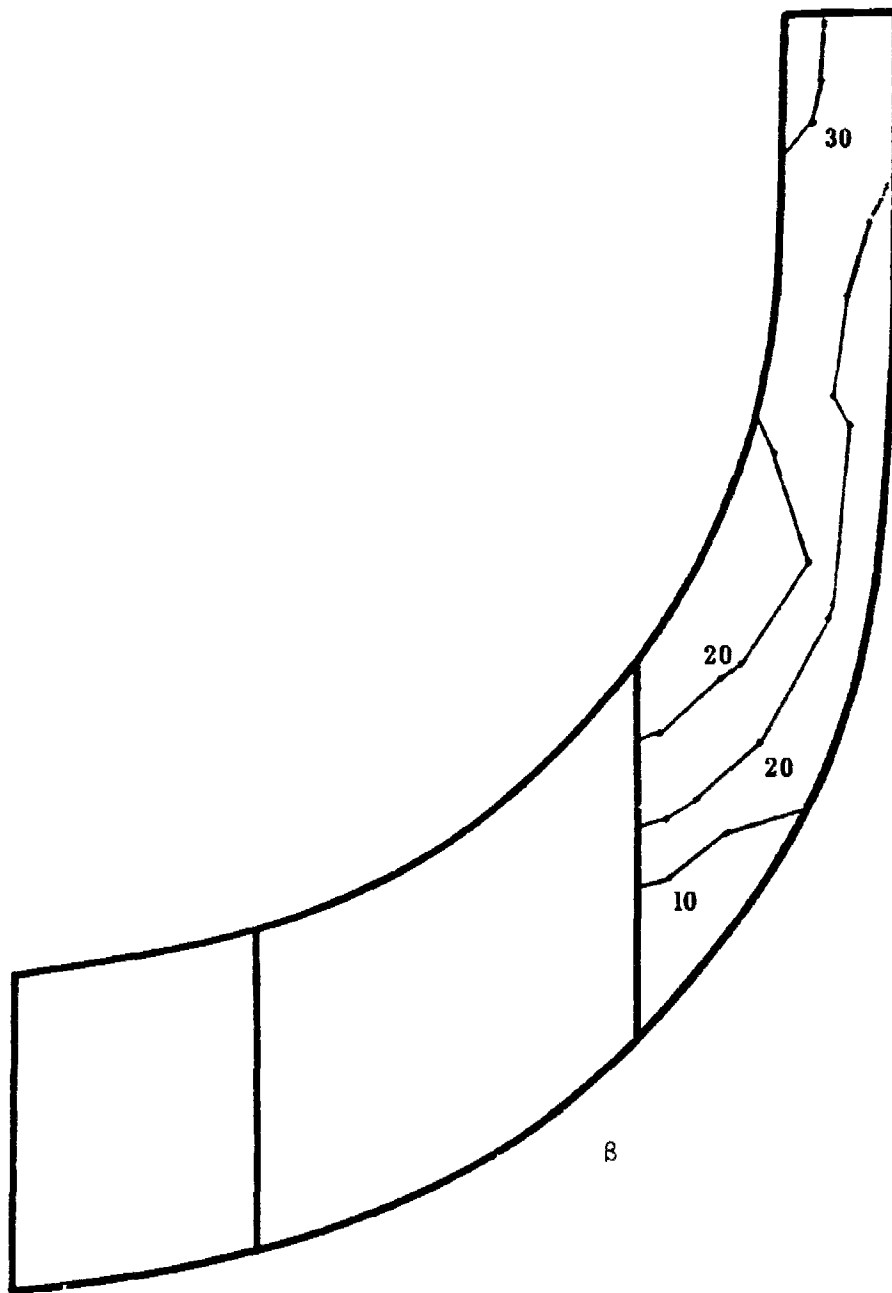
FIG. 50. DISTRIBUTION OF THE PARTICLE IMPACT ANGLES ON THE
PRESSURE SIDE OF THE SECOND SPLITTER VANE (DEGREES)
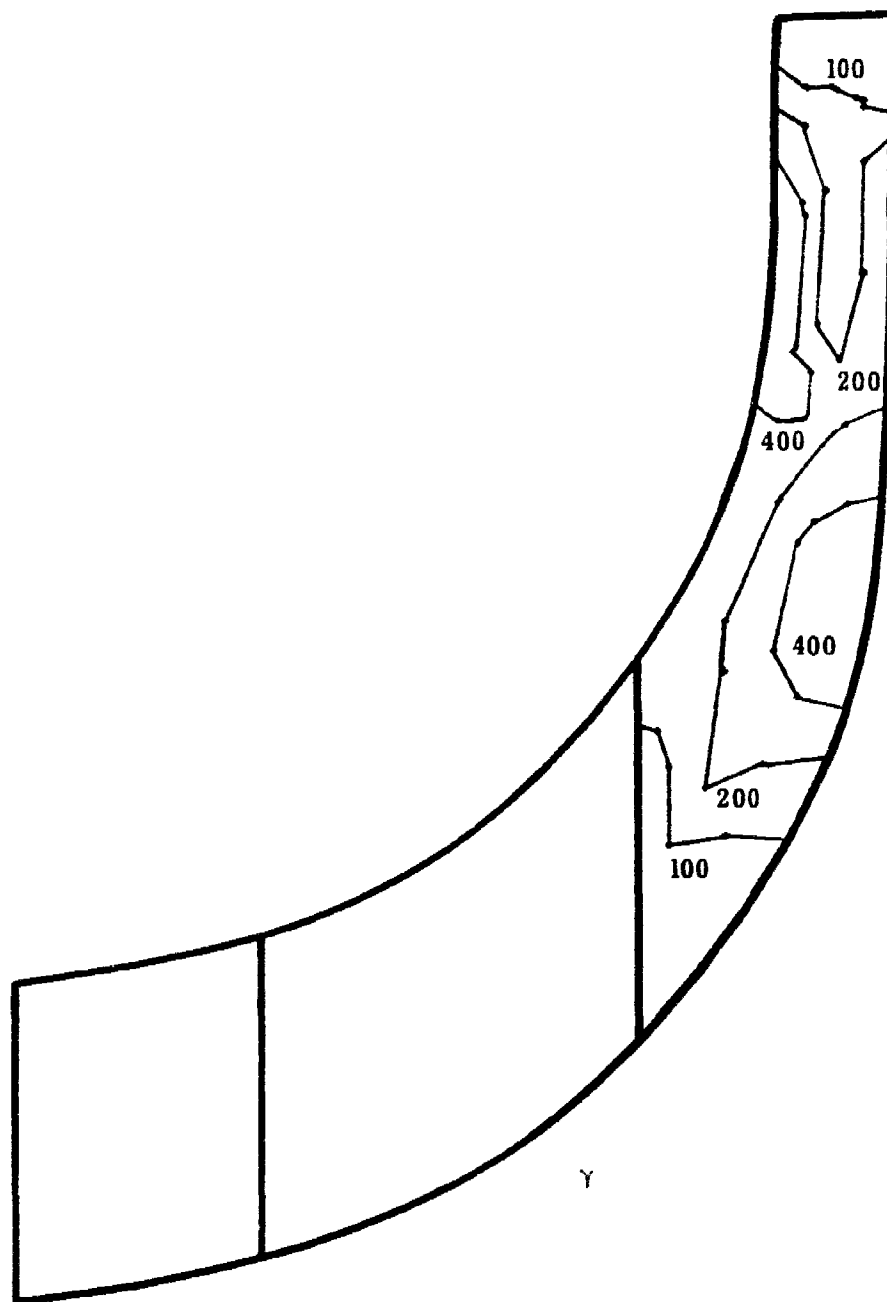
FIG. 51. DISTRIBUTION OF THE PARTICLE IMPACTS FREQUENCY ON THE PRESSURE SIDE OF THE SECOND SPLITTER VANE.
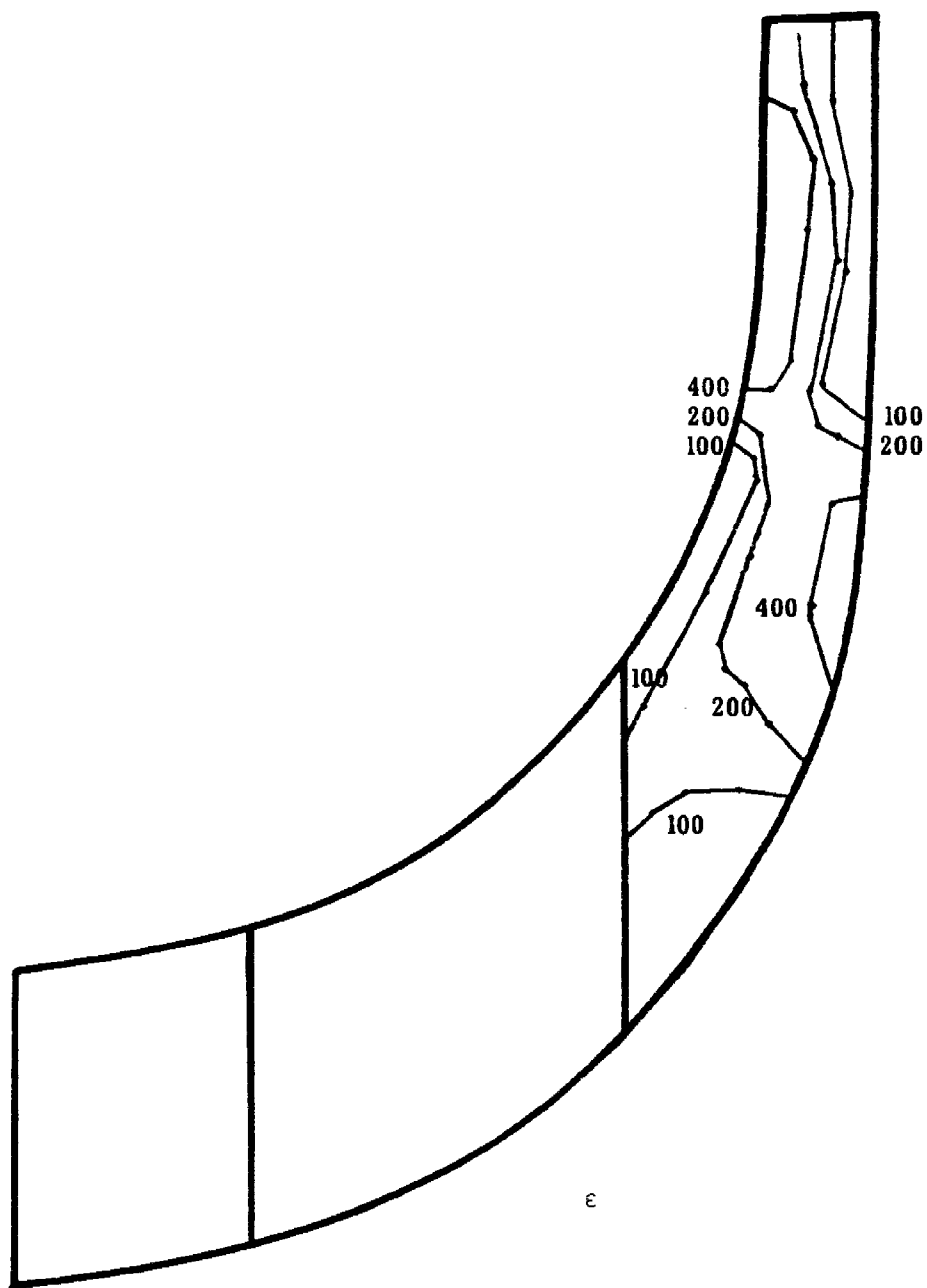
FIG. 52. DISTRIBUTION OF THE MASS EROSION PARAMETERS ON THE
PRESSURE SURFACE OF THE SECOND SPLITTER VANE.
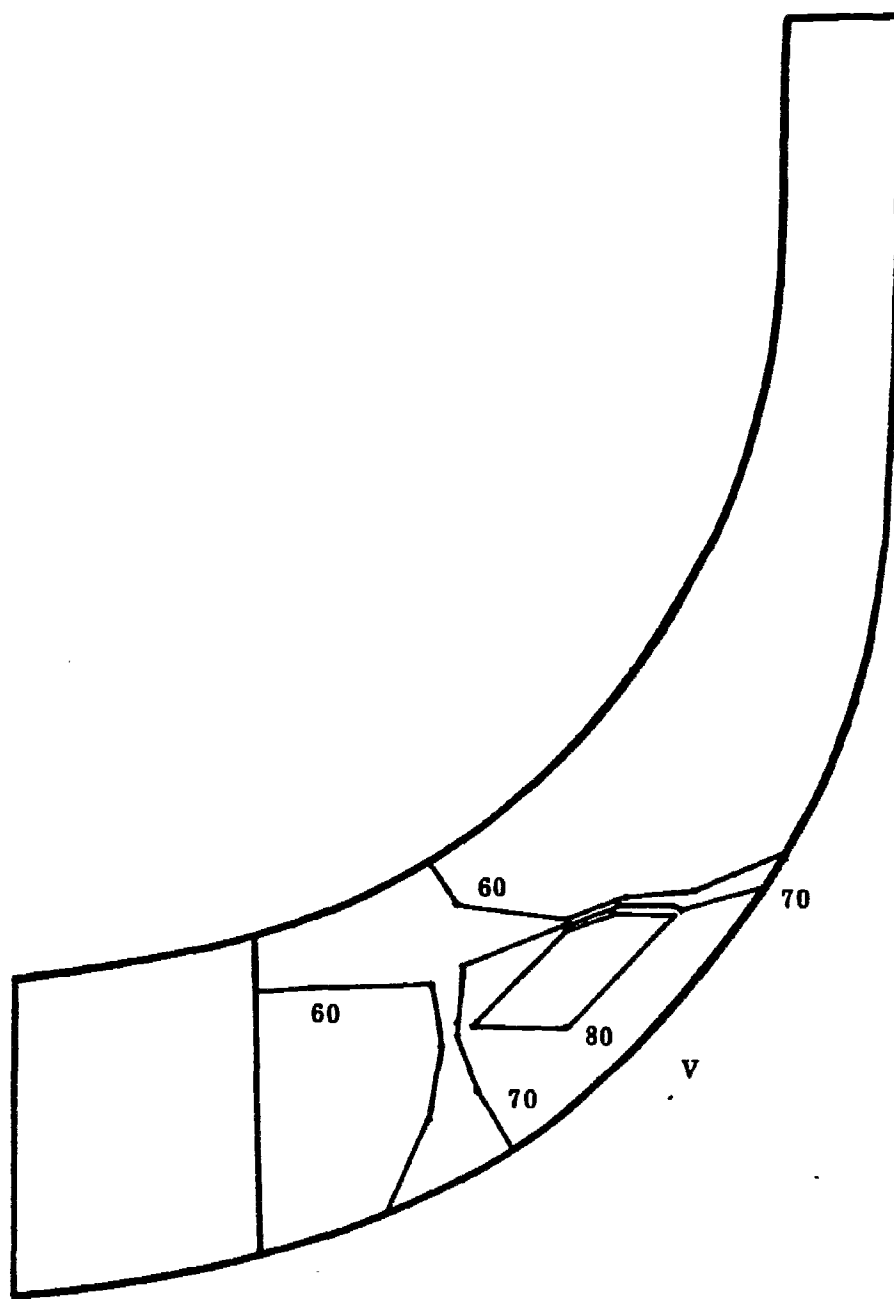
FIG. 53. DISTRIBUTION OF THE PARTICLE IMPACT VELOCITIES ON THE
SUCTION SIDE OF THE FIRST SPLITTER VANE (METER/SEC)
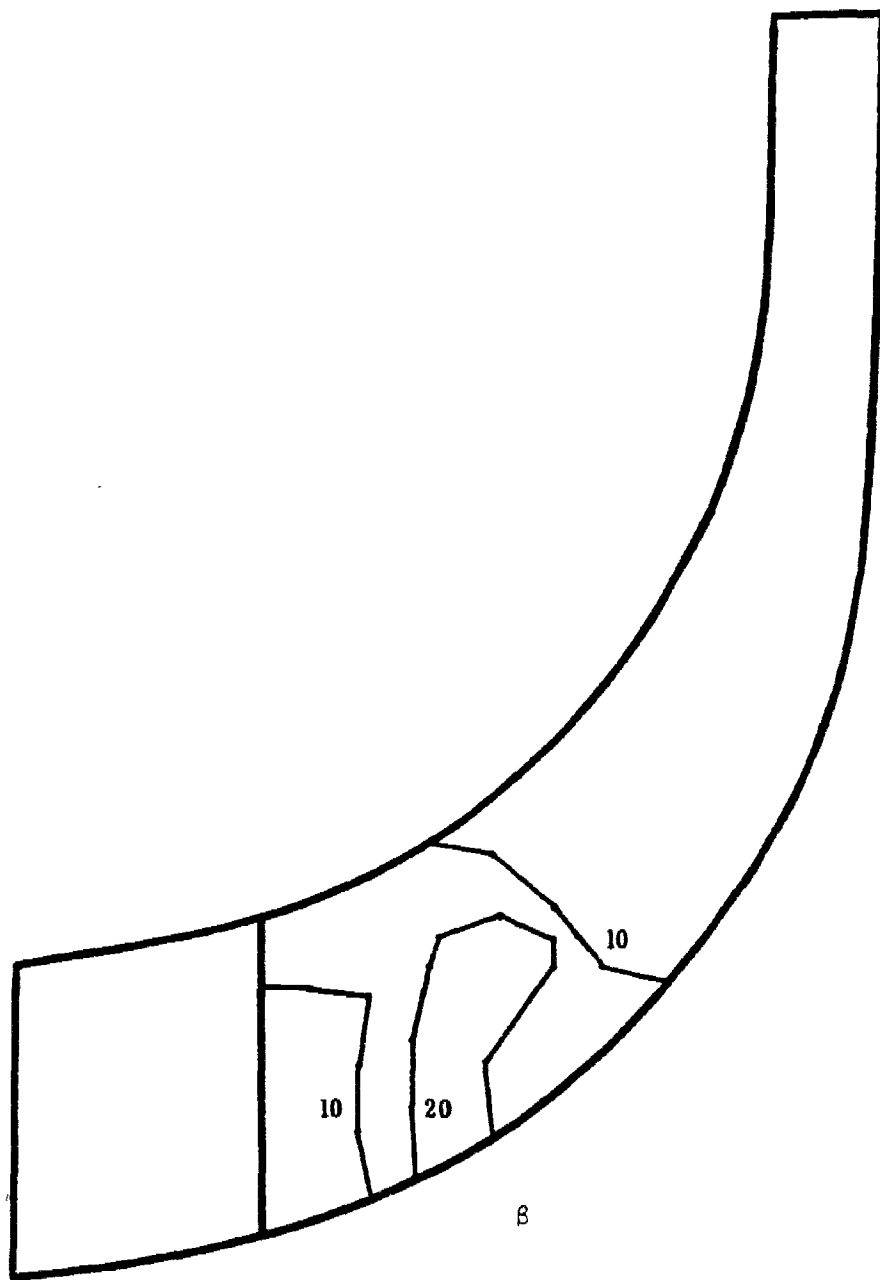
FIG. 54. DISTRIBUTION OF THE PARTICLE IMPACT ANGLE ON THE SUCTION
SIDE OF THE FIRST SPLITTER VANE (DEGREES).
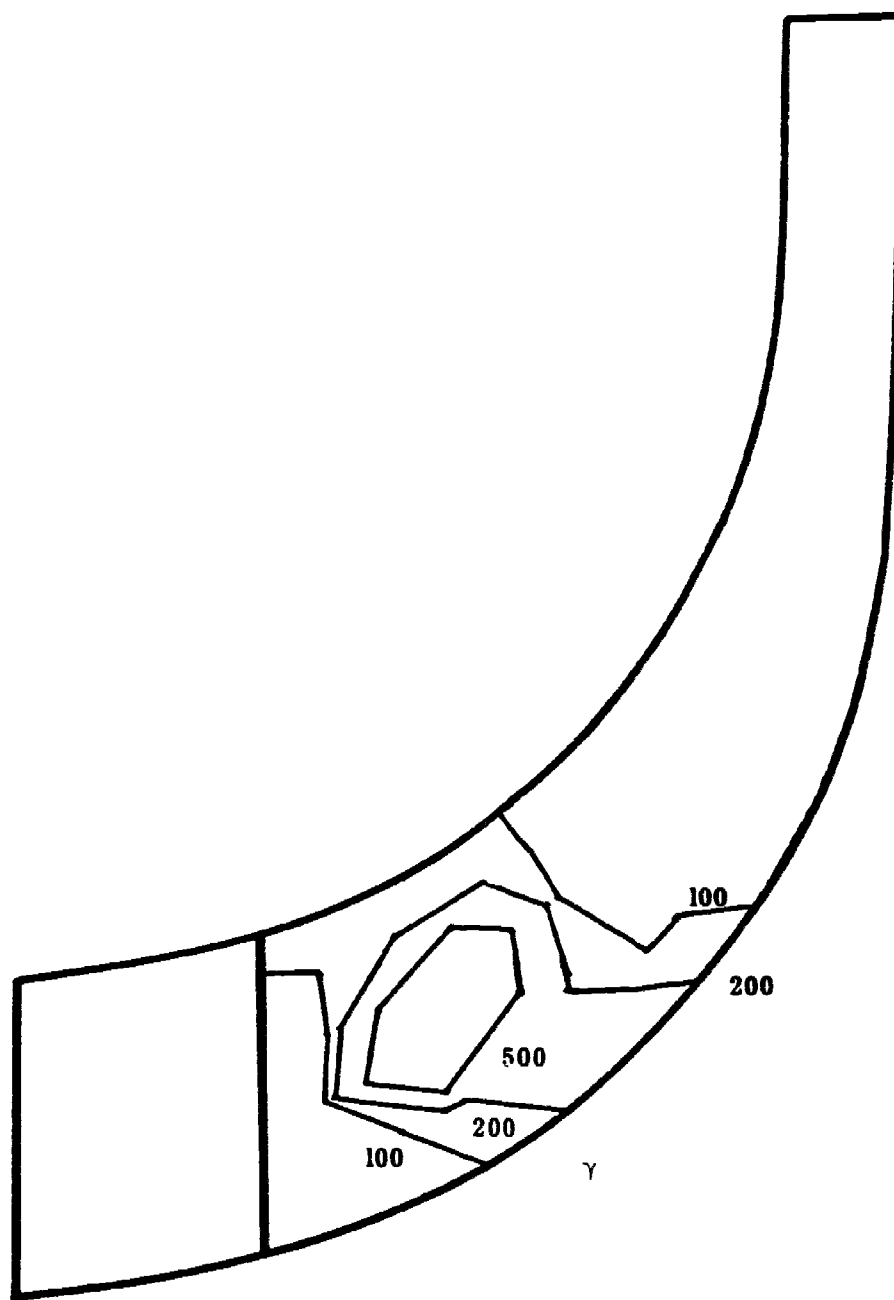
FIG. 55. DISTRIBUTION OF THE PARTICLE FREQUENCY OF IMPACTS ON THE SUCTION SURFACE OF THE FIRST SPLITTER VANE.
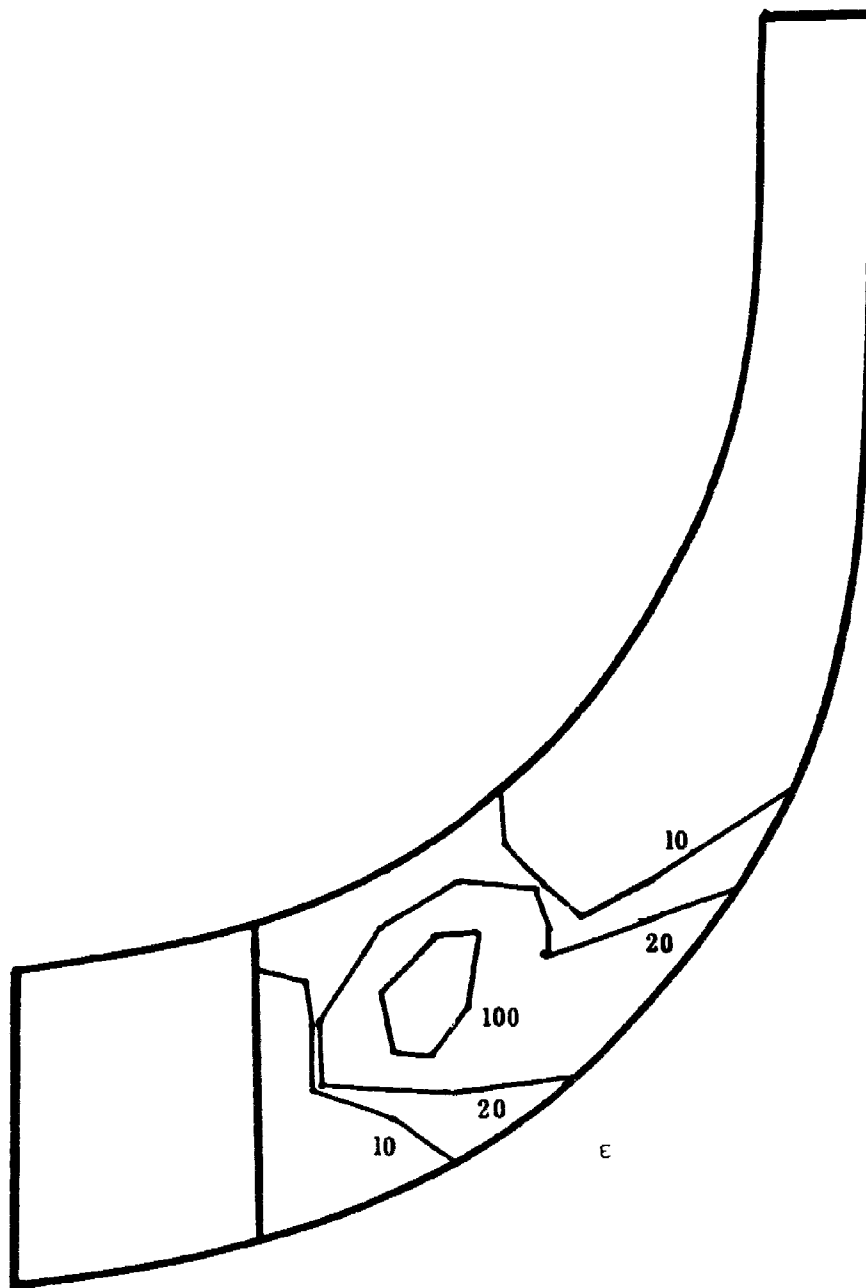
FIG. 56. DISTRIBUTION OF THE MASS EROSION PARAMETER ON THE
SUCTION SURFACE OF THE FIRST SPLITTER VANE.

AD-A173 288

REPORT DOCUMENTATION PAGE	READ INSTRUCTIONS BEFORE COMPLETING FORM	
1. REPORT NUMBER HRO 18560.29-EG	2. GOVT ACCESSION NO. N/A	3. RECIPIENT'S CATALOG NUMBER N/A
4. TITLE (and Subtitle) A Study of Erosion in Helicopter Engine With Inlet Separator	5. TYPE OF REPORT & PERIOD COVERED Technical Report	
	6. PERFORMING ORG. REPORT NUMBER 86-55	
7. AUTHOR(s) W. Tabakoff and A. Hamed	8. CONTRACT OR GRANT NUMBER(s) DAAG-29-82-K-0029	
9. PERFORMING ORGANIZATION NAME AND ADDRESS Dept. of Aerospace Engineering & Engg. Mechanics University of Cincinnati Cincinnati, OH 45223	10. PROGRAM ELEMENT, PROJECT, TASK AREA & WORK UNIT NUMBERS	
11. CONTROLLING OFFICE NAME AND ADDRESS U. S. Army Research Office Post Office Box 12211 Research Triangle Park, NC 27709	12. REPORT DATE August 1986	
	13. NUMBER OF PAGES 81	
14. MONITORING AGENCY NAME & ADDRESS(If different from Controlling Office)	15. SECURITY CLASS. (of this report) Unclassified	
	15a. DECLASSIFICATION/DOWNGRADING SCHEDULE	

16. DISTRIBUTION STATEMENT (of this Report)

Approved for public release; distribution unlimited.

17. DISTRIBUTION STATEMENT (of the abstract entered in Block 20, If different from Report)

NA

18. SUPPLEMENTARY NOTES

The view, opinions, and/or findings contained in this report are those of the author(s) and should not be construed as an official Department of the Army position, policy, or decision, unless so designated by other documentation.

19. KEY WORDS (Continue on reverse side If necessary and identify by block number)

Compressor Aerodynamics,
Erosion
Particualte Flow Trajectory Calculations

20. ABSTRACT (Continue on reverse side If necessary and identify by block number)

This report presents the results of an investigation of the solid particle dynamics and the resulting blade erosion through a helicopter engine with inlet particle separator. The particle trajectories are computed in the inlet separator which is characterized by considerable hub and tip contouring and radial variation in the swirling vane shape. The nonseparated particle trajectories are determined through the deswirling vanes and the five stage axial and one stage radial compressors. The impact data for a very large number of ingested particles is used to calculate the resulting blade surface erosion.

DD FORM 1473 EDITION OF 1 NOV 65 IS OBSOLETE